

## **INFORMATION TO USERS**

**This material was produced from a microfilm copy of the original document. While the most advanced technological means to photograph and reproduce this document have been used, the quality is heavily dependent upon the quality of the original submitted.**

**The following explanation of techniques is provided to help you understand markings or patterns which may appear on this reproduction.**

- 1. The sign or "target" for pages apparently lacking from the document photographed is "Missing Page(s)". If it was possible to obtain the missing page(s) or section, they are spliced into the film along with adjacent pages. This may have necessitated cutting thru an image and duplicating adjacent pages to insure you complete continuity.**
- 2. When an image on the film is obliterated with a large round black mark, it is an indication that the photographer suspected that the copy may have moved during exposure and thus cause a blurred image. You will find a good image of the page in the adjacent frame.**
- 3. When a map, drawing or chart, etc., was part of the material being photographed the photographer followed a definite method in "sectioning" the material. It is customary to begin photoing at the upper left hand corner of a large sheet and to continue photoing from left to right in equal sections with a small overlap. If necessary, sectioning is continued again — beginning below the first row and continuing on until complete.**
- 4. The majority of users indicate that the textual content is of greatest value, however, a somewhat higher quality reproduction could be made from "photographs" if essential to the understanding of the dissertation. Silver prints of "photographs" may be ordered at additional charge by writing the Order Department, giving the catalog number, title, author and specific pages you wish reproduced.**
- 5. PLEASE NOTE: Some pages may have indistinct print. Filmed as received.**

**Xerox University Microfilms**  
300 North Zeeb Road  
Ann Arbor, Michigan 48106

74-5519

ALLEN, John Joseph, 1943-  
THE EFFECTS OF NON-CONSTANT LATERAL PRESSURES  
ON THE RESILIENT RESPONSE OF GRANULAR  
MATERIALS.

University of Illinois at Urbana-Champaign,  
Ph.D., 1973  
Engineering, civil

University Microfilms, A XEROX Company , Ann Arbor, Michigan

THIS DISSERTATION HAS BEEN MICROFILMED EXACTLY AS RECEIVED.

**THE EFFECTS OF NON-CONSTANT LATERAL PRESSURES  
ON THE RESILIENT RESPONSE OF GRANULAR MATERIALS**

**BY**

**JOHN JOSEPH ALLEN**

**B.S., United States Air Force Academy, 1966  
M.S., University of Illinois, 1972**

**THESIS**

**Submitted in partial fulfillment of the requirements  
for the degree of Doctor of Philosophy in Civil Engineering  
in the Graduate College of the  
University of Illinois at Urbana-Champaign, 1973**

**Urbana, Illinois**

UNIVERSITY OF ILLINOIS AT URBANA-CHAMPAIGN

THE GRADUATE COLLEGE

April, 1973

I HEREBY RECOMMEND THAT THE THESIS PREPARED UNDER MY  
SUPERVISION BY JOHN JOSEPH ALLEN  
ENTITLED THE EFFECTS OF NON-CONSTANT LATERAL PRESSURES ON  
THE RESILIENT RESPONSE OF GRANULAR MATERIALS  
BE ACCEPTED IN PARTIAL FULFILLMENT OF THE REQUIREMENTS FOR  
THE DEGREE OF DOCTOR OF PHILOSOPHY

Marshall R. Thompson  
In Charge of Thesis

John G. Gernhardt  
Head of Department

Recommendation concurred in†

W. E. Blodgett  
William J. Hair  
Howard H. Thomassen  
Ernest J. Barenblat

Committee

on

Final Examination†

† Required for doctor's degree but not for master's.

#### ACKNOWLEDGEMENT

The author wishes to thank Marshall R. Thompson, Professor of Civil Engineering, University of Illinois at Urbana-Champaign, for his guidance during the course of this study.

Appreciation is also extended to personnel of the U.S. Army, Corps of Engineers, Construction Engineering Research Laboratory, where the experimental portion of this study was accomplished, for their assistance. Special thanks are given to Mr. Bob Neathammer for his help with the statistical analysis portion of this work and to Drs. Gene Marvin and Curt Eberhardt for their generous assistance with the finite elements analysis.

A special debt of gratitude is due the author's wife, Bette, whose continuing patience, understanding, and encouragement was essential to the successful completion of this study.

## TABLE OF CONTENTS

	Page
<b>CHAPTER</b>	
1. INTRODUCTION . . . . .	1
1.1 Statement of the Problem . . . . .	1
1.2 Objective and Scope . . . . .	3
2. LITERATURE SURVEY . . . . .	6
2.1 Constitutive Relations . . . . .	6
2.2 Models and Laboratory Investigations . . . . .	8
2.3 Concept of "Resilient" Response . . . . .	17
2.4 Factors Affecting the Resilient Response of Granular Materials. .	18
2.4.1 Stress History . . . . .	20
2.4.2 Duration of Load and Frequency of Application . . . . .	22
2.4.3 Aggregate Type and Gradation . . . . .	22
2.4.4 Density . . . . .	22
2.4.5 Degree of Saturation . . . . .	26
2.4.6 Stress Level . . . . .	26
2.5 Summary . . . . .	29
3. STRESS DISTRIBUTIONS IN FLEXIBLE PAVEMENTS AND EFFECTS OF NON-LINEAR MATERIAL PROPERTIES . . . . .	36
3.1 Surface Traction on a Semi-Infinite Elastic Halfspace . . . . .	36
3.1.1 Solution for Stresses and Displacements . . . . .	36
3.1.2 Advantages and Limitations of the Boussinesq Solution. . .	37

	Page
3.2 Elastic Layered System . . . . .	38
3.2.1 Development . . . . .	38
3.2.2 Advantages and Limitations of the Layered Elastic Solution . . . . .	41
3.3 Finite Element Analysis . . . . .	43
3.3.1 Development . . . . .	43
3.3.2 Advantages and Limitations of Finite Element Analysis . . . . .	47
3.4 Finite Element Analysis of Pavement Sections . . . . .	52
3.5 Comparison of Stress Pulses . . . . .	61
3.6 Implications of Stress-Dependent Properties for Pavement Performance . . . . .	67
4. LABORATORY TESTING PROGRAM . . . . .	79
4.1 Description of Materials . . . . .	79
4.2 Specimen Preparation . . . . .	81
4.3 Testing Equipment and Instrumentation . . . . .	88
4.3.1 Testing Equipment . . . . .	88
4.3.2 Instrumentation . . . . .	88
4.3.3 Triaxial Chamber . . . . .	92
4.4 Test Sequence . . . . .	92
4.4.1 Preliminary Tests . . . . .	92
4.4.2 Primary Tests . . . . .	95
5. PRESENTATION AND DISCUSSION OF RESULTS . . . . .	98
5.1 Methods of Computing the Resilient Modulus, $E_r$ , and Resilient Poisson's Ratio, $\nu_r$ . . . . .	98

	Page
5.2 Statistical Analysis of Data . . . . .	101
5.3 Results of the Preliminary Test Series . . . . .	103
5.3.1 Stress History Effects . . . . .	104
5.3.2 Stress Pulse Duration Effects . . . . .	107
5.3.3 Stress Sequence Effects . . . . .	107
5.3.4 Summary of Preliminary Test Results . . . . .	109
5.4 Results of Primary Test Series . . . . .	111
5.4.1 Effects of State of Stress . . . . .	111
5.4.2 Effects of Density . . . . .	124
5.4.3 Effects of Material Type . . . . .	133
5.4.4 Plastic Deformations . . . . .	143
5.4.5 Anisotropic Behavior . . . . .	148
5.4.6 Comparison of VCP and CCP Test Results . . . . .	150
5.5 Summary of Laboratory Results . . . . .	158
6. IMPLICATIONS OF THE LABORATORY RESULTS FOR PAVEMENT ANALYSIS . . .	160
6.1 Introduction . . . . .	160
6.2 K and n Varied Simultaneously . . . . .	162
6.3 K Varied - n Unchanged . . . . .	166
6.4 n Varied - K Constant . . . . .	169
6.5 Poisson's Ratio Varied . . . . .	169
6.6 Interaction of K and n . . . . .	170
6.7 Significance of Variations in the Resilient Material Parameters . . . . .	171

	Page
7. SUMMARY AND CONCLUSIONS . . . . .	173
7.1 Summary . . . . .	173
7.2 Conclusions . . . . .	173
7.3 Recommended Research . . . . .	177
 LIST OF REFERENCES . . . . .	 178
APPENDIX A - DATA FROM PRIMARY TEST SERIES . . . . .	184
APPENDIX B - NOMENCLATURE . . . . .	203
VITA . . . . .	205

## LIST OF TABLES

Table	Page
2.1 INFLUENCE OF DEGREE OF SATURATION ON THE RESILIENT PROPERTIES OF GRANULAR BASE MATERIALS . . . . .	28
2.2 SUMMARY OF REPEATED-LOAD TRIAXIAL TESTS TO EVALUATE THE RESILIENT PROPERTIES OF GRANULAR MATERIALS . . . . .	35
3.1 DIMENSIONS AND MATERIAL PROPERTIES OF PAVEMENT SECTIONS ANALYZED BY FINITE ELEMENTS TECHNIQUE . . . . .	57
4.1 ATTERBERG LIMITS AND SPECIFIC GRAVITY . . . . .	79
4.2 TEST SPECIMENS . . . . .	84
4.3 TEST SCHEDULE . . . . .	96
5.1 RESULTS OF STRESS PULSE DURATION TESTS . . . . .	108
5.2 RESULTS OF STRESS SEQUENCE TESTS . . . . .	110
5.3(a) REGRESSION EQUATIONS FOR $E_r$ FROM PRIMARY TEST DATA . . . . .	112
5.3(b) REGRESSION EQUATIONS FOR $v_r$ FROM PRIMARY TEST DATA . . . . .	113
5.4 TOTAL PLASTIC AXIAL STRAIN . . . . .	146
5.5 PERCENTAGE TOTAL AXIAL STRAIN ACCUMULATED DURING VCP AND CCP TESTS .	157
6.1 RESILIENT MATERIAL PARAMETERS USED IN SENSITIVITY ANALYSIS . . . . .	165
6.2 EFFECTS OF VARIATIONS IN RESILIENT PARAMETERS ON INDICATORS OF PAVEMENT PERFORMANCE . . . . .	167

## CHAPTER 1

### INTRODUCTION

#### 1.1 Statement of the Problem

To accurately predict the performance of a proposed pavement section, the designer must be able to quantify the response of each component of the pavement to the anticipated traffic loads. To date, this has been done primarily by assigning to each pavement material parameters which are thought to most adequately characterize the material as linearly elastic. These parameters are then used in various analytical procedures which have their bases in elastic theory. It is generally accepted, however, that the stress-strain behavior of flexible pavement materials is neither linear nor elastic. In reality traffic induced pavement deformations consist of elastic (recoverable) portions, viscous (time dependent) components, and plastic (permanent) components. Proper characterization of such viscoelastic materials is complex and too involved for ready use as an analytical tool. It appears that, while computational techniques ranging from elastic layered solutions to finite element solutions are available and readily adaptable to pavement structure, the ability to properly quantify the necessary material parameters for use in these techniques is lacking. The applicability of elastic theory and present computational schemes to pavements as well as the difficulty of characterizing pavement components has been recognized in the United States and abroad. Seed, et al. (61)\* state, "In view of the availability of tabulated solutions for stresses and deflections in elastic systems and the development of numerical procedures for use with electronic computers, there would seem to be no obstacle to at least an approximate determination of the transient and recoverable pavement deflections, other than the diffi-

---

\* Numbers in parentheses refer to entries in the List of References, page 178.

culty of evaluating the appropriate properties (elastic modulus and Poisson's ratio) of the pavement materials."

From England, Burt (14) has written, "The adequacy of linear elastic theory has been demonstrated for many conditions provided that the appropriate dynamic moduli are used..."

Two major types of flexible pavement distress which limit performance are excessive rutting (plastic deformation) and fatigue cracking of the asphalt surface. Occurrence of the former has been considerably reduced through application of current, empirically-derived design procedures. On the other hand, the latter is becoming more prominent. Fatigue cracking results from repeated, instantaneous, and recoverable deflections brought about by the transient traffic loadings. The instantaneous and recoverable nature of these deflections has led many researchers to conclude that they can be predicted by suitable use of elastic theory. They have been termed "resilient" deflections rather than elastic in order to avoid confusion.

The importance of deflections in determining pavement performance has been recognized. Certain design schemes seek to limit the load-induced surface deflections as a means of preventing fatigue cracking. Others have attempted to correlate surface cracking with the radius of curvature of deflection basins and, thus, limit the radius. More recently, engineers have become aware that to reliably predict pavement performance it is necessary to assess the states of stress and strain existing in a pavement structure under moving loads. Therefore, efforts have been made to determine constitutive stress-strain relations for paving materials.

In developing constitutive relations and applying them to boundary value problems such as the transient loading of a pavement section, it is necessary that the materials be tested under the appropriate conditions. For example,

it is thought that granular material responds differently to dynamic loadings than to static loads. Therefore, in order to develop predictive equations for the material parameters of a granular base-coarse material, it should be tested using stresses of the magnitudes expected in service, and these stresses should be applied dynamically. Several dynamic testing procedures have been used. In-situ tests on pavement sections include vibratory techniques and repeated plate-load tests. Laboratory tests include resiliometer and repeated-load triaxial testing. The triaxial test has several advantages. It is relatively inexpensive compared to field tests and it requires less time. In addition, stresses can be applied to a specimen as pulses that simulate those applied to an element in an actual pavement. Several investigators have reported the results obtained from repeated-load triaxial tests on pavement materials (24)(31)(51)(52). Specimens in these tests were subjected to constant confining pressures and pulsed axial loads. There have been no reports, however, regarding studies in which the confining pressure was varied simultaneously with the axial pressure on such a time scale as to accurately simulate a moving wheel load. In effect, previous investigations have approximated the maximum levels of radial stresses to be found at various locations in a pavement system, but the effects of time-dependent variations in these stresses as they reach these maxima have not been explored. Because the material parameters of certain pavement components have been found to be highly stress dependent, it appears desirable to ascertain the effects of non-constant lateral pressures on the resilient properties of these granular materials.

### 1.2 Objective and Scope

The objective of this research was to assess the effects of non-constant lateral pressures on the resilient response of granular materials. Predictive

equations for material stiffnesses and Poisson's ratios were developed and are considered accurate for use in various analytical techniques, insofar as they are applied to the proper boundary value problem. That is, these are pseudo-elastic material parameters that define the response of an unbound granular base course material to stresses applied at typical vehicle speeds. It is not intended that these results serve as a model for predicting accumulated plastic deformations (rutting). However, it is suggested that these results have direct application to the problem of predicting transient, resilient pavement deflections, and therefore, serve as a step toward the successful prediction of asphalt concrete pavement fatigue life.

The project was divided into several phases. Phase I consisted of a literature survey concerned chiefly with the factors involved in developing constitutive relations for granular materials, previous experimental methods of determining material properties of cohesionless soils, factors affecting the resilient properties of granular materials, and the various predictive models for material resilient moduli and Poisson's ratio that have been proposed. Phase I is discussed in Chapter 2.

Phase II, reported on in Chapter 3, included the study of stress distributions in flexible pavement systems under load and the subsequent development of stress pulses for use in repeated-load triaxial testing.

Phase III was the laboratory testing program. As reported in Chapter 4, compacted samples of granular materials were subjected to repeated stress pulses which were accurate simulations of the stresses applied to an element of a flexible pavement section under moving wheel loads. Lateral stresses were varied simultaneously with axial stresses. Such factors as density, stress pulse duration, number of stress repetitions, and type of material were varied in order to assess their effects on resilient response. For comparison purposes,

tests were run in which specimens were subjected to constant lateral pressures and repeated axial loads. At each stress level resilient radial and axial strains were measured.

Phase IV, discussed in Chapter 5, consisted of reduction and presentation of data acquired during the testing phase. The significance of each testing variable is discussed and predictive equations for the resilient modulus and Poisson's ratio are presented.

A sensitivity analysis is presented in Chapter 6 in which the effects of changes in granular material parameters on the quantitative indicators of pavement performance are investigated for typical pavement sections.

Chapter 7 contains conclusions reached as a result of this study as well as recommendations for further research.

A list of pertinent references is included at the end of this report. It should be noted that little mention is made of reports published prior to 1967 because these are comprehensively summarized by Seed, et al. (61).

CHAPTER 2  
LITERATURE SURVEY

### 2.1 Constitutive Relations

Before a solution to a boundary value problem can be obtained, it is necessary to quantify the stress-strain properties of the materials involved. The relationship between stress and strain in a material is known as the "constitutive" law. In general terms, stress (strain) in a material is a function of location, time, temperature, and strain (stress). For example, Westmann (72) uses the following nomenclature:

$$\epsilon_{xx} = F_{xx} (\tau_{xx}, \tau_{yy}, \dots, X, Y, Z, t, T) \quad (2.1)$$

where,  $t$  represents time

$T$  represents temperature

$X, Y, Z$  represent location

$\epsilon$  represents strain

$\tau$  represents stress

It has been verified experimentally that for rates of loading corresponding to those applied by moving highway or aircraft traffic, unbound granular materials respond essentially independently of temperature and rate of loading. (Seed, et al., Ref. 61) Therefore, the response of materials may be characterized as either linear, rate-independent or nonlinear, rate-independent. That the response of granular materials is non-linear has also been well-documented. (Hicks, 31) In addition, the instantaneous and recoverable nature of the strains in highway pavement components subjected to moving loads has led previous investigators to model granular materials as non-linear, elastic.

Dehlen(18) describes a constitutive relation for non-linear, elastic materials which is represented by the strain matrices corresponding to a large number

of differing stress matrices.

It is common(18)(31) to express a nonlinear, elastic constitutive law in terms of stress-strain increments, where the increment of strain is a linear function of the stress increment superimposed on the reference stress level.

In matrix form:

$$\begin{bmatrix} \epsilon_{xx} \\ \epsilon_{yy} \\ \epsilon_{zz} \\ \epsilon_{xy} \\ \epsilon_{yz} \\ \epsilon_{zx} \end{bmatrix} = \begin{bmatrix} A_{11} & A_{12} & A_{13} & A_{14} & A_{15} & A_{16} \\ A_{21} & A_{22} & A_{23} & A_{24} & A_{25} & A_{26} \\ A_{31} & A_{32} & A_{33} & A_{34} & A_{35} & A_{36} \\ A_{41} & A_{42} & A_{43} & A_{44} & A_{45} & A_{46} \\ A_{51} & A_{52} & A_{53} & A_{54} & A_{55} & A_{56} \\ A_{61} & A_{62} & A_{63} & A_{64} & A_{65} & A_{66} \end{bmatrix} \begin{bmatrix} \sigma_{xx} \\ \sigma_{yy} \\ \sigma_{zz} \\ \tau_{xy} \\ \tau_{yz} \\ \tau_{zx} \end{bmatrix} \quad (2.2)$$

Expressed in cylindrical coordinates and for an axisymmetric condition:

$$\epsilon_{xx} = \epsilon_{rr}, \epsilon_{yy} = \epsilon_{\theta\theta}, \epsilon_{zz} = \epsilon_{zz}, \epsilon_{xy} = \epsilon_{r\theta} = 0, \epsilon_{yz} = \epsilon_{\theta z} = 0, \epsilon_{zx} = \epsilon_{rz}.$$

Assuming no coupling between volumetric and shear stress and strains:

$$\begin{bmatrix} \epsilon_{rr} \\ \epsilon_{\theta\theta} \\ \epsilon_{zz} \\ \epsilon_{rz} \end{bmatrix} = \begin{bmatrix} A_{11} & A_{12} & A_{13} & 0 \\ A_{12} & A_{11} & A_{13} & 0 \\ A_{31} & A_{31} & A_{33} & 0 \\ 0 & 0 & 0 & A_{66} \end{bmatrix} \begin{bmatrix} \sigma_{rr} \\ \sigma_{\theta\theta} \\ \sigma_{zz} \\ \tau_{rz} \end{bmatrix} \quad (2.3)$$

For the triaxial test, confining stresses and axial stresses are principal stresses. Therefore,  $\epsilon_{rz} = 0$  and:

$$\begin{bmatrix} \epsilon_{rr} \\ \epsilon_{zz} \end{bmatrix} = \begin{bmatrix} A_{11} + A_{12} & A_{13} \\ 2A_{31} & A_{33} \end{bmatrix} \begin{bmatrix} \sigma_{rr} \\ \sigma_{zz} \end{bmatrix} \quad (2.4)$$

For an isotropic material Equation (2.4) reduces to the standard Hook's law formulation:

$$\begin{bmatrix} \epsilon_{rr} \\ \epsilon_{zz} \end{bmatrix} = \begin{bmatrix} \frac{1-\nu}{E} & -\frac{\nu}{E} \\ -\frac{2\nu}{E} & \frac{1}{E} \end{bmatrix} \begin{bmatrix} \sigma_{rr} \\ \sigma_{zz} \end{bmatrix} \quad (2.5)$$

where, E is Young's modulus and  $\nu$  is Poisson's ratio.

Note that the use of the standard triaxial test allows the determination of only two constants in Equation (2.4)  $A_{33}$  and  $A_{13}$ . In this case  $A_{33}$  represents the stiffness in the direction of applied stress and  $A_{13}$  represents Poisson's ratio perpendicular to the applied stress. The assumption of isotropy must be made. Hence,  $A_{33} = A_{11}$   $A_{13} = A_{31} = A_{12}$ .

The following section discusses various models and laboratory procedures that have been employed to describe the behavior of granular materials.

## 2.2 Models and Laboratory Investigations

Seed, et al.(61) have summarized the results of repeated load tests conducted on granular materials confined in rigid, hollow cylinders and in the Hveem Resiliometer. Although the Resiliometer is used by the California Highway Department, these types of tests have not been utilized too extensively. Recent laboratory and theoretical studies have yielded interesting and sometimes contradictory results. The first of these, conducted by Ko and Scott (41)(42), involves the use of a soil test box that can apply three different normal stresses to the sides of cubical samples. These principal stresses can be varied independently by use of a mechanical-hydraulic device. Results of tests conducted on cubical sand samples indicate that the volumetric compression of sand stressed hydrostatically is nonlinear but nearly elastic for pressures up to about 80 psi.

Hardin(29) developed a shear stress-strain relation to be applied to non-destructive testing of airport pavements. Using an apparatus capable of applying repeated torque to soil samples he measured the shear modulus over an extreme range of strain levels.

A theoretical study by Nelson and Baron (55) resulted in their proposal of an isotropic relation between stress and strain for soils. They state that no unique stress-strain relation, per se, exists, but that the bulk and shear moduli are functions of the stress and/or strain invariants.

Barenberg (5) reported the results of repeated loads on granular materials on a prepared subgrade. The testing apparatus was a two dimensional box 4 feet long by 6 inches wide by 18 inches deep. The load was applied through a steel plate 6 inches long by 4 inches wide. The results showed that the response of the granular-subgrade layered system was greatly influenced by the moisture content of the granular layer, with degrees of saturation above 80 percent having a particularly detrimental effect.

Figure 2.1 relates permanent deformation to magnitude of load, number of applications, and moisture content. Figure 2.2 relates the recoverable deformation after 20,000 load applications to the dry density of the granular material.

Huang (34) presented an analytical technique for determining stresses and displacements in nonlinear soil media in which he represented the material stiffness by:

$$E = E_0 (1 + \beta \theta) \quad (2.6)$$

a relationship originally suggested by Barkan (7). In this equation,  $E$  = elastic modulus under the given stress invariant;  $E_0$  = initial elastic modulus;  $\beta$  = a soil constant ( $\text{psi}^{-1}$ ) indicating the percentage increase in elastic modulus per 1 psi increase in stress invariant;  $\theta$  = the first stress invariant.

In recent years the applicability and desirability of using laboratory

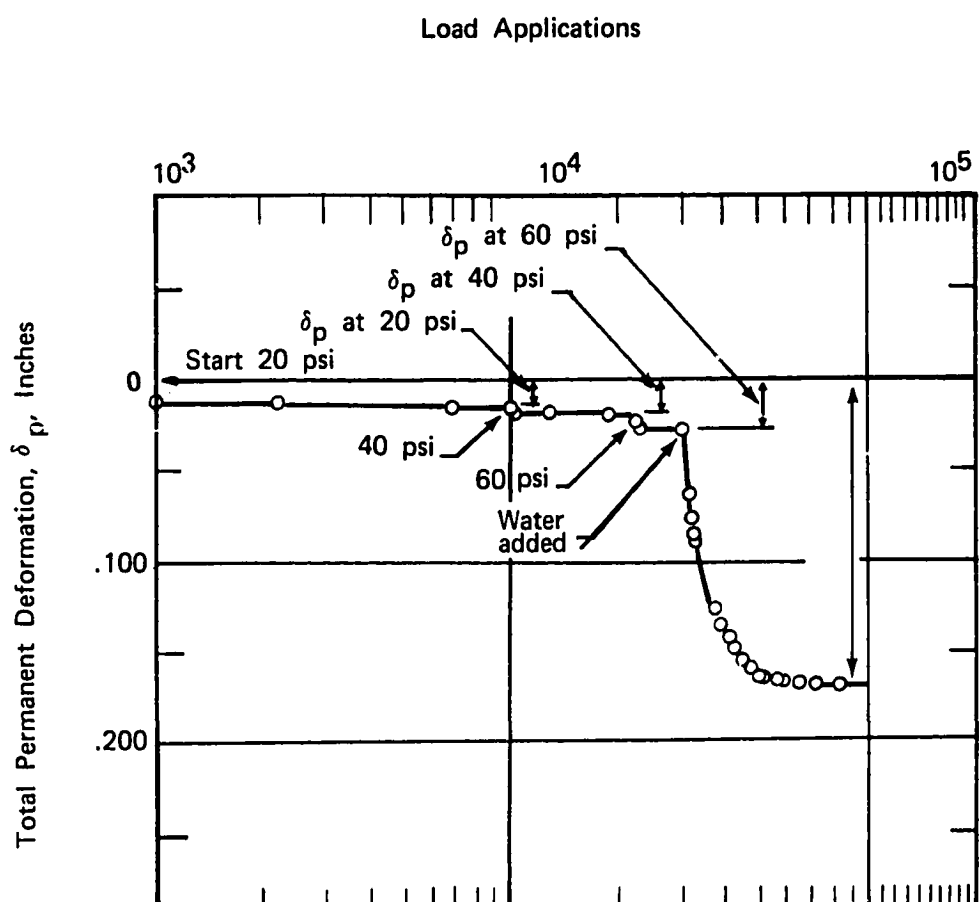
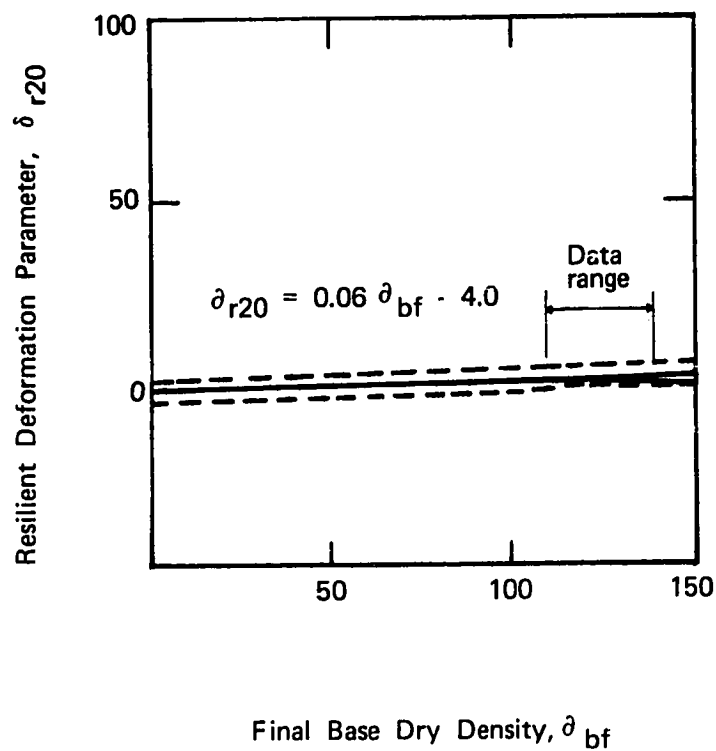


**Figure 2.1**  
Typical Performance of Samples Subjected to Repeated Loads  
in the Two Dimensional Model (After Barenberg (5)).



Note: Dotted lines show range of 3 times standard error of the estimate.

$\delta_{r20}$  = Resilient deformation divided by load magnitude at 20,000 load repetitions.

Figure 2.2  
Resilient Deformation Versus Dry Density of Base (After Barenberg (5)).

tests to characterize paving materials has been widely recognized (18)(31)(48)(61). In particular, the triaxial test has received increasing interest primarily because this apparatus can be programmed to apply repeated stresses of such duration and magnitude as to simulate the stresses applied to a pavement element under moving wheel load. There are varieties of the triaxial test. Bamert, Schmitter, and Weber (3) reported on the use of a standard triaxial cell modified to include a dropping weight to apply the dynamic load, a spring device to preset  $\sigma_1$ , and seismic measuring equipment. With this device they measured the static and dynamic moduli of sand.

Dunlap (24) reported the results of Texas triaxial tests on compacted specimens of crushed limestone base course materials as well as the results of repeated-load triaxial tests on the same materials. In the Texas triaxial test, 6 - by 8- inch specimens are tested to failure at a loading rate of 0.15 inches per minute after undergoing a drycuring and capillary absorption treatment. Because in-situ pavement base courses are subjected to a large number of short duration stresses of less than failure magnitude, only Dunlap's repeated load test results are presented herein. Specimens at various constant lateral pressures were subjected to repeated vertical stresses of varying magnitude and applied by means of a solenoid actuated hydraulic cylinder. Dunlap's proposed deformation law is as follows:

$$M_z = K_2 + K_3 (\sigma_r + \sigma_\theta) \quad (2.7)$$

where,  $M_z$  = modulus of deformation measured in the direction of applied stress,  $\sigma_z$

$K_2$  = modulus of deformation in the unconfined condition and is analogous to Young's modulus in elastic theory.

$\sigma_r, \sigma_\theta$  = radial and tangential stresses.

For the triaxial test, (2.7) becomes:

$$M_z = K_2 + 2K_3 (\sigma_r) \quad (2.8)$$

Figure 2.3 depicts Equation (2.8) graphically. Dunlap determined  $M_z$  by dividing the repeated deviator stress by the recoverable strain, which was measured by dial extensometers. Figure 2.4 is typical of his results.

In an attempt to better simulate field conditions, Dunlap ran a series of tests in which the lateral pressures were varied simultaneously with the deviator stresses. The assumption was made that the lateral stresses were a constant percentage of the deviator stresses, and in order to maintain this proportionality, both stresses were varied manually at a strain rate of 0.005 inches per minute. He concluded that the deformation constants ( $K_2$  and  $K_3$ ) were reduced by increasing the moisture content of the sample and by reducing the density. In addition, he found that  $M_z$  was greater for rates of loading corresponding to those in the field than for slower rates. Finally, he stated that sample densification under greater numbers of load repetitions tended to increase the deformation constants.

Moore, Britton, and Schrivner (51) used an optical tracking system to measure lateral and axial displacements on samples of compacted crushed limestone subjected to repeated loads in a triaxial machine. Using the relation:

$$M_z = K_2 + K_3 \sigma_r^2 \quad (2.9)$$

they investigated the effects of number of load applications, stress history, and rate of loading on the modulus of deformation,  $M_z$ . They concluded that: (1) the modulus increases as the number of repetitions increases, partly because of loss of moisture from the sample during testing; (2) it is not possible to predict the stiffness of a granular material unless its entire stress history is known; (3) the effect of rate of loading is small for rates varying from 200 to 650 psi/sec. Figure 2.5 is typical of these results relating the modulus to number of load applications.

Kirwan and Glynn (38) reported the results of repeated triaxial tests on

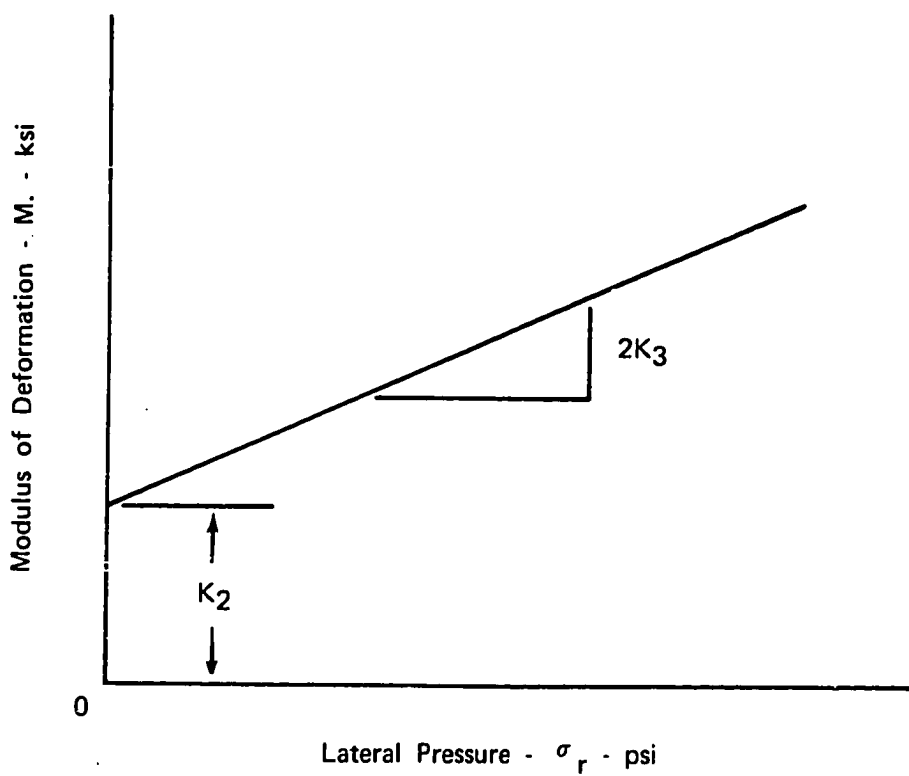


**Figure 2.3**  
Relationship between Modulus of Deformation and Lateral Pressure (After Dunlap (24)).

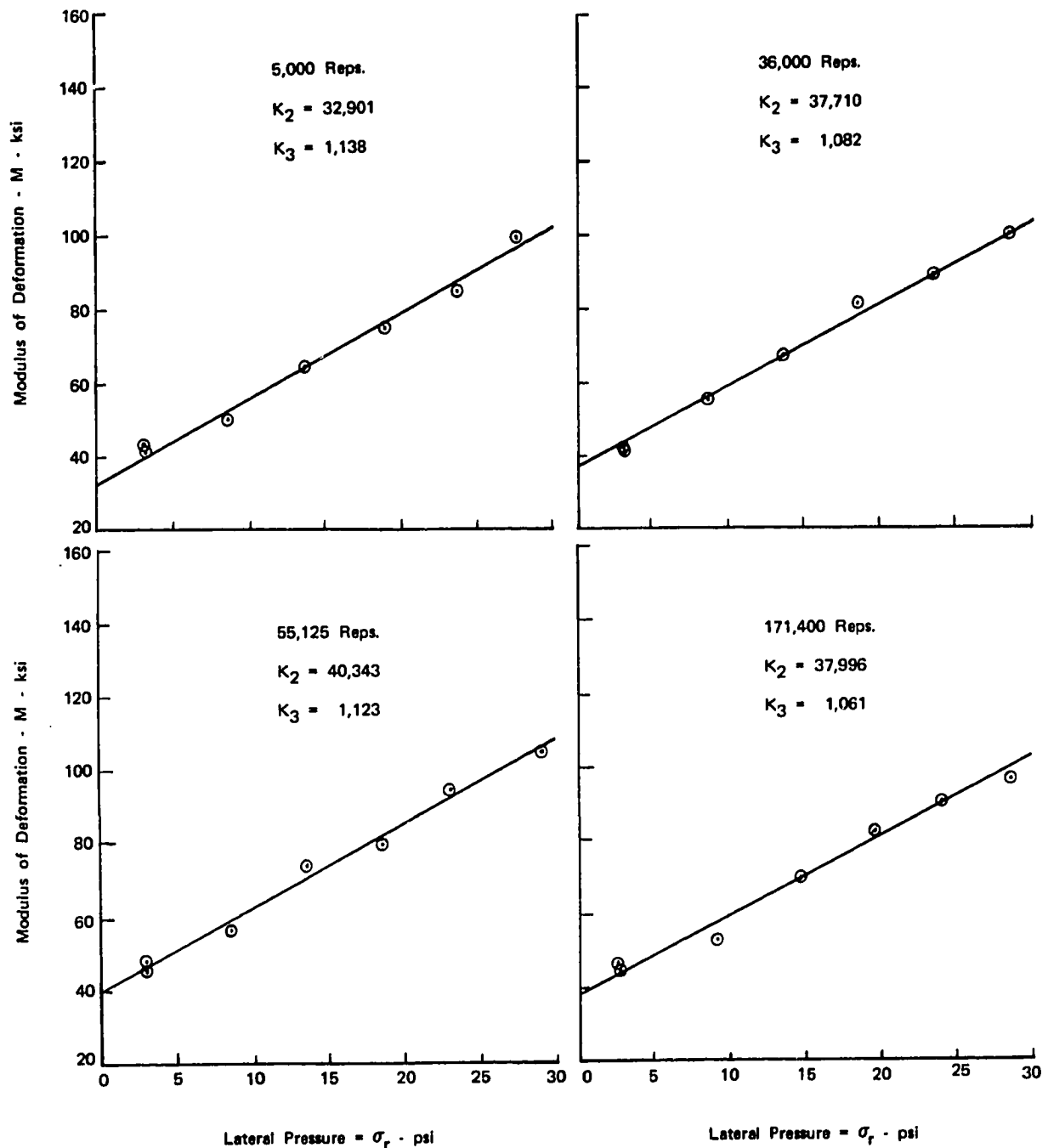


**Figure 2.4**  
**Effect of Lateral Pressure on Modulus of Deformation for Repeated Deviator Stress of 51.8 psi**  
(After Dunlap (24)).

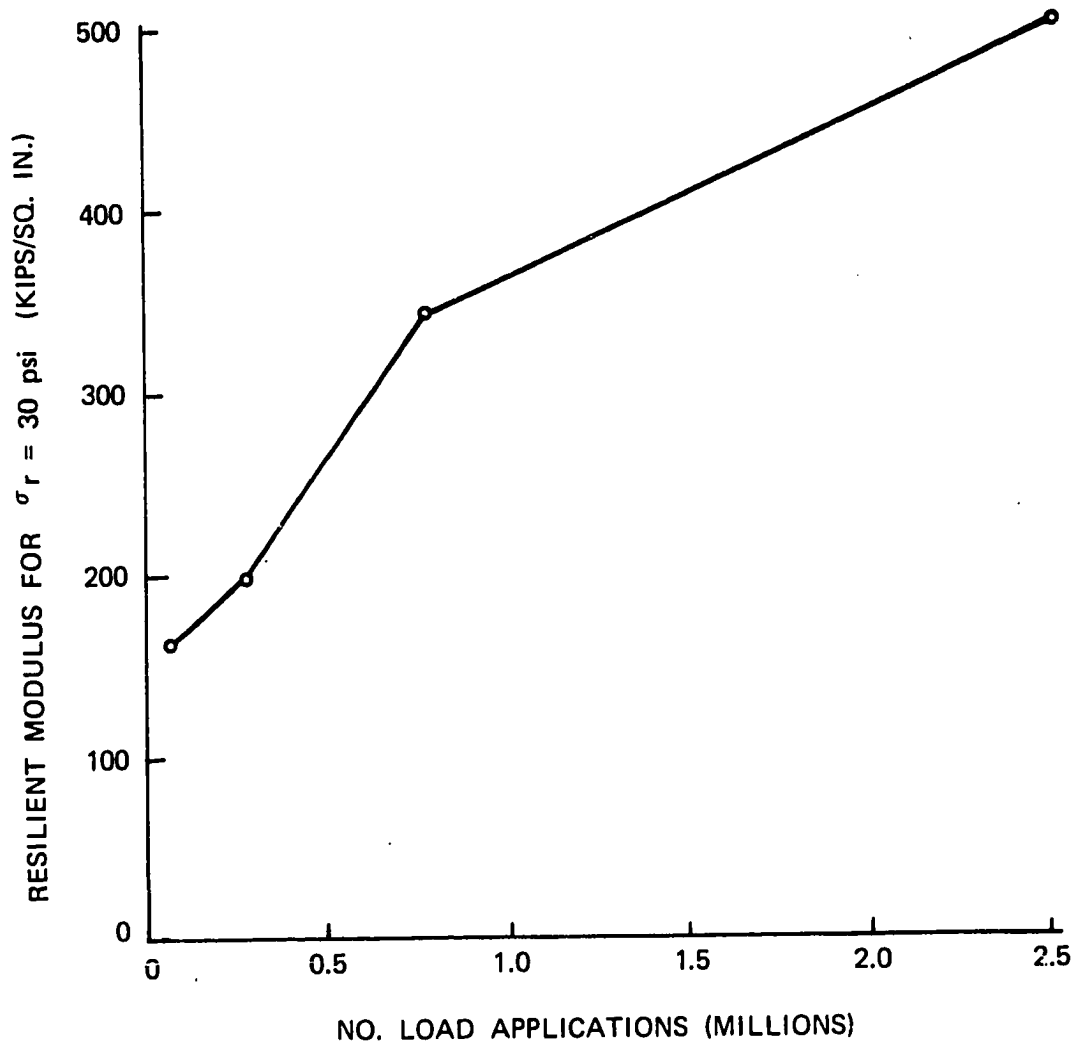


**Figure 2.5**  
Increase with Load Applications of the Modulus  $K_2 + K_3 \sigma_r^2$   
for Deviator Stress = 34 psi (After Moore, et al. (51)).

granular soils subjected to constant confining pressure. They, too, preferred Barkan's model, Equation (2.6).

Morgan (52) tested sands in a triaxial apparatus. He applied constant lateral pressures and repetitive axial loads. He found: (1) After a certain number of repetitions, permanent deformations remain essentially constant. (2) Confining pressure is the most significant factor affecting stiffness. At constant confinement, an increase in deviator stress reduces the modulus only slightly. (3) Poisson's ratio appears to be unrelated to confining pressure, deviator stress, or number of load repetitions. For these sands, Poisson's ratio ranged from 0.2 to 0.4.

Makhlof and Stewart (47) reported the following results of cyclic triaxial tests on air-dry, clean, Ottawa sand: (1) Sand in the loose or dense state exhibits strain-hardening characteristics over the range of stresses studied. (2) Inelastic strains continue in a decreasing manner with continued loading cycles. (3) The modulus of elasticity increases as the confining pressure increases.

### 2.3 Concept of "Resilient" Response

The applicability of the concept of resilient (or pseudo-elastic) response of granular materials is widely recognized (18)(31)(61). Basically, this approach seeks to formulate predictive equations for the resilient modulus and resilient modulus and resilient Poisson's ratio through the use of repeated-load triaxial tests. By expressing these parameters as functions of the state of stress in the materials, it is possible to account for nonlinear material response. The derived modulus and Poisson's ratio may then be used to characterize the granular layer in the numerical solution for transient pavement deflections.

Two models have been used to describe the resilient modulus:

$$M_r = K_1 \sigma_3^{K_2} \quad (2.10)$$

$$M_r = K_1' \theta^{K_2'} \quad (2.11)$$

where,  $M_r$  = resilient modulus

$K_1$ ,  $K_2$ ,  $K_1'$ ,  $K_2'$  = constants from regression analysis

$\sigma_3$  = confining pressure, psi

$\theta$  = sum of principal stresses,  $\sigma_1 + 2\sigma_3$

Hicks (31) tested compacted samples of granular materials using a conventional triaxial testing apparatus. At each of several constant confining pressures, he applied a series of repeated axial loads of varying magnitude. Figure 2.6 illustrates his methods of determining the resilient modulus and Poisson's ratio for a given confining stress. Note that either secant or tangent coefficients may be obtained. It is believed that secant values are most applicable to iterative type solutions and tangent values are best used with incremental solutions (see Chapter 3). Regression analysis of the results of tests conducted at various levels of confining stress yields values for the constants in Equations 2.10 and 2.11. He also modeled Poisson's ratio as a function of the principal stress ratio:

$$\nu = A_0 + A_1 \left( \frac{\sigma_1}{\sigma_3} \right) + A_2 \left( \frac{\sigma_1}{\sigma_3} \right)^2 + A_3 \left( \frac{\sigma_1}{\sigma_3} \right)^3 \quad (2.12)$$

where, the A constants were found by least squares techniques.

#### 2.4 Factors Affecting the Resilient Properties of Granular Materials

Following is a discussion of the factors affecting the resilient response of granular materials. This information has been gathered from the results of

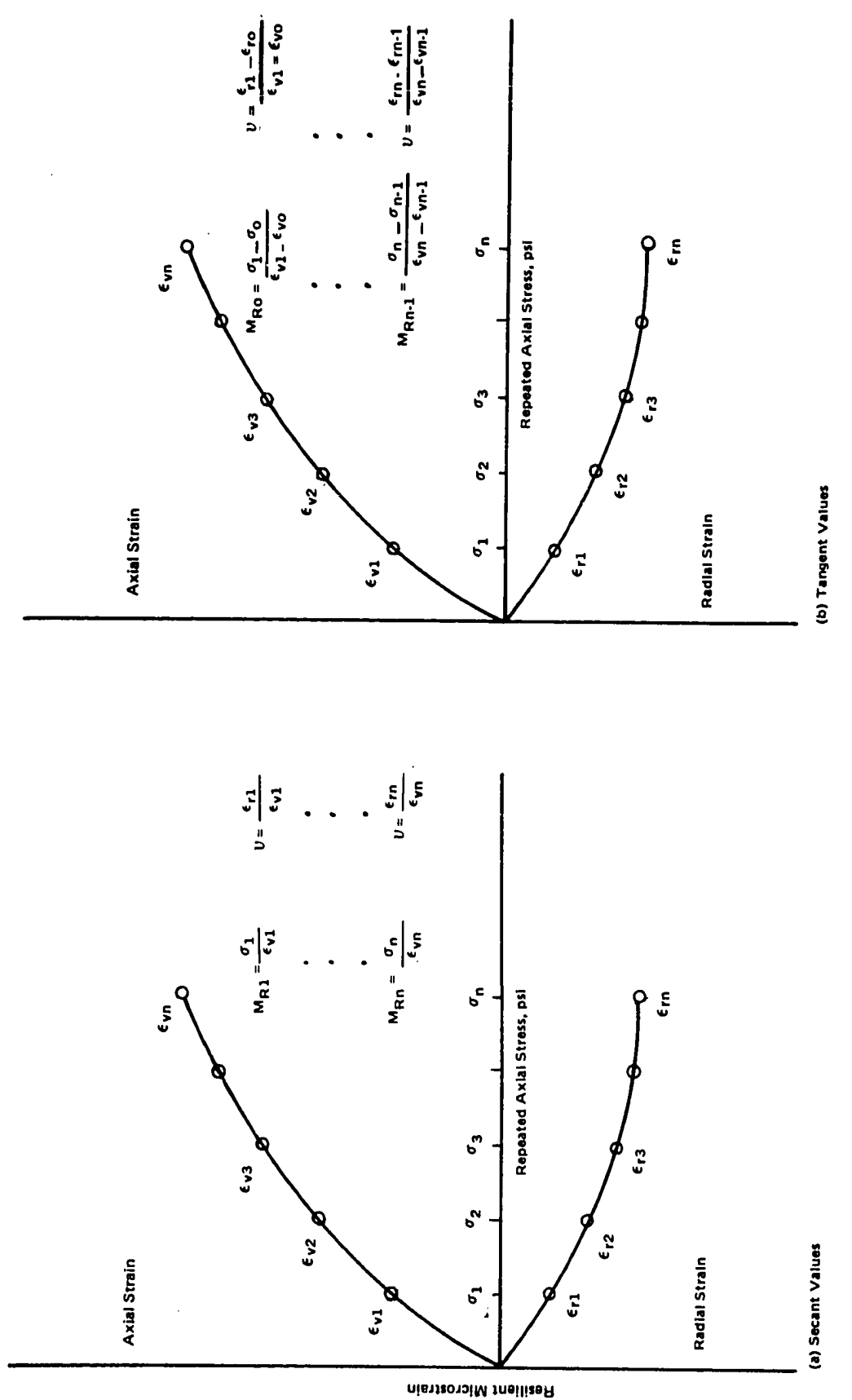


Figure 2.6  
Methods Employed for Computing Resilient Modulus and Poisson's Ratio (After Hicks (31)).

repeated-load triaxial tests on compacted specimens of typical base and subbase course aggregates.

#### 2.4.1 Stress History

One of the more important findings was reported by Hicks (31). Investigating the influence of stress sequence and number of repetitions on the resilient response, he subjected a series of specimens to 25,000 load applications and observed the change in resilient modulus and Poisson's ratio. In this test he used two stress sequences, one increasing and the other, decreasing. These stress sequences are illustrated in Figure 2.7. This series of tests revealed that, as long as the stresses were representative of those found in an actual pavement system, the resilient response of dry and partially saturated granular materials measured after 50 to 100 stress repetitions is an accurate representation of the response of that material when subjected to a complex stress history. In addition, he found that one specimen may be used to measure the resilient response at all stress levels and that these different stress levels could be applied in any sequence.

It has been found by others (51)(18) that the resilient modulus does depend somewhat on stress history. Herein, stress history is used to refer to the complex totality of stresses, normal and shear, that have been applied to a specimen in service or in the laboratory. Dehlen (18) proposed the following reasons for stress history effects on the resilient properties of granular materials: (a) progressive densification, (b) particle rearrangement, and (c) development and dissipation of pore pressures under repeated applications of stress. He also reported that the resilient response of sands and clays subjected to complex stress histories could be estimated adequately after 50 to 100 load repetitions.

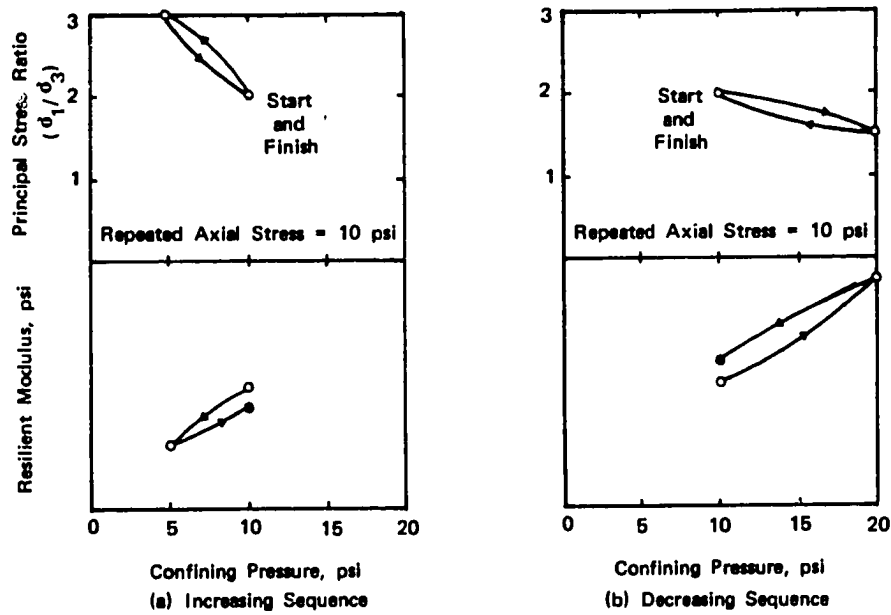


**Figure 2.7**  
Types of Stress Sequences used in Preliminary Experiments (After Hicks (31))

#### 2.4.2 Duration of Load and Frequency of Application

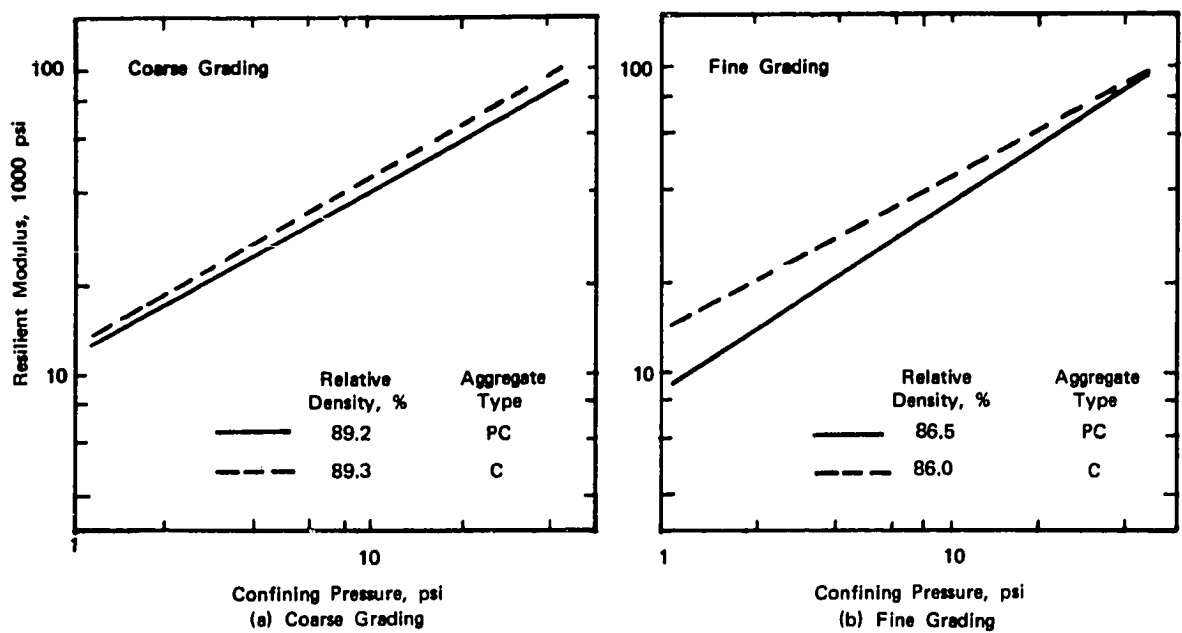
Seed, et al., (61) reported that the resilient modulus for sands increased from 23,000 psi to 27,000 psi as the duration of load decreased from 20 minutes to 1/3 second. Hicks conducted tests at stress durations of 0.1, 0.15 and 0.25 seconds and found no change in the resilient modulus or Poisson's ratio. Similarly, Mitry (48) found that the duration of load has no pronounced effect on the resilient modulus of sand and gravel. Although the resilient modulus generally increases with an increase in the frequency of load application (Seed, et al., 61), there is little effect for frequencies in the range of those expected to occur in a pavement structure. Consequently, most investigators have used testing frequencies on the order of 20 to 30 repetitions per minute (30)(31)(48) (61).

#### 2.4.3. Aggregate Type and Gradation

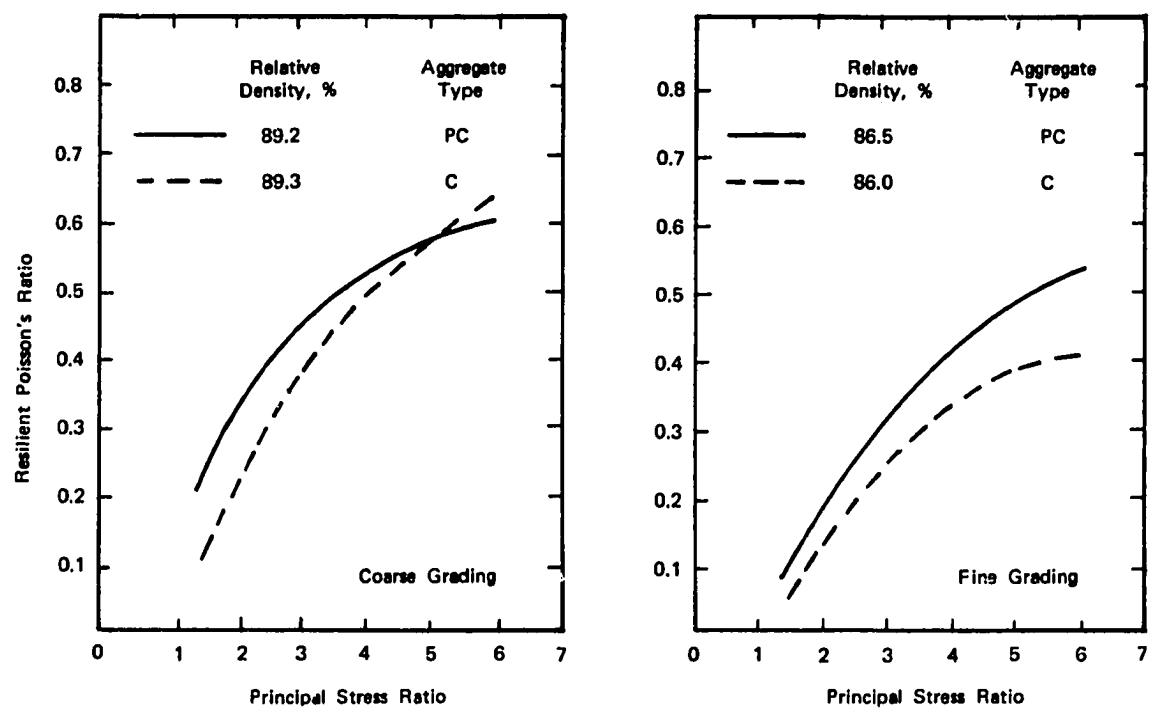
Hicks (31) found that the resilient modulus increased with increasing particle angularity or surface roughness and that Poisson's ratio generally was lower for the same conditions. Figure 2.8 shows the effect of aggregate types on the resilient modulus, and Figure 2.9 the effect on Poisson's ratio. For a given aggregate, varying the percentage finer than the number 200 sieve has a small effect on the resilient response of the material (31) for a range of fines from 2 to 10 per cent.

#### 2.4.4 Density

Previous test results from Hicks (31) indicate that the resilient modulus is greater for samples compacted to higher relative densities and subjected to identical stresses. Figures 2.10 and 2.11 graphically illustrate this effect and the effect of density on Poisson's ratio. It should be noted that the



**Figure 2.8**  
**Effect of Aggregate Type (Partially Crushed vs. Crushed) on the Relationship between Resilient Modulus and Confining Pressure ( $\sigma_3$ ). Dry Test Series.(After Hicks (31)).**



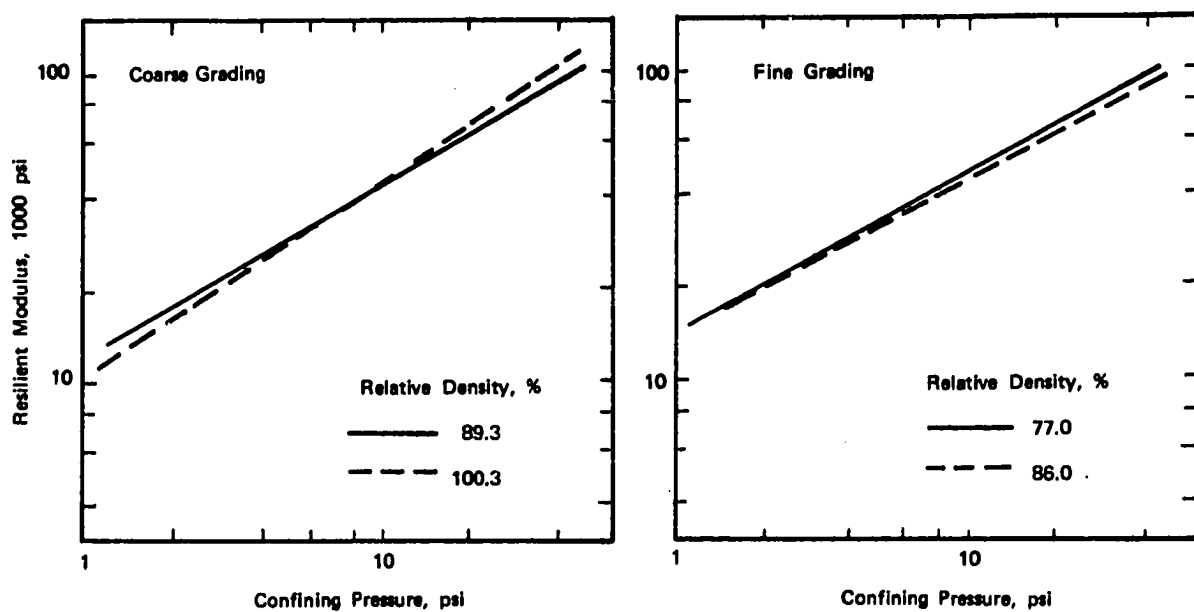


**Figure 2.10**  
Effect of Density on Relationship between Resilient Modulus and Confining Pressure ( $\sigma_3$ ).  
Crushed Aggregate. Dry Test Series. (After Hicks (31))

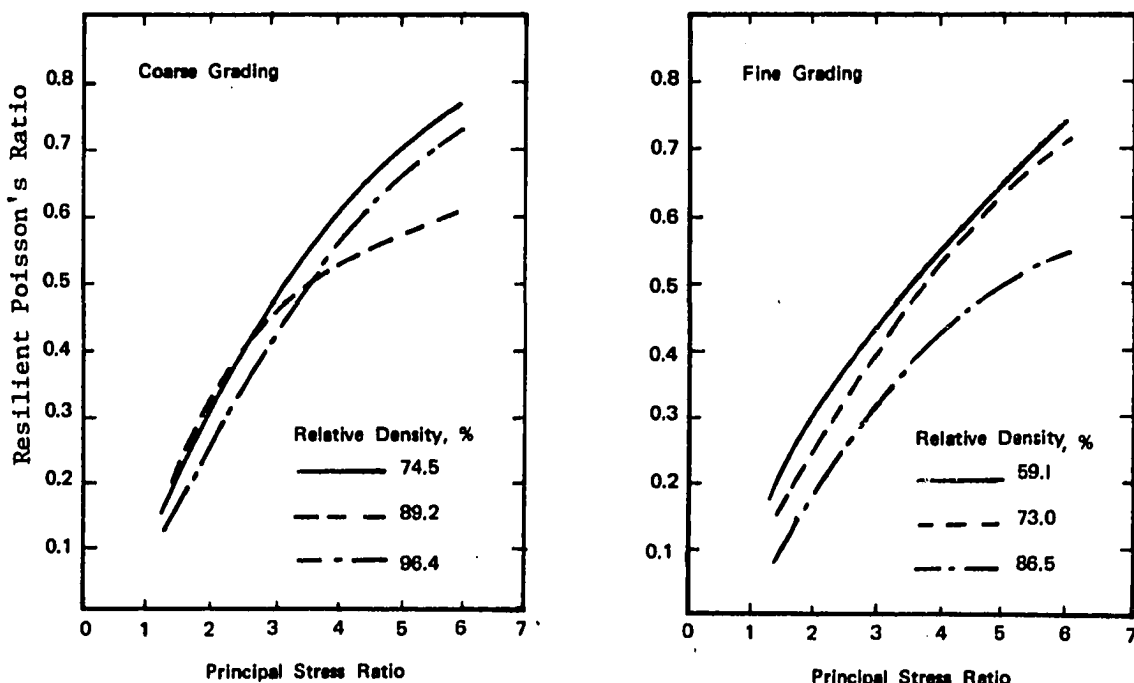


**Figure 2.11**  
Effect of Density on the Relationship between Resilient Poisson's Ratio and Principal Stress Ratio ( $\sigma_1/\sigma_3$ ). Partially Crushed Aggregate. Dry Test Series.  
(After Hicks (31)).

density effect is shown to be rather slight, particularly as compared with the effect of confining pressure. This is an encouraging development, since the density of base and subbase courses in a pavement structure will change during the pavement's service life.

#### 2.4.5 Degree of Saturation

Haynes and Yoder (30) found that the resilient moduli of gravels were more affected by an increase in the degree of saturation than were the moduli of crushed stone. Figure 2.12, from Reference 49, shows the relationship between  $K_1$  ( $M_r = K_1 \sigma_3^{K_2}$ ) and water content. Table 2.1 summarizes the influence of degree of saturation on the resilient properties of granular materials. In general, it can be stated that an increase in the percent saturation of a granular material has an adverse effect on its resilient properties. This reduction in stiffness is thought to be caused by the development of excess pore water pressure under repeated loads with an accompanying reduction in effective confining stress (Kasianchuk, 37). As regards Poisson's ratio, Hicks (31) found that, generally, it decreased as the degree of saturation increased, Figure 2.13.

O. O. Thompson (69) conducted repeated load tests on compacted granular specimens in which a pore pressure gage was installed. Such factors as gradation, density, and axial pressure were varied. Permanent and resilient deformations were recorded. Thompson's results confirmed the findings of Haynes and Yoder that at high degrees of saturation resilient and permanent deformations increased substantially and also the measured pore water pressures increased.

#### 2.4.6 Stress Level

Without exception, previous investigators have found that stress level has the most significant effect on the resilient properties of granular materials.

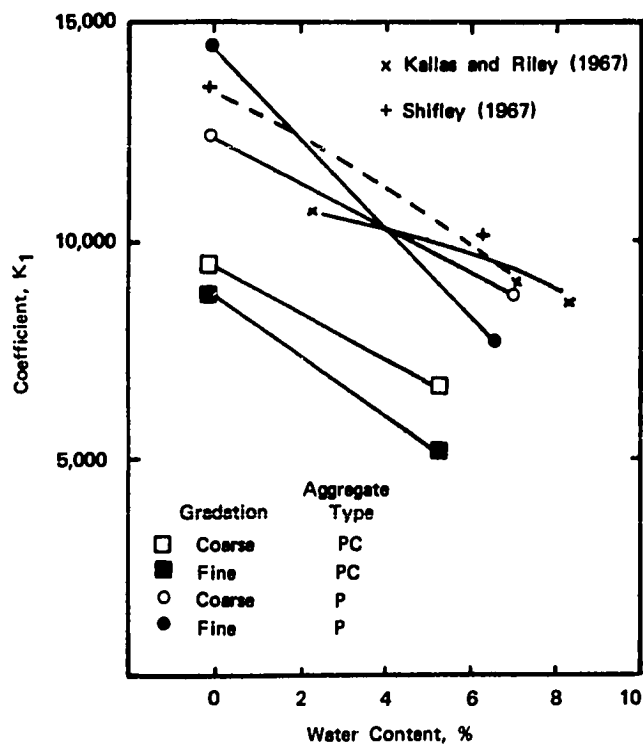


**Figure 2.12**  
Variation in Regression Constant ( $K_1$ )  $M_r = K_1 \sigma_3^{K_2}$   
with Water Content (After Hicks (31)).

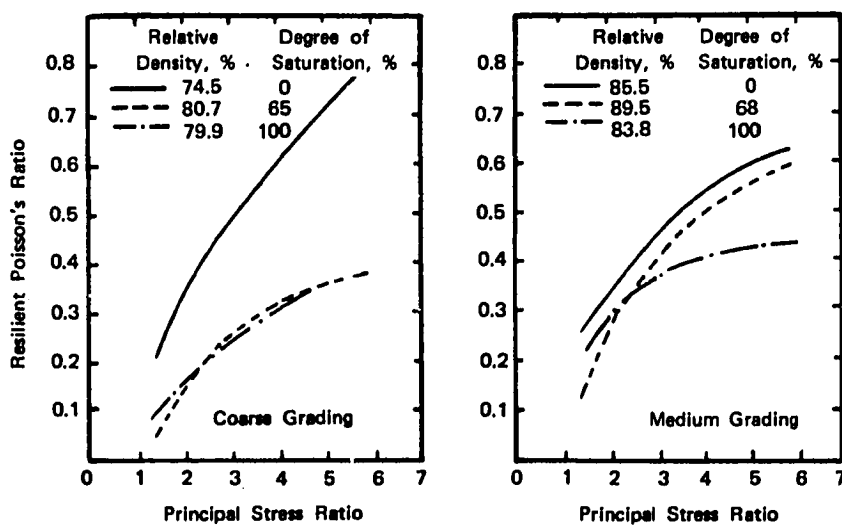


**Figure 2.13**  
Effect of Degree of Saturation on the Relationship between Resilient Poisson's Ratio and Principal Stress Ratio. Partially Crushed Aggregate. (After Hicks (31)).

TABLE 2.1  
INFLUENCE OF DEGREE OF SATURATION ON THE  
RESILIENT PROPERTIES OF GRANULAR BASE MATERIALS  
(After Hicks, Ref 31)

Percent Passing No. 200	Relative Density Percent	Degree of Saturation Percent	K <sub>1</sub>	K <sub>2</sub>	Mean Poisson's Ratio
<u>Partially Crushed Aggregate</u>					
3	80.0*	0	9,620	.57*	0.48*
	80.1	65	6,786	.59	0.25
	79.9	100	9,598	.55	0.25
5	85.5	0	10,252	.64	0.45
	89.5	68	6,937	.57	0.39
	83.8	100	9,430	.50	0.35
8	86.5	0	8,939	.61	0.34
	82.8	75	5,204	.64	0.50
	87.5	100	9,063	.52	0.25
<u>Crushed Aggregate</u>					
3	89.3	0	12,338	.55	0.41
	86.1	70	8,818	.57	0.29
5	87.0	0	13,435	.56	0.27
	87.3	81	9,032	.58	0.22
10	86.0	0	14,672	.50	0.23
	91.8	94	7,759	.57	0.45

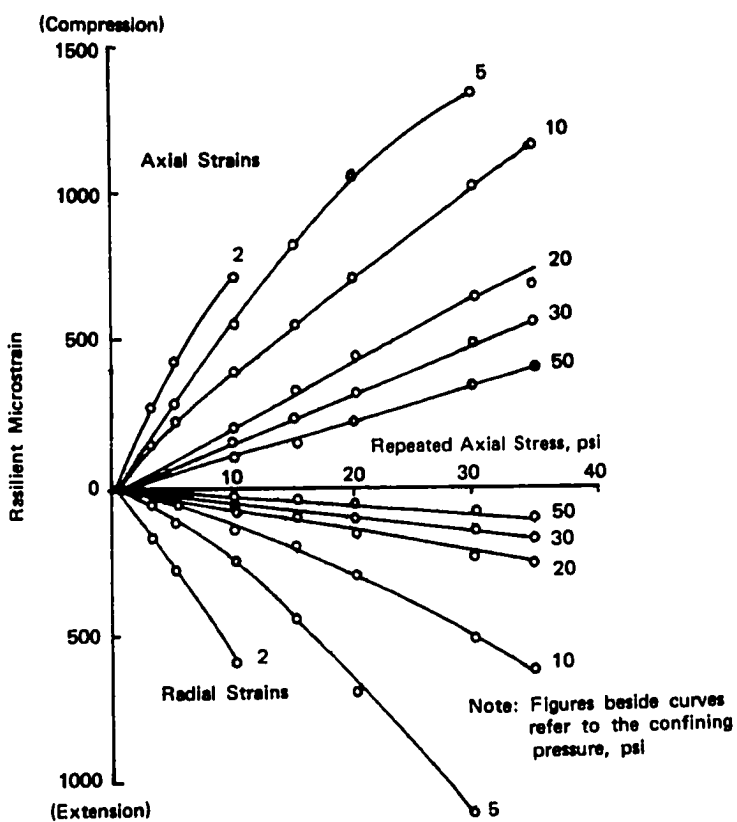
\* Values obtained using linear interpolation.

Figure 2.14 shows the influence of radial and axial stresses on recoverable strains. Several points are illustrated in this figure. First, the higher degree of nonlinearity at lower confining pressures is apparent. Second, the decrease in resilient strain with increase in confinement is also obvious. Third, it is shown that radial strains show a softening effect with increased axial stress, while axial strains exhibit a stiffening-type response.

Figure 2.15 shows the variation in resilient modulus with principal stress ratio (effect of increasing axial stress). The stiffening response shown for increasing ratios is also apparent in Figure 2.14, but less obviously. Hicks (31) found this stiffening effect to continue up to a principal stress ratio of 11, but Seed, et al.,(61), in testing similar materials at a stress ratio of 10, observed the specimen to fail in shear at about 1000 load repetitions. Hicks concluded that, as long as shear failure does not occur, this stiffening effect is a real aspect of the material and also that Equations 2.10, 2.11, and 2.12 are valid indicators of the resilient modulus and Poisson's ratio. Figures 2.16, 2.17 and 2.18 are typical representations of these equations.

## 2.5 Summary

The response of granular base and subbase course materials to repeated dynamic loadings such as those applied to a pavement section by moving traffic has been widely characterized by use of the resilience approach. The recoverable or "resilient" strains observed in these pavements to be caused by dynamic loads can be predicted through application of appropriate material parameters and standard elastic theory. It appears that, at present, the repeated-load triaxial test offers the most promising means of applying simulated field loading conditions to specimens of pavement components, and thus, this test procedure yields the most accurate estimation of a material's resilient modulus and Poisson's



**Figure 2.14**  
**Variation in Axial and Radial Strains with Axial Stress.**  
**(Partially Crushed Aggregate, Low Density, Coarse Grading, Dry )**  
**(After Hicks (31)).**

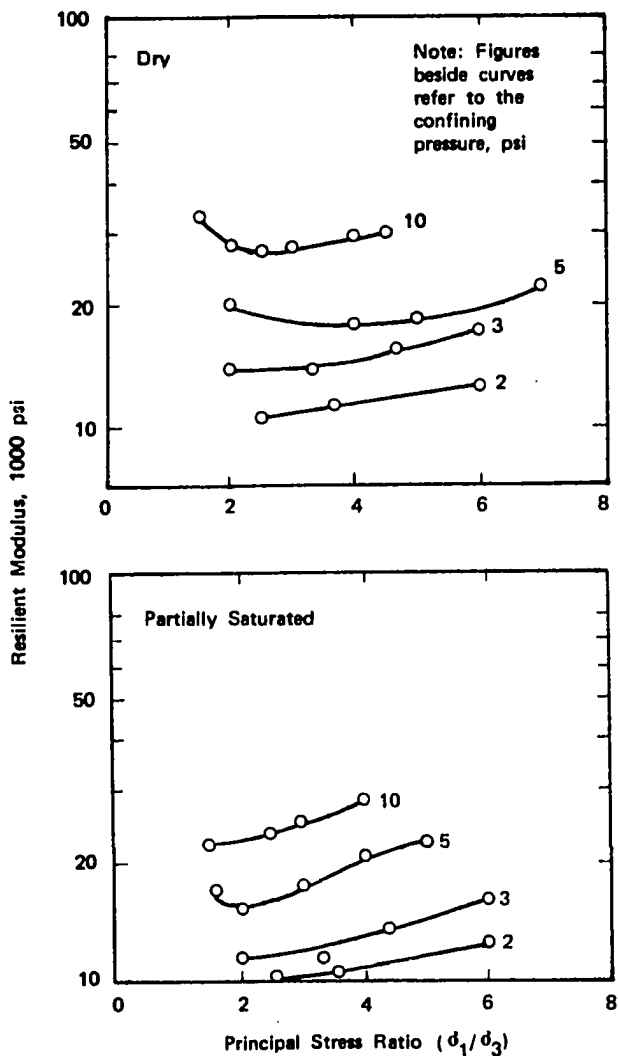


**Figure 2.15**  
**Variation in Secant Modulus with Principal Stress Ratio.**  
**(Partially Crushed Aggregate, Low Density, Coarse Grading.)**  
**(After Hicks (31)).**

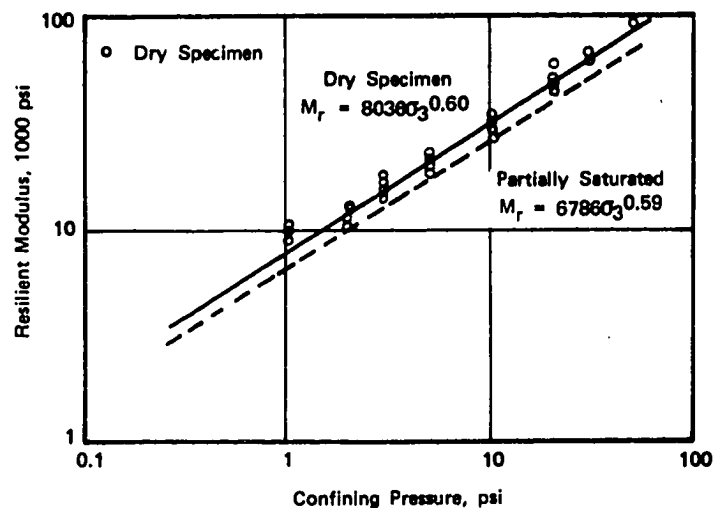


**Figure 2.16**  
**Variation in Secant Modulus with Confining Pressure.**  
**(Partially Crushed Aggregate, Low Density, Coarse Grading.) (After Hicks (31)).**

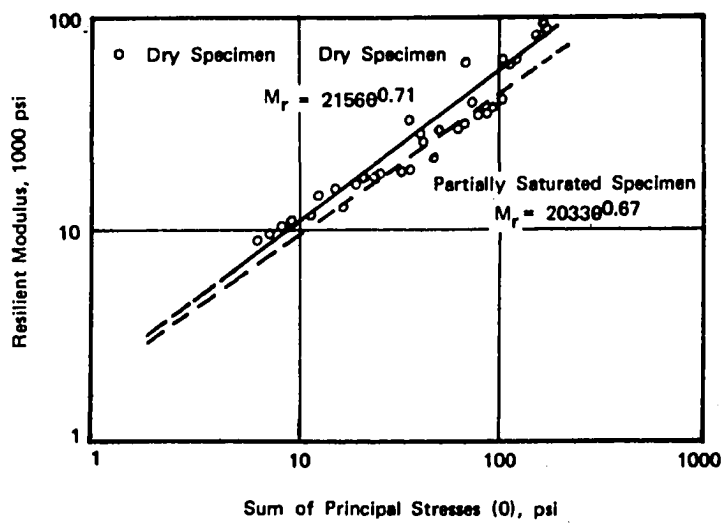


**Figure 2.17**  
**Variation in Secant Modulus with Sum of Principal Stresses**  
**(Partially Crushed Aggregate, Low Density, Coarse Grading)**  
**(After Hicks (32))**

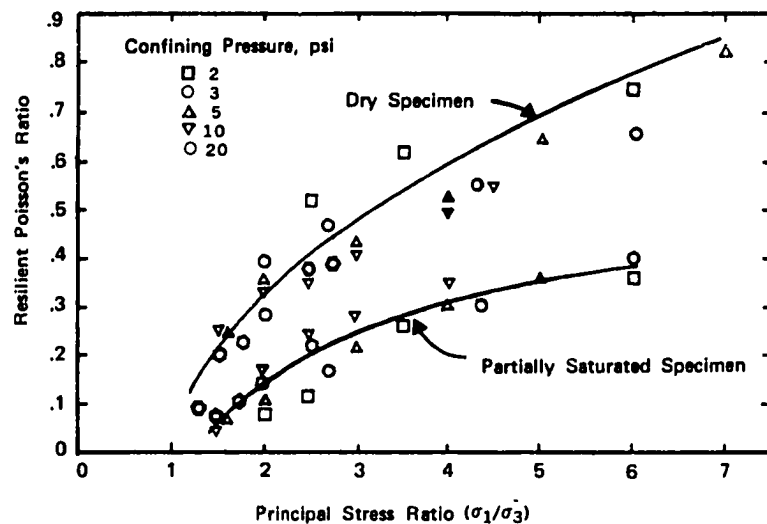


**Figure 2.18**  
Secant Poisson's Ratio as a Function of Principal Stress Ratio. (Partially Crushed Aggregate, Low Density, Coarse Grading.) (After Hicks (31))

ratio. The highly stress-dependent nature of these parameters necessitates consideration of the state of stress throughout a granular layer of a pavement structure when attempting to predict transient deformations. Figure 2.16 shows the drastic increase in resilient modulus that occurs when the confining pressure is increased from 1 to 10 psi.

In addition, it has shown that such factors as degree of saturation, aggregate type, gradation, and density affect the resilient properties of granular materials, but much less significantly than does the state of stress. Table 2.2 summarizes the results of previous repeated-load triaxial tests conducted to ascertain the factors affecting the resilient properties of granular specimens.

Despite the knowledge of the heavy influence of confining stresses on the resilient parameters, there have been no published results of tests where lateral stresses were varied simultaneously with the axial stress. Since this condition is representative of the state of stress occurring in an actual pavement structure subjected to moving wheel loads, the purpose of this research was to simulate field conditions by means of repeated-load, variable-confining-pressure, triaxial tests in the laboratory. Chapter 3 describes the procedures used to obtain the axial and radial stress pulses which were applied to the granular specimens.

TABLE 2.2  
 SUMMARY OF REPEATED-LOAD TRIAXIAL TESTS TO EVALUATE THE RESILIENT  
 PROPERTIES OF GRANULAR MATERIALS  
 (After Seed, et al., (61) and Hicks (31))

Researcher	Material	Resilient Modulus, psi	Comments
1. Seed and Chan	Silty Sand	21,300 to 27,300	Varied frequency and duration of load.
2. Haynes and Yoder	Gravel and Crushed Stone	28,000 to 63,000	Varied moisture content and gradation
3. Biarez	Rounded Aggregate	16,700 to 54,500	Varied stress levels and void ratio.
4. Trollope, Lee and Morris	Poorly graded Dry Sand	35,000 to 95,000	Varied stress levels, dry density, rate of deformation.
5. Dunlap	Well graded Aggregate	30,000 to 160,000	Varied stress levels.
6. Mitry	Dry Gravel	7,000 $\sigma_3^{0.55}$ 1,900 $\theta_{61}$	Varied Stress levels.
7. Schiffley	Crushed Gravel	13,000 $\sigma_3^{0.50}$ to 9,000 $\sigma_3^{0.50}$	Varied moisture content
8. Kasiianchuk	Aggregate Base Aggregate Subbase	3,830 $\theta^{0.53}$ 2,900 $\theta^{0.47}$	Varied stress levels.
9. Hicks and Finn	Aggregate Base	5,400 $\theta^{0.50}$ to 21,000 $\theta^{0.50}$	Varied moisture content.

### Chapter 3

#### STRESS DISTRIBUTIONS IN FLEXIBLE PAVEMENTS AND EFFECTS OF NON-LINEAR MATERIAL PROPERTIES

The purpose of this chapter is to discuss the procedures leading to the development of the stress pulses that were applied by the triaxial apparatus to the granular specimens. Of the many available models for analysis of pavement systems, three have been applied most often to flexible-type pavements. These three models, with their accompanying assumptions are described herein:

##### 3.1 Surface Traction on a Semi-Infinite Elastic Halfspace

###### 3.1.1 Solution for Stresses and Displacements

The problem of a point load applied to a linearly elastic, homogeneous, halfspace was solved by Boussinesq in 1885. Hence, the solution for stresses and displacements in such a halfspace loaded at the surface is often termed the "problem of Boussinesq". Boussinesq's results may be expanded to solve for stresses and displacements within soil masses subjected to uniformly distributed surface loadings. Equations 3.1 have been widely used for this purpose.

$$\begin{aligned}\sigma_z &= p \left[ 1 - \frac{z^3}{(a^2 + z^2)^{3/2}} \right] \\ \sigma_r &= p/2 \left[ 1 + 2\nu - \frac{2(1+\nu)z}{(a^2 + z^2)^{1/2}} + \frac{z^3}{(a^2 + z^2)^{3/2}} \right] \\ w_z &= p/E \left[ 2(1-\nu^2) (a^2 + z^2)^{1/2} - \frac{(1+\nu)z^2}{(a^2 + z^2)^{1/2}} + (\nu + 2\nu^2 - 1) z \right]\end{aligned}\quad (3.1)$$

where,  $\nu$  = Poisson's ratio

$p$  = distributed surface load

$a$  = load radius at surface

$z$  = depth below the surface

$\sigma_z$  = vertical stress at depth  $z$

$\sigma_r$  = radial stress at depth  $z$

$w_z$  = vertical displacement at depth  $z$

$E$  = Young's modulus

In 1916 Terazawa (66) extended Boussinesq's solution by use of the stress function concept, which forms the basis for the layered-elastic model described in the next section.

Newmark (56) developed charts for the solution of stresses in elastic masses from the equations of Boussinesq. Foster and Ahlvin (27) developed curves for the solution of vertical, horizontal, and shear stresses in an elastic mass due to circular loaded plates. These curves allow for stress computations at any depth and at any offset distance from the center of the loaded area.

### 3.1.2 Advantages and Limitations of the Boussinesq Solution

Although the solution of the Boussinesq problem has the advantage of permitting quick and easy determination of the state of stress within the mass, it is nevertheless not well suited for application to flexible pavement systems. The requirement that the halfspace be infinite in horizontal extent precludes the use of this model in solving for stresses and displacements resulting from wheel loads at the edge of a pavement. In addition, because flexible pavement systems are not made up of linearly elastic, homogeneous materials, the Boussinesq solution fails to take account of the changes in the pattern of stresses as effected by the varying material properties from layer to layer. In fact, this model usually overestimates the values of vertical stresses throughout the pavement structure and the upper part of the subgrade, thus negating the load-spreading and stress-reducing properties of the stiffer upper layers.

### 3.2 Elastic Layered System

#### 3.2.1 Development

The solution for stresses and displacements in a symmetrically-loaded elastic layered system, Figure 3.1a, was proposed by Burmister in 1943 (13). The following assumptions were made:

1. Each layer is composed of linearly elastic, isotropic, homogeneous material.
2. All layers are weightless. The upper layers are infinite in horizontal extent, but of finite thickness. The bottom layer is infinite in extent horizontally and vertically downward.
3. The surface of the top layer is free of normal and shear stresses outside the loaded area. The load consists of symmetrically applied normal stresses. The displacements and stresses approach zero as the depth in the lower layer approaches infinity.
4. The layers are in continuous contact. That is, normal and shear stresses as well as vertical and horizontal displacements are equal on either side of the interfaces. It should be noted that this requirement allows a discontinuity in radial stresses across an interface, since for a given equality of strains the stresses will be determined by the material parameters.

In Figure 3.1b  $u$ ,  $v$ , and  $w$  are defined as displacements in the  $r$ ,  $\theta$  and  $z$  directions, respectively. As a consequence of the assumed symmetry of loading and deformations, the shear stresses  $\tau_{r\theta}$  and  $\tau_{\theta z}$  and the tangential displacement component  $v$ , are identically zero. The solutions to boundary value problems in the linear theory of elasticity require that the equations of equilibrium and compatibility be satisfied. This requirement can be facilitated by defining stress functions  $\phi_i$  for each layer so that:

$$\nabla^2 \nabla^2 \phi_1 = 0$$

where,  $\nabla^2$  is the Laplace Operator:

$$\nabla^2 = \frac{\partial^2}{\partial r^2} + \frac{1}{r} \frac{\partial}{\partial r} + \frac{\partial^2}{\partial z^2} \quad (3.2)$$

The stress equations of equilibrium can be written in terms of the assumed stress function:

$$\begin{aligned} \sigma_r &= \frac{\partial}{\partial z} [\nu \nabla^2 \phi - \frac{\partial^2 \phi}{\partial r^2}] \\ \sigma_\theta &= \frac{\partial}{\partial z} [\nu \nabla^2 \phi - \frac{1}{r} \frac{\partial \phi}{\partial r}] \\ \sigma_z &= \frac{\partial}{\partial r} [\nu \nabla^2 \phi - \frac{\partial^2 \phi}{\partial z^2}] \\ \tau_{rz} &= \frac{\partial}{\partial r} [(1-\nu) \nabla^2 \phi - \frac{\partial^2 \phi}{\partial z^2}] \end{aligned} \quad (3.3)$$

The displacements can be expressed as follows:

$$\begin{aligned} w &= \frac{1+\nu}{E} [(1-2\nu) \nabla^2 \phi + \frac{\partial^2 \phi}{\partial r^2} + \frac{1}{r} \frac{\partial \phi}{\partial r}] \\ u &= \frac{1+\nu}{E} [-\frac{\partial^2 \phi}{\partial r \partial z}] \end{aligned} \quad (3.4)$$

The following stress function has been found to satisfy the necessary conditions:

$$\phi_i = J_0(mr) [ (A_i + B_i z)e^{mz} + (C_i + D_i z)e^{-mz} ] \quad (3.5)$$

In this equation  $J_0(mr)$  is the Bessel function of first kind and zero order,  $m$  is a dimensionless parameter of integration, and the  $i$  subscript refers to the  $i$  th layer. The constants  $A_i$ ,  $B_i$ ,  $C_i$  and  $D_i$  are evaluated from the boundary and interface conditions.

For the bottom layer, the requirement that stresses and displacements vanish at infinity leads to this stress function:

$$\phi_b = J_0(mr) [(C_b + D_b z) e^{-mz}] \quad (3.6)$$

For the special case of a single layer system (problem of Boussinesq), Equation 3.6 is the stress function utilized by Terazawa (66).

Burmister (13) presented the theory for 2 and 3 layer systems but did not solve for specific values of stress. Computer solutions for layered systems have been developed by several groups. Jones (36) solved the 3 layer problem and presented tables of coefficients by which the stresses at the interfaces may be computed in terms of the applied load. These coefficients were calculated for various layer modular and thickness ratios. Jones' solution was applicable to the problem defined by Burmister's boundary and interface conditions and Poisson's ratio equal to 0.5. Peattie (58) presented Jones' results in graphical form on three-dimensional plots.

Burmister's work has been extended by Schiffman (63) to include surface shears and general asymmetry. He introduced a second stress function,  $\Psi$ , into the equations of equilibrium and solved by means of Hankel transforms.

Charyulu and Sheeler (15) presented a computer solution for any arbitrary number of layers and for different interface conditions. Specifically they assumed a parabolic surface stress distribution instead of circular. In addition, they permitted different radial displacements on either side of an interface. As a result of this disparity in horizontal displacement, shear stresses on either side of an interface were defined as being equal and as being a function of the relative displacement.

Peutz, Van Kempen, and Jones (60) developed a computer solution for stresses and displacements within multilayered, elastic systems induced by one or more

vertical axisymmetric surface loads. This solution permits the use of two interface conditions. The rough interface condition assumes no slip between adjacent layers, and thus, requires that shear stress and radial displacement be constant across the interface. The smoother interface condition allows the layers to slip over each other without any shear stresses.

### 3.2.2 Advantages and Limitations of the Layered Elastic Solution

The layered elastic model has the advantage that one may divide a pavement cross section into any number of layers and specify different material parameters for each layer. In this manner, an investigator can determine the effects on derived stresses and displacements of placing stiffer layers beneath less stiff layers (inverted sections). Also, various interface conditions can be simulated between layers.

Although possessing advantages over the elastic halfspace model, the elastic layered model suffers from several deficiencies. Because of the assumed symmetry of the model, it cannot be applied to pavement structures that are limited in extent. Here again, the problem of edge loads cannot be examined. As pointed out by Barksdale and Hicks (11) the effects of vibrations are neglected in the layered elastic solution. This omission could be significant for unbound granular materials which would densify due to traffic-induced vibrations and lead to rutting.

Probably the most serious deficiency of this approach lies in its assumption that each layer is linearly elastic, isotropic, and homogeneous. Although this deficiency is less pronounced for portland cement concrete and bituminous concrete layers, which behave almost as linearly elastic materials over the range of stresses and rate of stress application encountered in most pavement structures, it may be more significant for other pavement components, particularly unbound

granular materials. The response to load of these materials may vary from slightly nonlinear to significantly nonlinear, depending upon such factors as stress level, position in the structure, and the nature of the overlying layers. For example, Duncan, Monismith, and Wilson (23) found that the resilient modulus of the granular base course was less affected by the surface loading with a stiffer surface course than with a less stiff asphalt concrete layer. In Chapter 2 it was reported that the modulus of a granular material is a function of the state of stress in the material.

To account for this stress dependency of the modulus, Huang (34) has developed an iterative computer solution for the layered elastic problem which employs the boundary and continuity conditions proposed by Burmister. The moduli for the various layers are derived from the model suggested by Barkan (7),  $E = E_0(1 + \beta\theta)$ , which has been discussed previously. In this solution the modulus for an entire layer is computed from the stresses at the center of the layer. Huang's results indicate that the stresses computed for highly non-linear materials may be as much as 30 per cent different from those computed by linear theory. However, linear theory will not account for the stress-dependent modulus, and, hence, significantly overestimate deflections throughout the system.

The Chev 5L iterative layered elastic solution, available from the University of California at Berkeley, also takes account of the stress-dependent material properties of pavement components. In this program the modulus of granular materials is computed as a function of the first stress invariant and the modulus of cohesive materials is described as a function of the principal stress difference,  $\sigma_1 - \sigma_3$ . The surface load is applied in one step and the program performs successive iterations until the moduli from step to step differ by less than a prescribed value. Although the modulus can vary only in the vertical direction (i.e., the modulus is constant within any one layer), such an approach is a

reasonable and inexpensive method of accounting for nonlinear material properties.

### 3.3 Finite Element Analysis

#### 3.3.1 Development

The finite element technique of analysis, as applied to pavement systems, possesses many advantages over previously discussed techniques; although it, too, has certain limitations. The purpose of this section is to briefly describe the manner in which this type of solution may be applied to pavement systems and to mention the advantages and limitations inherent in the process.

The first step is to reduce the continuum to a system of discrete bodies. In the analysis of layered systems this is done by dividing the continuous structure into an assemblage of axisymmetric elements, which are interconnected at circumferential joints. This characterization is illustrated in Figure 3.2. Equilibrium equations, in terms of nodal point displacements are solved by the direct stiffness method:

$$[Q] = [K] [U] \quad (3.7)$$

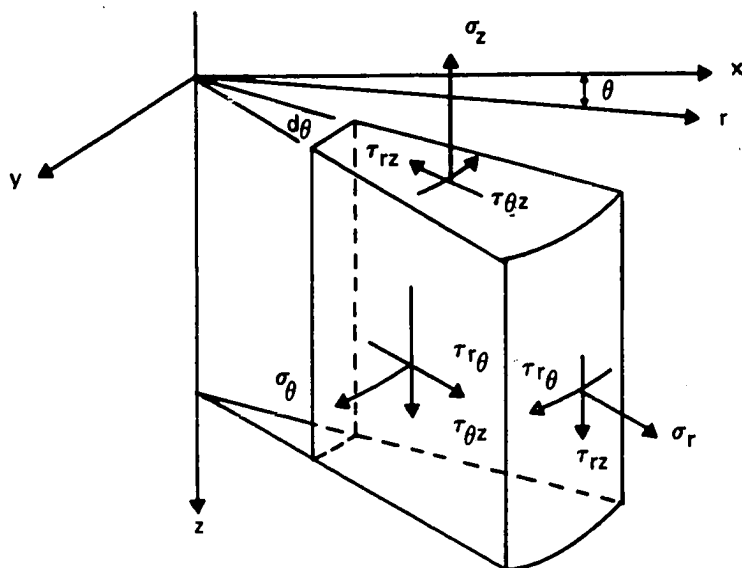
where,  $[Q]$  is the matrix of concentrated node point loads,

$[K]$  is the stiffness matrix

$[U]$  is the matrix of node point displacements in the  $r-z$  plane.

The form of the displacement field within each element must be assumed. Most often this is done by defining displacements at any point  $(r,z)$  within an element,  $m$ , as linear functions of position; this condition assures continuity between elements. The displacement field may then be stated in terms of the nodal point displacement,  $\{U_n\}$ . Strain at any point within an element is related to displacements by:

(a) Coordinate System and Differential Element



(b) Layered System

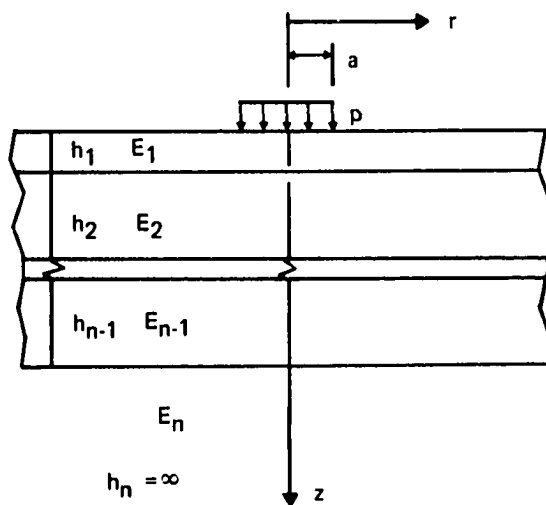
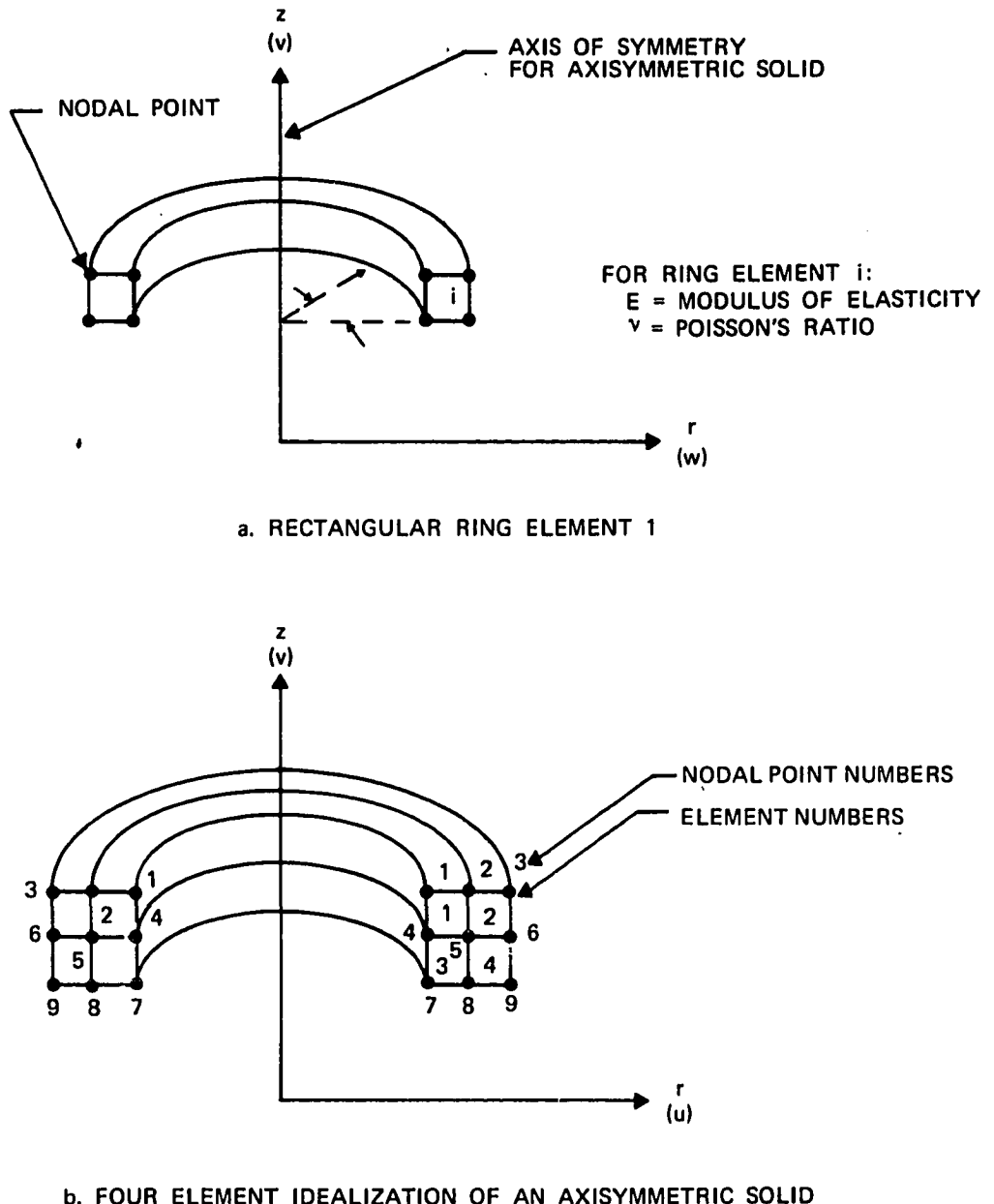


Figure 3.1  
Typical Layered System and Differential Element



**Figure 3.2**  
Notation Used in the Finite Element Idealization of an  
Axisymmetric Solid (After Barksdale (8))

$$\begin{Bmatrix} \epsilon_z \\ \epsilon_r \\ \epsilon_\theta \\ \gamma_{rz} \end{Bmatrix} = \begin{Bmatrix} \partial U_z / \partial z \\ \partial U_r / \partial r \\ U_r / r \\ \partial U_r / \partial r + \frac{\partial U_z}{\partial r} \end{Bmatrix} \quad (3.8)$$

Substituting the displacement function:

$$\{\epsilon\} = [B] \{U\} \quad (3.9)$$

where,  $\{\epsilon\}$  = strain vector

$[B]$  = coefficient matrix relating strain to nodal displacement.

$\{U\}$  = nodal point displacement vector

The relationship between stress and strain at a point in an element may be expressed in terms of an elasticity matrix.

$$\{\sigma\} = [D] \{\epsilon\} \quad (3.10)$$

where,  $\{\sigma\}$  = stress vector

$[D]$  = elasticity matrix

$\{\epsilon\}$  = strain vector

For a linear, isotropic material Equation 3.10 may be stated:

$$\begin{Bmatrix} \sigma_z \\ \sigma_r \\ \sigma_\theta \\ \tau_{rz} \end{Bmatrix} = \frac{E(1-\nu)}{(1+\nu)(1-2\nu)} \begin{Bmatrix} 1 & \frac{\nu}{1-\nu} & \frac{\nu}{1-\nu} & 0 \\ \frac{\nu}{1-\nu} & 1 & \frac{\nu}{1-\nu} & 0 \\ \frac{\nu}{1-\nu} & \frac{\nu}{1-\nu} & 1 & 0 \\ 0 & 0 & 0 & \frac{1-2\nu}{2(1-\nu)} \end{Bmatrix} \begin{Bmatrix} \epsilon_z \\ \epsilon_r \\ \epsilon_\theta \\ \gamma_{rz} \end{Bmatrix} \quad (3.11)$$

The stiffness matrix for element  $m$  may now be formed. Wilson (73) defines it in this manner:

$$[K^m] = \int_{\text{vol}} [B]^T [D] [B] dv \quad (3.12)$$

where, the integral must be integrated over the entire volume of the ring element. Wilson further defines the stiffness matrix for the entire assemblage of  $m$  elements as:

$$[K] = \sum_{m=1}^M [K^m] \quad (3.13)$$

In developing the load vector,  $[Q]$ , concentrated loads at the node points may be placed directly in the proper position. However, distributed surface tractions must first be transformed into equivalent concentrated nodal loads. One method of accomplishing this transformation is to replace the surface tractions with nodal loads that accomplish the same amount of work as the node points are displaced.

Once the stiffness and load matrices are formed, Equation 3.7 may be solved for the node point displacements. Then Equation 3.9 may be solved for strains and Equation 3.10 will yield the stresses in each element.

### 3.3.2 Advantages and Limitations of Finite Element Analysis

The finite element method has numerous advantages as compared with other numerical techniques. It is completely general as regards material properties. Bodies composed of different materials are easily specified. Anisotropic materials may be handled by specifying the proper coefficients in the elasticity matrix. Displacement or stress boundary conditions may be specified at any node points. Errors associated with the assumed linearity of the displacement fields may

be reduced by decreasing the sizes of elements. Possibly the greatest benefit from using the method stems from its ability to handle non-linear materials. Duncan, Monismith and Wilson (23) utilize an iterative scheme, in which the entire surface load is applied in one step and the modulus for each iteration is calculated as some function (depending on the type of material) of the state of stress calculated from the previous iteration. The process continues until the calculated moduli for successive iterations differ by less than a prescribed value. Barksdale (8) developed incremental analytical techniques in which the material stress-strain curve is broken into a series of tangent sections. The surface load is applied in increments and each material modulus is determined from the slope of the tangent at the appropriate stress level.

The flexibility of the finite element model for predicting stresses and displacements within pavement structures is evident from test results published in "Basic Properties of Pavement Components" (49) by Monismith, Hicks, and Salam. In this study the measured results of plate load tests on a prototype highway flexible pavement were compared with results computed by the following three analytical procedures;

1. An iterative multilayer elastic solution in which the modulus was permitted to vary with depth; constant Poisson's ratio for each layer.
2. Incremental finite element solution which permitted horizontal and vertical variation of moduli; constant Poisson's ratio for each material.
3. Incremental finite element solution in which moduli and Poisson's ratio were specified as functions of stress.

It was found that the elastic layered solution overestimated resilient plate deflections, but that both finite element solutions yielded plate deflections that agreed well with measured values. Overestimation of surface deflections by the elastic-layered solution may be brought about by two factors. The first

is the assumed infinite depth of the lower layer. Even though the computed strains at great depth are small, when summed over such a large distance, they can lead to an exaggerated estimate of deflections. The second factor is that the load was assumed to be applied to the layered system through a flexible plate, whereas the plate configuration in a finite element solution may be specified as part of the problem by describing the geometry and material parameters of the plate. The latter procedure appears to be a better approximation of field loading conditions. However, if the deflections computed by the elastic layered solution are arbitrarily reduced by about 20 per cent (as has been noted to be a reasonable correction for a flexible plate (49) ) then good agreement among all three solutions results. Figure 3.3 shows measured and computed surface deflections for 8- and 12- inch plates.

The same study compared calculated and measured values of the vertical stress in the subgrade. While all three computer solutions gave reasonably good agreement with measured values, the finite element technique appears to compare more favorably (Figure 3.4). In all cases the finite element solution yielded higher values for subgrade stresses.

Limitations associated with the finite element model are primarily related to the assumed condition of axial symmetry. This condition restricts the use of the model to static loads on systems of great horizontal extent. Here again is a solution that will not handle loads applied along a pavement edge. In addition, dynamic effects are not considered.

Although this form of numerical approximation becomes more accurate as the size of each element is reduced, the number of elements involved increases with an accompanying increase in the amount of computer storage and computation time required. Thus, computer costs are quite large as compared with those incurred by the elastic layered model.

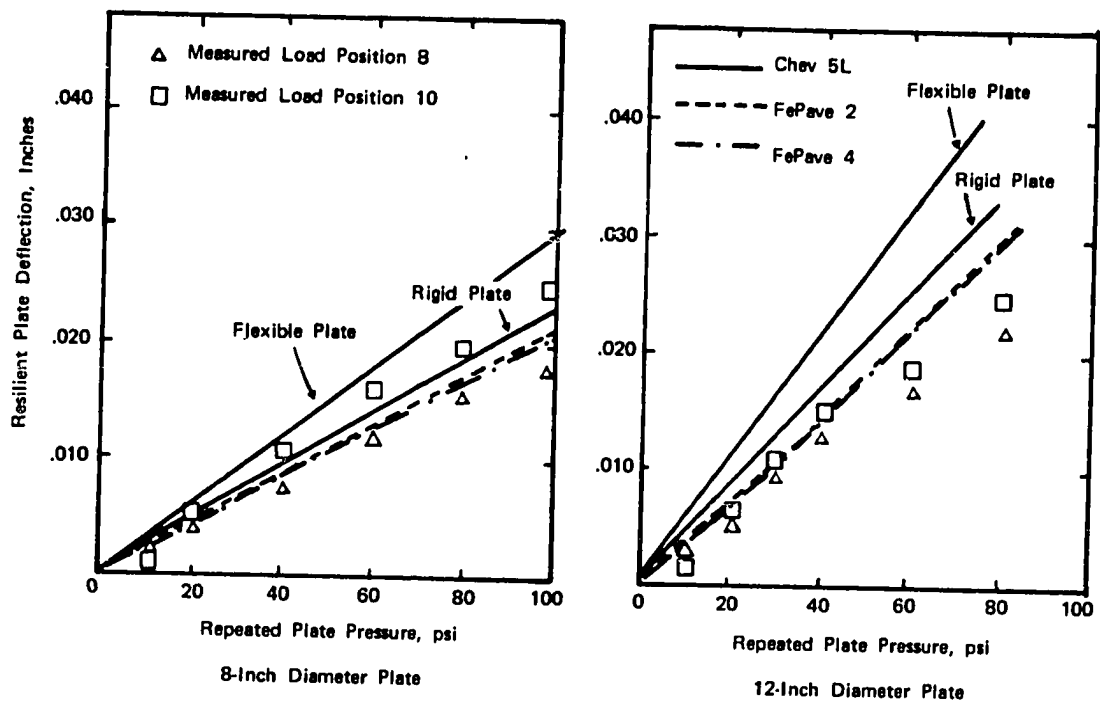


**Figure 3.3**  
**Computed and Measured Surface Deflections for Three Layer System.**  
**Base Partially Saturated (Fe Pave 2 and 4 are Finite Element Solutions)**  
**(After Monismith, et al. (49))**

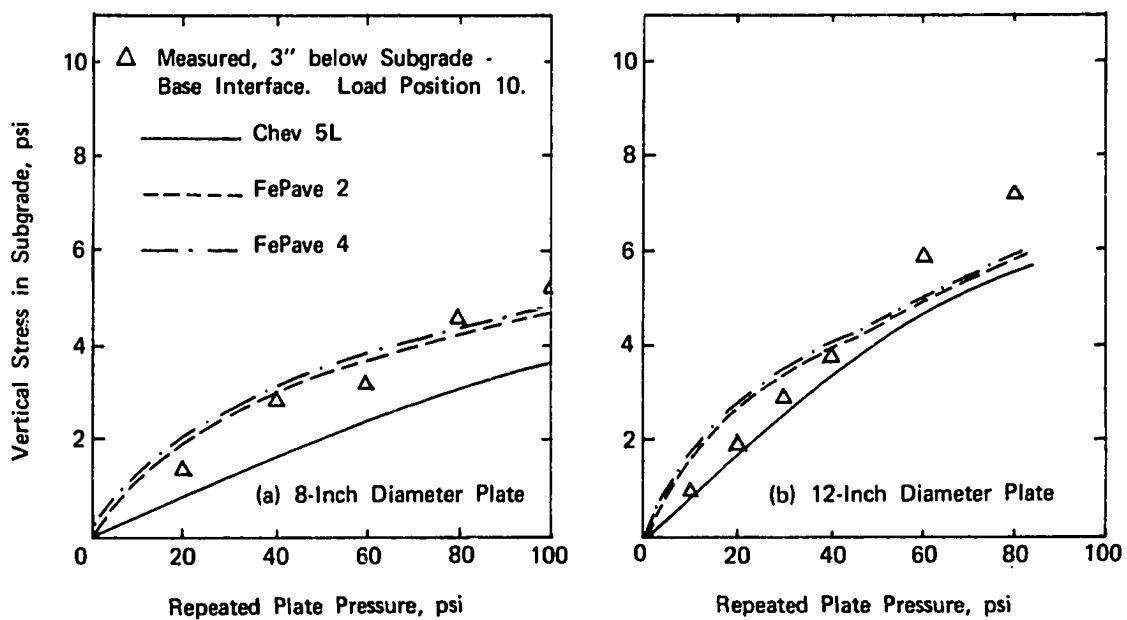


**Figure 3.4**  
**Computed and Measured Vertical Stress in Subgrade for Three Layer System. Plate Load at Top of Surface. Base Partially Saturated.**  
**(Fe Pave 2 and 4 are Finite Element Solutions) (After Monismith, et al. (49))**

A further limitation of this method, a limitation shared by any model that represents granular materials as an elastic continuum, is that there is no provision for slip along interparticle surfaces of contact. However, at present no model has been developed which can be readily applied to pavement systems and which incorporates such a feature.

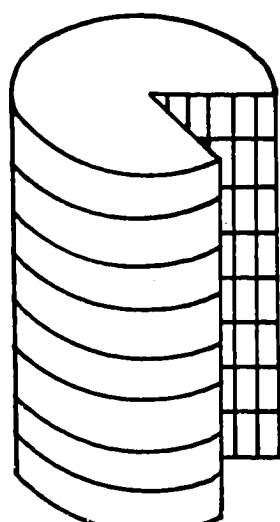
It is felt that for use as a research tool, the advantages of the finite element model far outweigh its disadvantages. Hence, an incremental, finite element solution was selected for use in this project. The following section describes this model and the pavement sections which were analyzed.

### 3.4 Finite Element Analysis of Pavement Sections

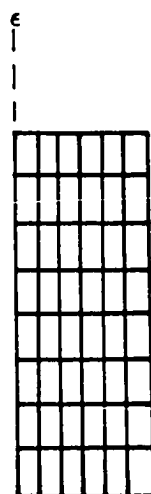
The pavement structures to be analyzed were idealized as cylinders as shown in Figure 3.5\*. Rectangular elements were specified. To assure the compatibility of displacements (i.e., no gaps develop in the deformed structure), linear displacement fields were assumed within each element. Output consisted of radial and vertical displacement at the four exterior nodes of each rectangle and the complete state of stress at the center of each rectangle. Input to the program included the locations of vertical and horizontal element boundaries, surface load and load radius, number of increments, layer thicknesses, and material properties. Specified material properties included the unit weight, coefficient of earth pressure at rest, Poisson's ratio, and resilient modulus. Poisson's ratio is input as a constant for each material, but the resilient moduli may be specified in a number of ways:

---

\* The finite element model used in this study was developed by E. L. Wilson at the University of California at Berkeley and subsequently modified by J. M. Duncan, also at California, so as to (a) utilize elements bounded by horizontal and vertical lines, (b) handle nonlinear materials and (c) apply the surface load in a series of increments.



Oblique View



Half - Section

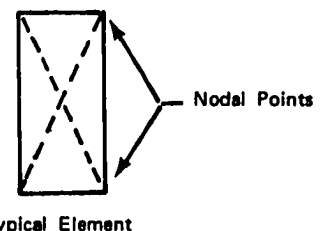


**Figure 3.5**  
Finite Element Idealization of a Cylinder

1. The material may be considered to be linear elastic, with a constant modulus.

2. For materials with temperature-dependent moduli, values of temperature and the associated modulus may be input for various points. The program interpolates for the modulus between the specified points.

3. The modulus may be input as a function of the confining pressure:

$$M_r = K_1 \sigma_3^{K_2} \quad (3.14)$$

4. The modulus may be defined as a function of principal stress difference:

$$M_r = K_2 + K_3 [K_1 - (\sigma_1 - \sigma_3)] \quad K_1 > (\sigma_1 - \sigma_3) \quad (3.15a)$$

$$M_r = K_2 + K_4 [(\sigma_1 - \sigma_3) - K_1] \quad K_1 < (\sigma_1 - \sigma_3) \quad (3.15b)$$

This model is shown in Figure 3.6. In this analysis asphalt concrete layers were specified by material 2, granular layers by material 3, subgrade layers by material 4, and lime-stabilized layers by material type 1.

Three pavement structural sections were analyzed: a runway section, a highway section, and an "inverted" section similar to the highway section except that the subbase was replaced by a 10-inch thick layer of stabilized subgrade. The dimensions of the runway section were similar to those of a pavement test section at the U. S. Army Waterways Experiment Station, Reference (1). The dimensions of the highway section were derived by means of the Asphalt Institute design method (Reference 68). The subgrade CBR for each section was assumed to be about 4.0. The three cross sections are shown in Figure 3.7. The dimensions and material properties of each are summarized in Table 3.1. The material parameters were selected as being average values reported in the literature for similar type materials.

The applied load is divided into a number of equal increments, 5 for this

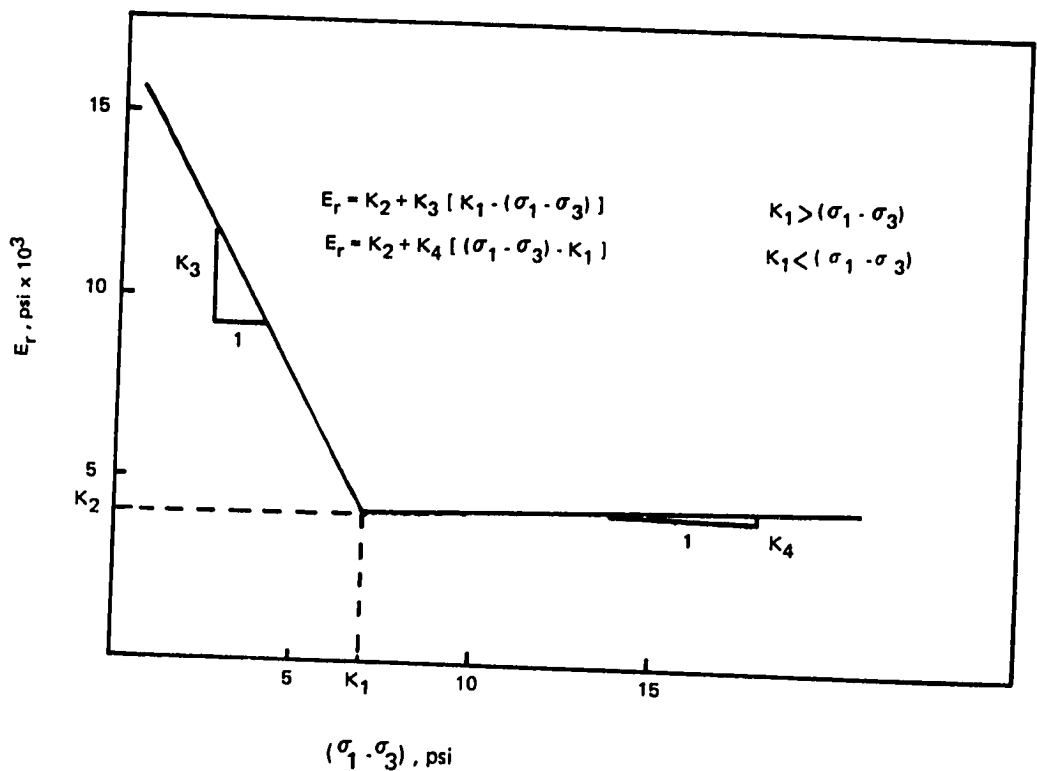
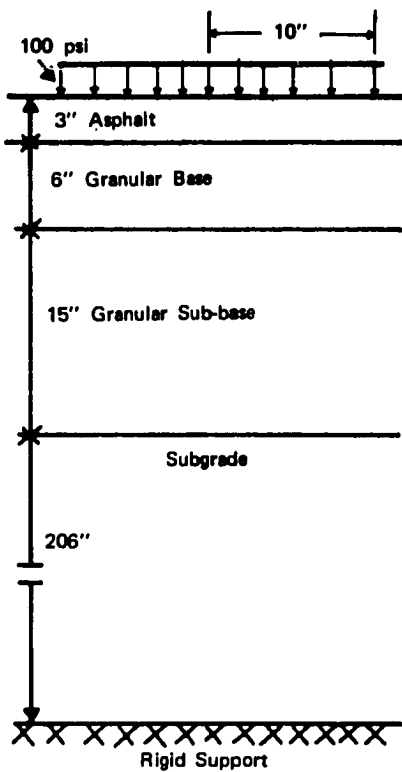
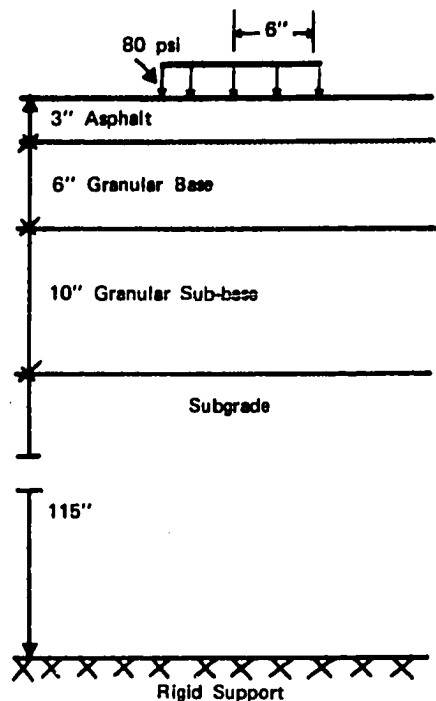


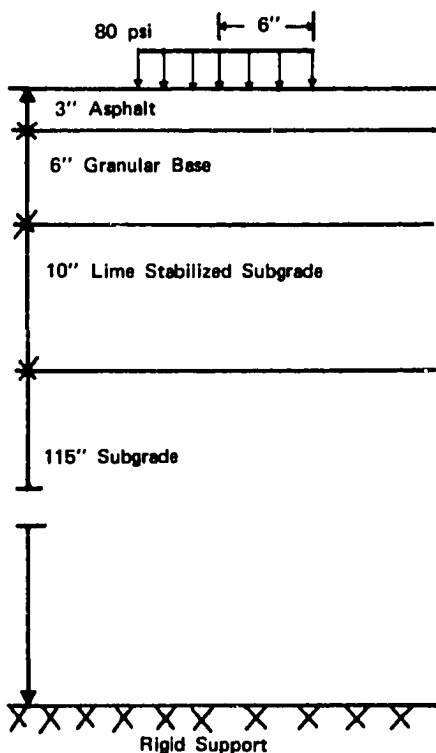
Figure 3.6  
Subgrade Resilient Modulus as a Function of Principal Stress Difference ( $\sigma_1 - \sigma_3$ )



(a) RUNWAY SECTION



(b) HIGHWAY SECTION



(c) INVERTED SECTION

**Figure 3.7**  
Three Pavement Sections Analyzed by Finite Elements Technique

TABLE 3.1  
DIMENSIONS AND MATERIAL PROPERTIES OF PAVEMENT SECTIONS ANALYZED  
BY FINITE ELEMENTS TECHNIQUE

Section	Layer	Thickness, inches	Coefficient of Earth Pressure at Rest, $K_o$	Poisson's Ratio	Unit Weight (lb/in <sup>3</sup> )	Modulus, psi
Runway Section	1. Asphalt Concrete	3	0.6	0.40	.085	800,000 (top), 650,000 (bottom)
	2. Base	6	0.6	0.40	.085	13,500 $\sigma_3^{0.52}$
	3. Subbase	15	0.6	0.40	.085	9,500 $\sigma_3^{0.56}$
	4. Subgrade	206	0.5	0.47	.070	4,000 + 1,800 [7 - ( $\sigma_1 - \sigma_3$ )] $> (\sigma_1 - \sigma_3)$ 4,000 + 32 [ $(\sigma_1 - \sigma_3) - 7$ ] $< (\sigma_1 - \sigma_3)$
Highway Section	1. Asphalt Concrete	3	0.6	0.40	.085	800,000 (top), 650,000 (bottom)
	2. Base	6	0.6	0.40	.085	13,500 $\sigma_3^{0.52}$
	3. Subbase	10	0.6	0.40	.085	9,500 $\sigma_3^{0.56}$
	4. Subgrade	115	0.5	0.47	.070	4,000 + 1,800 [7 - ( $\sigma_1 - \sigma_3$ )] $> (\sigma_1 - \sigma_3)$ 4,000 + 32 [ $(\sigma_1 - \sigma_3) - 7$ ] $< (\sigma_1 - \sigma_3)$
Inverted Section	1. Asphalt Concrete	3	0.6	0.40	.085	800,000 (top), 650,000 (bottom)
	2. Base	6	0.6	0.40	.085	13,500 $\sigma_3^{0.52}$
	3. Lime Stabilized	10	0.3	0.10	.070	150,000
	4. Subgrade	115	0.5	0.47	.070	4,000 + 1,800 [7 - ( $\sigma_1 - \sigma_3$ )] $> (\sigma_1 - \sigma_3)$ 4,000 + 32 [ $(\sigma_1 - \sigma_3) - 7$ ] $< (\sigma_1 - \sigma_3)$

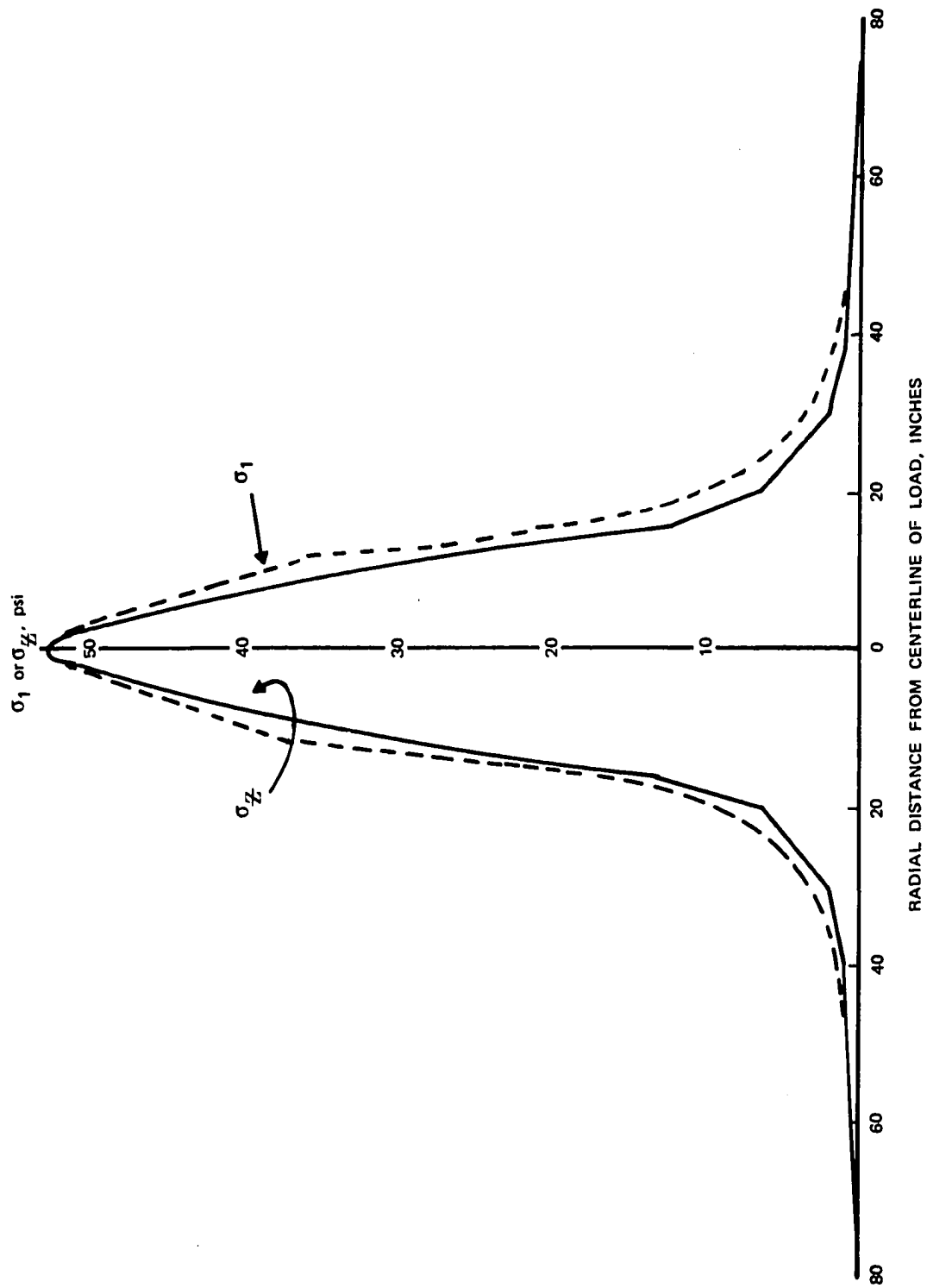


**Figure 3.8**  
Distribution of Vertical ( $\sigma_Z$ ) and Major Principal ( $\sigma_1$ ) Stresses  
One Inch Below Base-Asphalt Concrete Interface in Runway Section

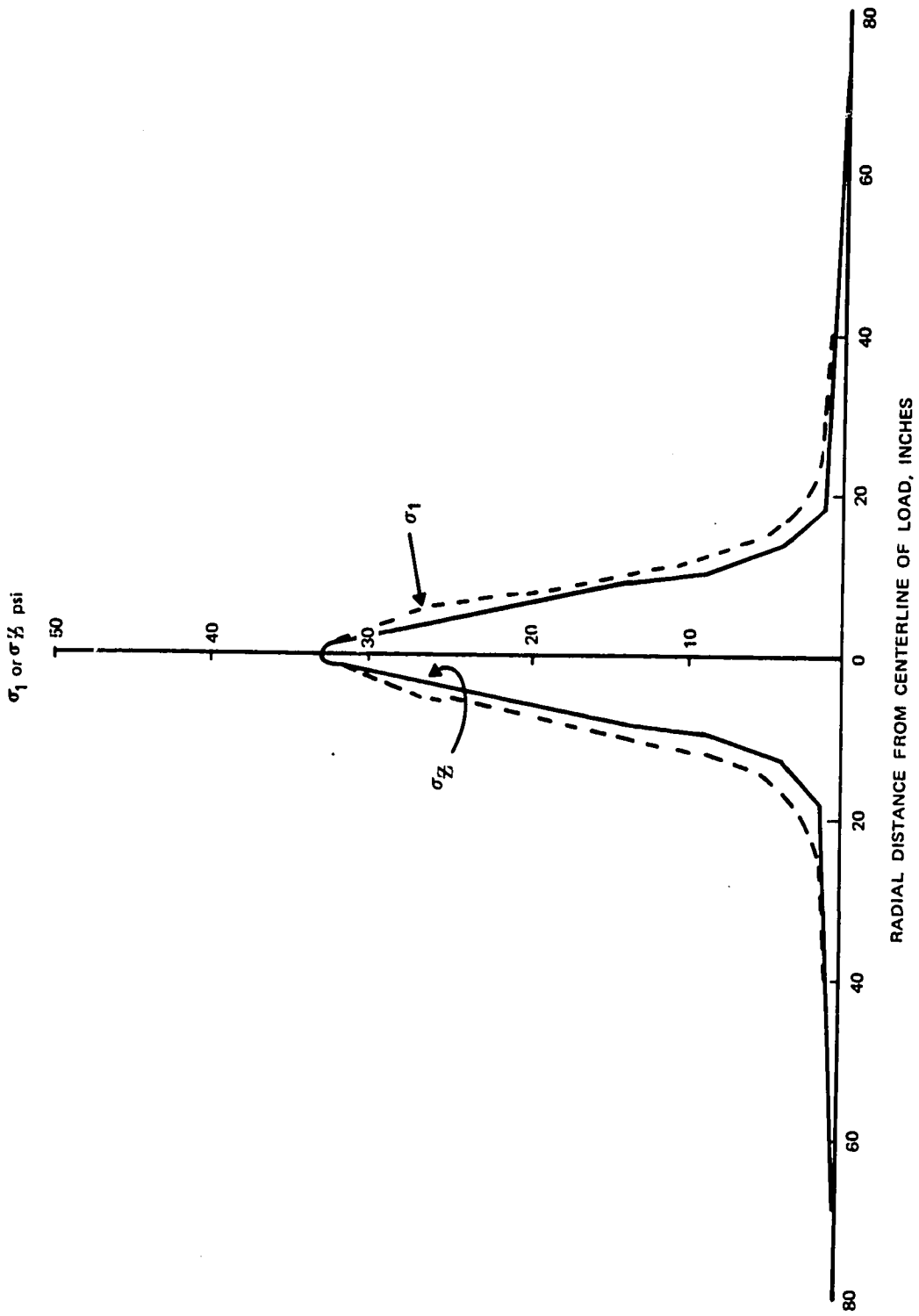


Figure 3.9  
Distribution of Vertical ( $\sigma_z$ ) and Major Principal ( $\sigma_1$ ) Stresses One Inch  
Above Base-Stabilized Layer Interface in Inverted Section

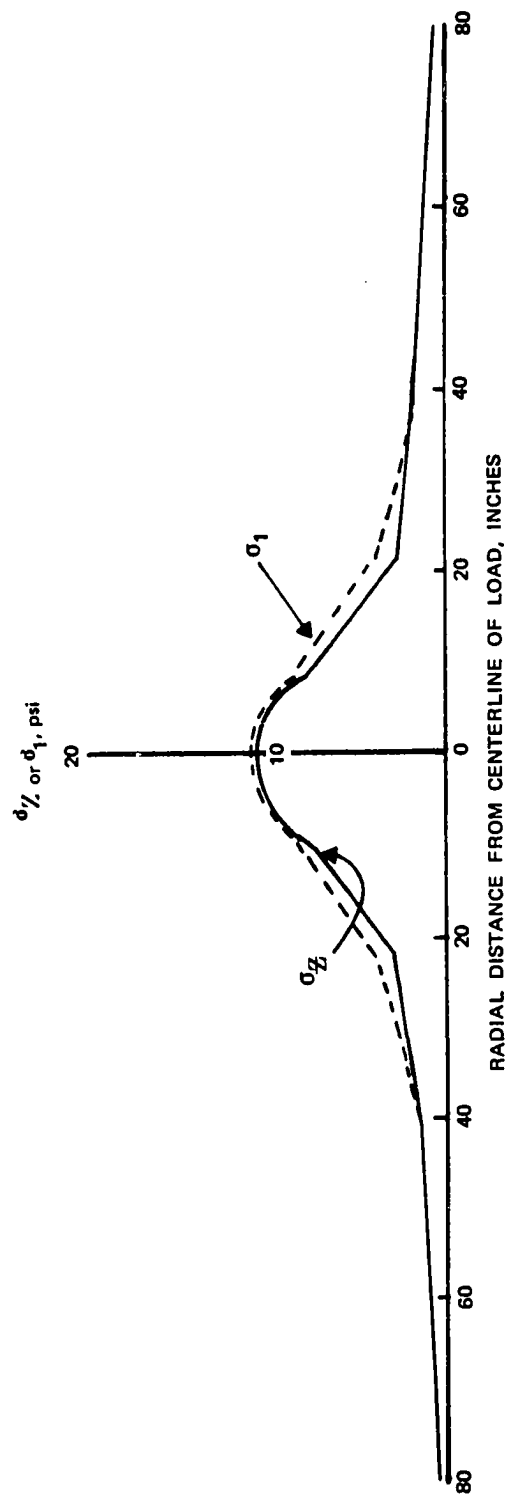


Figure 3.10  
Distribution of Vertical ( $\sigma_z$ ) and Major Principal ( $\sigma_1$ ) Stresses at  
Center of Subbase in Highway Section

portion of the study. Before the first increment is applied, gravity stresses are computed for each element from the specified unit weights, coefficients of earth pressure at rest, and the depth below the surface of each element. The component of  $\sigma_3$  due to gravity stress was included in each calculation of the moduli of the granular materials. However, for the subgrade material only the load-induced stress difference ( $\sigma_1 - \sigma_3$ ) was used to calculate the moduli. To calculate the moduli of the stress dependent material (granular layers and subgrade) for the initial load increment, an initial stress distribution was approximated by means of a one-to-one load spread concept. From this stress distribution and the gravity stresses (where applicable), initial moduli were computed and the stiffness matrix was formed. Displacements and stresses resulting from the first increment were then calculated. From these stresses, new moduli were computed and the process was repeated. Final values of stresses and displacements were arrived at in this step-by-step manner.

### 3.5 Comparison of Stress Pulses

For all three sections the shapes of the stress distributions appeared to be related to depth within the section. The major principal stress pulse and vertical stress pulse, while generally of sinusoidal shape, were more sharply peaked in the upper part of the base course, with shallower slopes in the lower base and subbase. Since principal stresses are everywhere greater than vertical stresses, except directly under the center of the load, where they are equal, the major principal stress pulse would therefore be of somewhat longer duration than the vertical stress pulse. This difference increases with depth. The same trends were reported by Barksdale (9). Figures 3.8 through 3.10 are typical of the results derived from all three sections.

Transformation of these spatially distributed stress pulses to time-

distributed pulses is a simple matter of dividing the width of the pulse by vehicle speed. In addition, empirical corrections for inertia and viscous effects have been derived from AASHO Road Test results (32). On the basis of those corrections, Barksdale (9) applied correction factors of 1.11, 1.13, and 1.14 to the durations determined by elastic analysis to obtain pulse durations corresponding to vehicle speeds of 15, 30, and 45 mph respectively. However, for the purposes of this study no such corrections were applied since the granular materials tested by Hicks displayed little or no change in behavior as load durations varied. As reported in Chapter 5, the response of materials tested in this study was also negligibly affected by changes in load duration.

Radial and minor principal stress pulses were similar in shape for the runway and highway sections. These pulse shapes, too, appeared to be related to depth within the system. In the upper portions of the base, these pulses were more or less flat-topped, although in the extreme upper portion of the base the stresses were slightly less directly under the center of the load than at a slight radial offset. Both types of pulse became more sinusoidal as the depth increased. Figures 3.11 and 3.12 show typical horizontal stress distributions for the runway and highway sections.

Analysis of the inverted section revealed significant changes in stress distributions. Although the vertical and major principal stress pulses were of the same shape as those for the highway section, their magnitudes were greater throughout the granular layer. Figure 3.13 compares vertical stresses one inch below the base-asphalt concrete interface. It is important to note that the inclusion of the stiffer layer beneath the base almost doubled the vertical stress beneath the center of the load at this point. The same effect was found throughout the base.

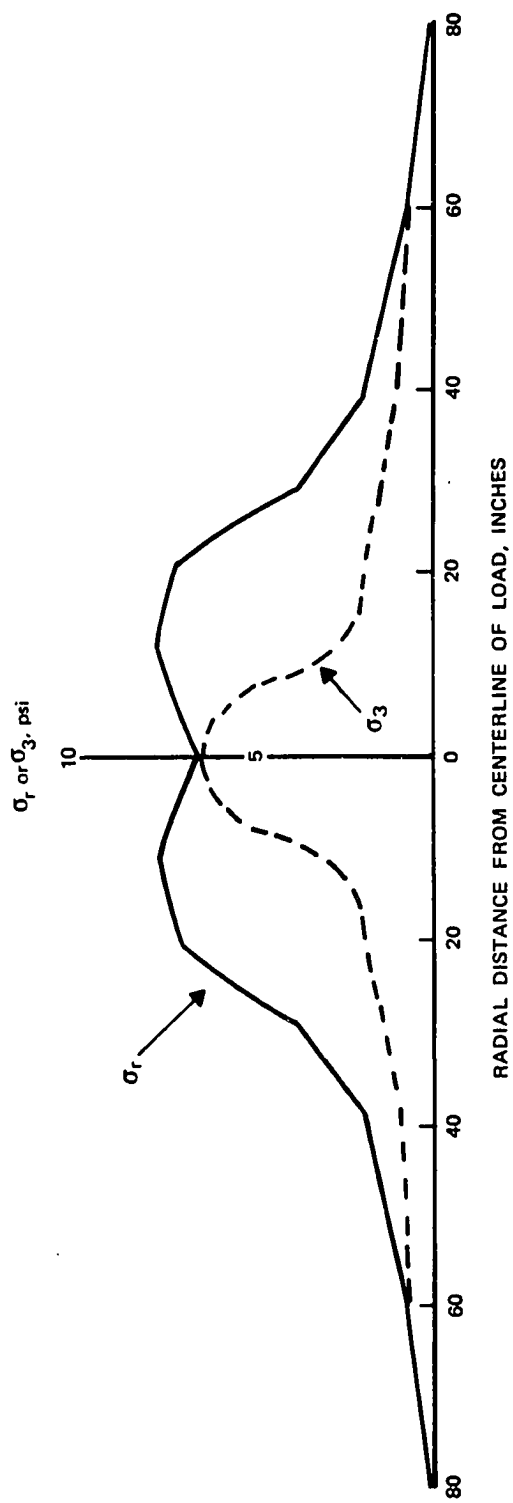


Figure 3.11  
Distribution of Radial ( $\sigma_r$ ) and Minor Principal ( $\sigma_3$ ) Stresses  
One Inch Above Base-Subbase Interface in Runway Section

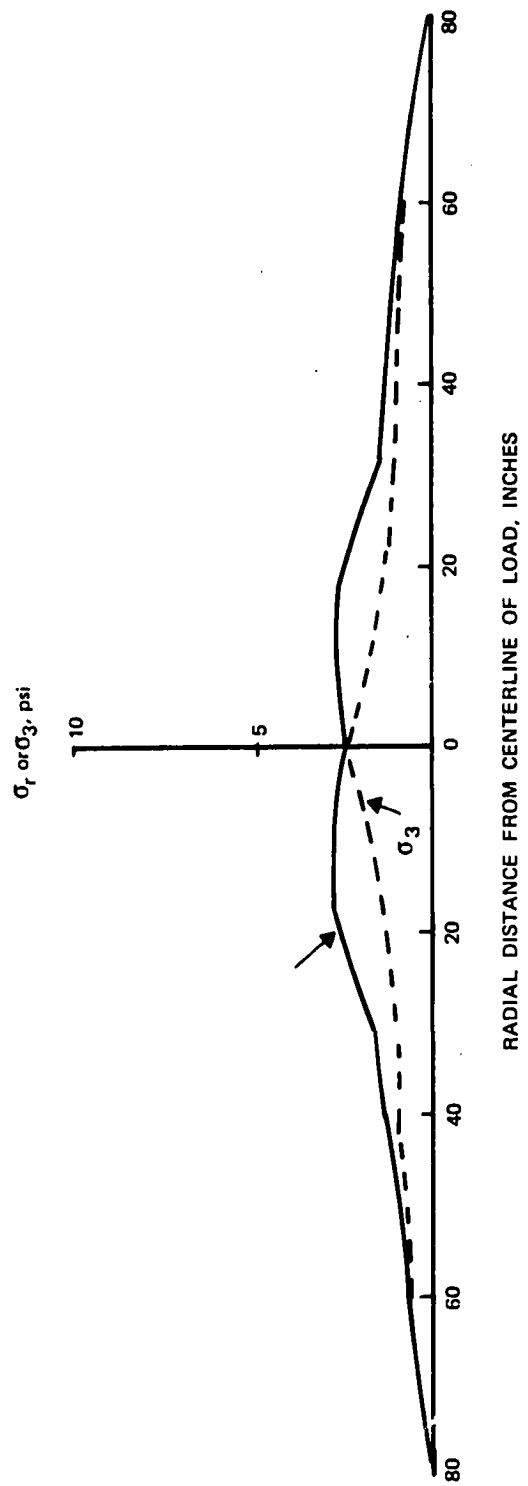


Figure 3.12  
Distribution of Radial ( $\sigma_r$ ) and Minor Principal ( $\sigma_3$ ) Stresses  
at Center of Subbase in Highway Section

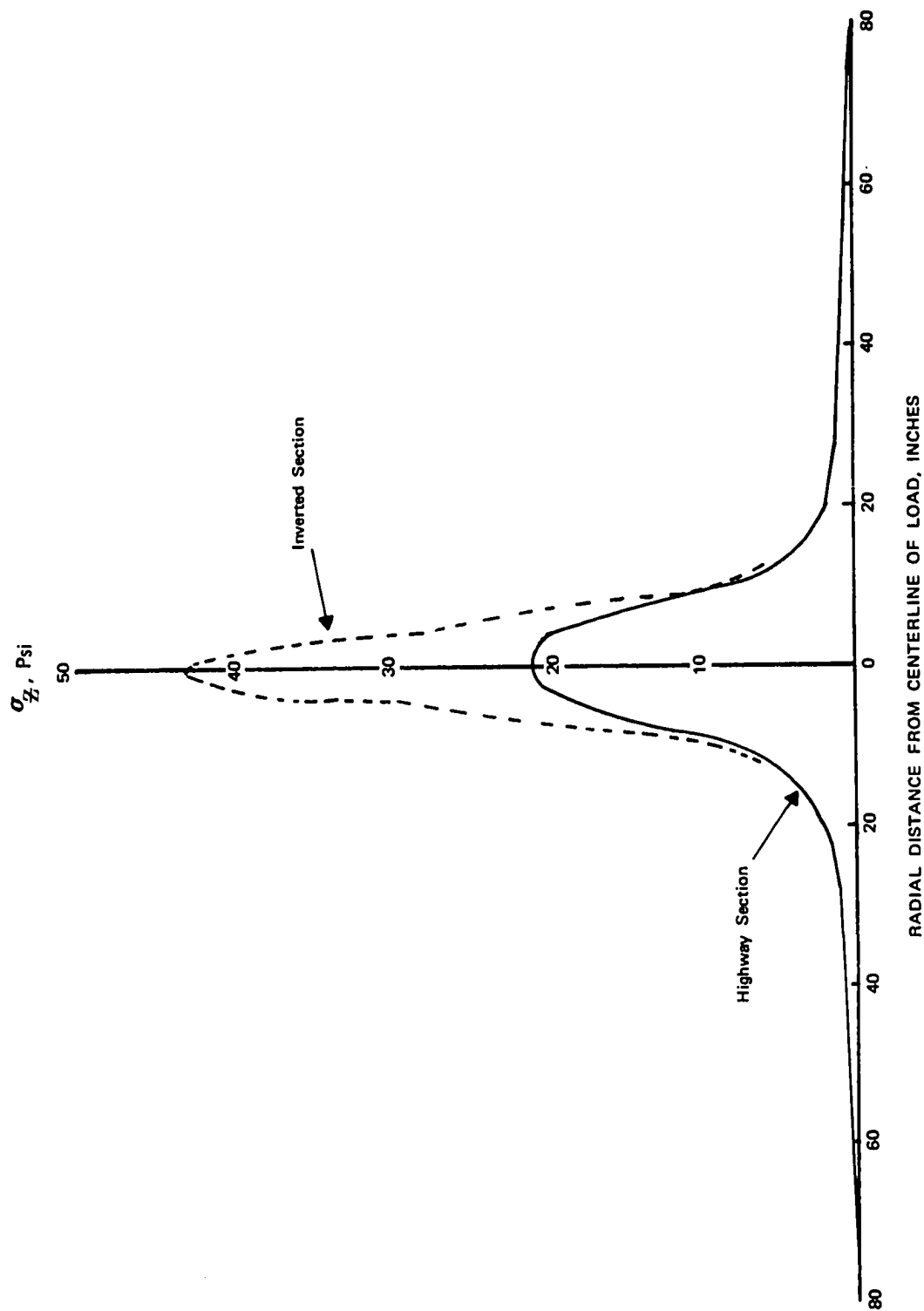


Figure 3.13  
Comparison of Vertical Stresses One Inch Below Asphalt Concrete—  
Base Course Interface in Highway and Inverted Sections

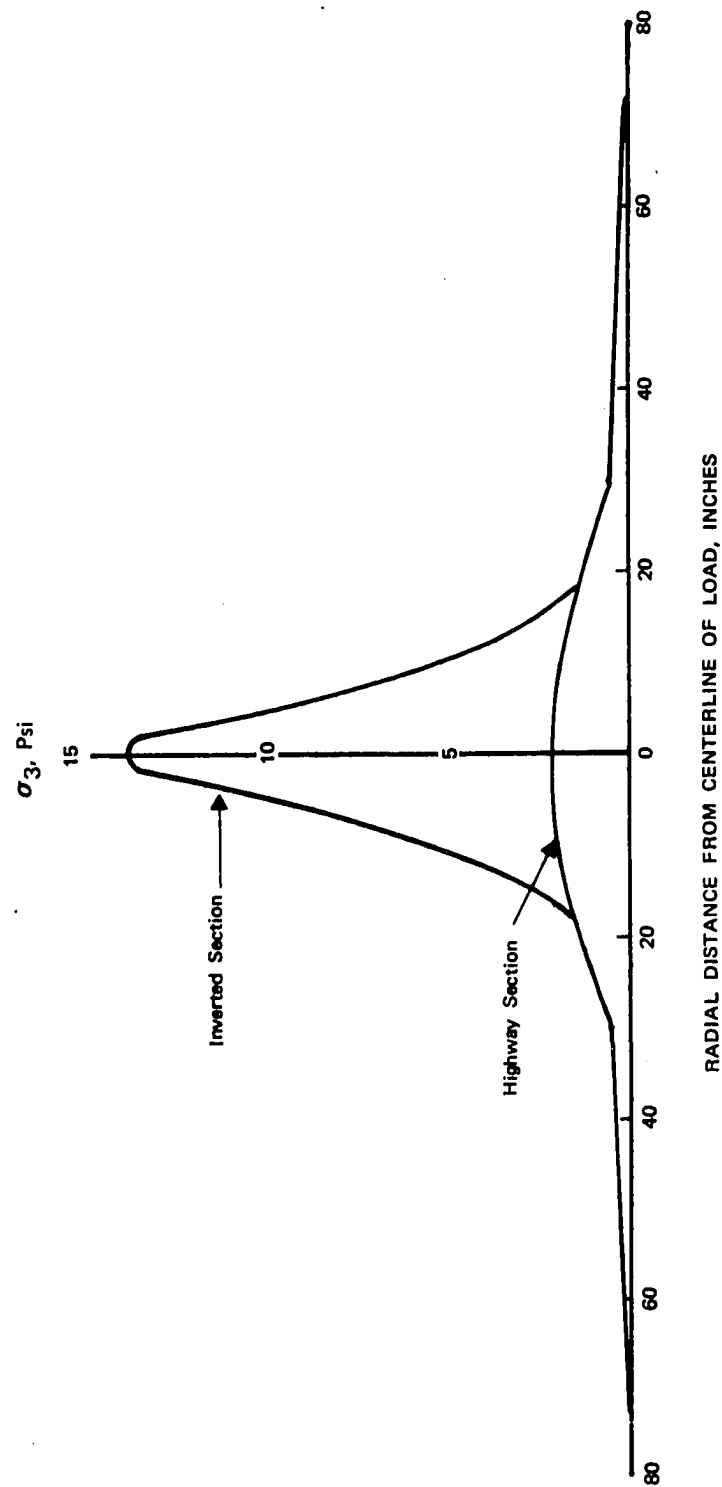


Figure 3.14  
Comparison of Minor Principal Stresses at Center of Base Course  
in Highway and Inverted Sections

More significant was the drastic increase in the radial and minor principal stresses throughout the granular layer of the inverted section. The reduction in confining pressure beneath the center of the load was completely eliminated with a resulting sinusoidal pulse shape. The magnitude of the minor principal stress pulse directly under the load increased by 500 to 800 percent. Figure 3.14 compares the distribution of minor principal stresses for the highway and inverted sections.

It is evident from Figures 3.8 through 3.14 that a half-sinusoid is the most general shape of all the stress distributions. For this reason and because most standard laboratory function generators, in combination with hydraulic testing equipment, have the capability of applying such a pulse shape, the half sinusoid was selected as the basic pulse shape for use in this study. Simulation of states of stress at various depths within the granular layer could be accomplished by varying the pulse duration and magnitude. This was done, and the testing procedures and results are presented in subsequent chapters.

In the following section, the response of the three pavement sections is discussed, with an emphasis on the significance of the stress-dependent material parameters.

### 3.6 Implications of Stress-Dependent Properties for Pavement Performance

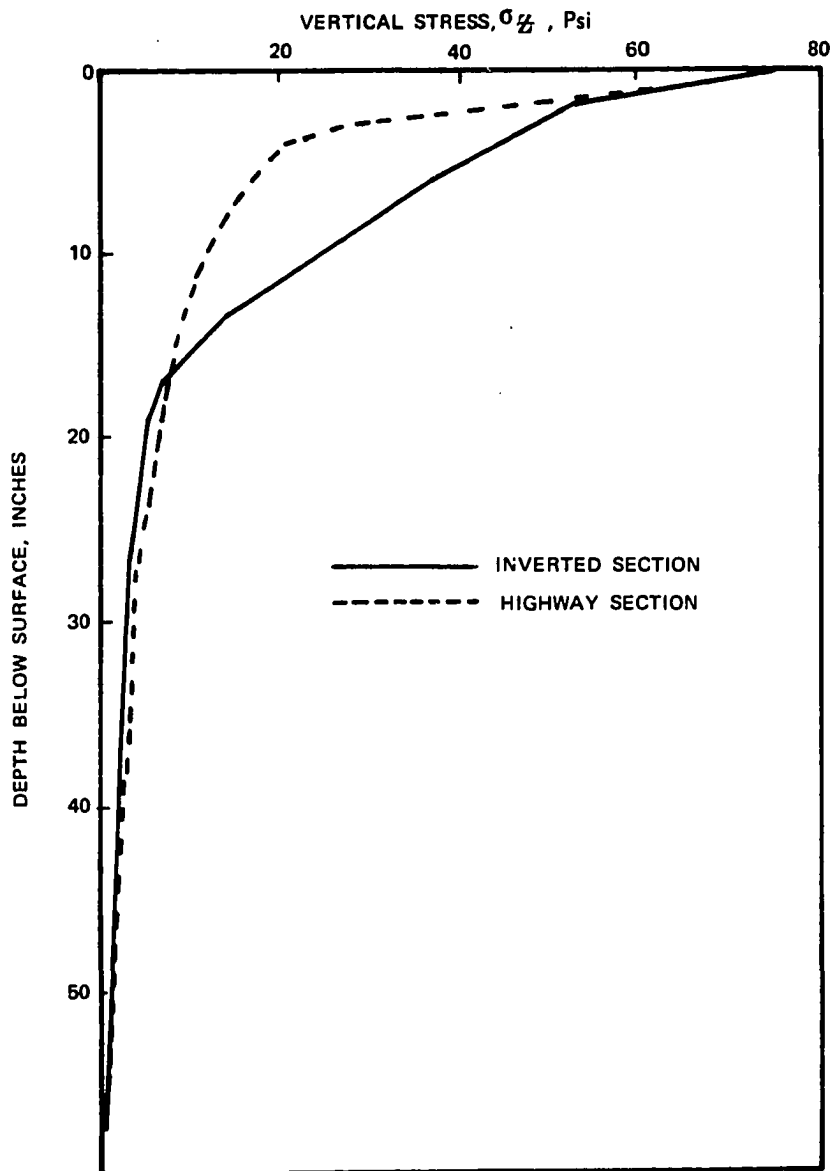
The most obvious conclusion to be reached from the literature survey concerning the stress-dependent resilient modulus is that, for an increase in  $\sigma_3$  or the first invariant, an increase in the modulus results. Since an increased modulus yields decreased strains, it might be assumed that any arrangement of pavement components that causes higher confining stresses in the granular layers will result in lower surface deflections and longer pavement serviceability. The effects of deflections on pavement performance have been recognized. Zube

and Forsyth (76) and (77), discuss the importance of prediction of resilient deflections and limiting criteria for deflections. Lister (45) presented deflection criteria for flexible pavements and discussed a method by which such criteria could be used to estimate future pavement performance.

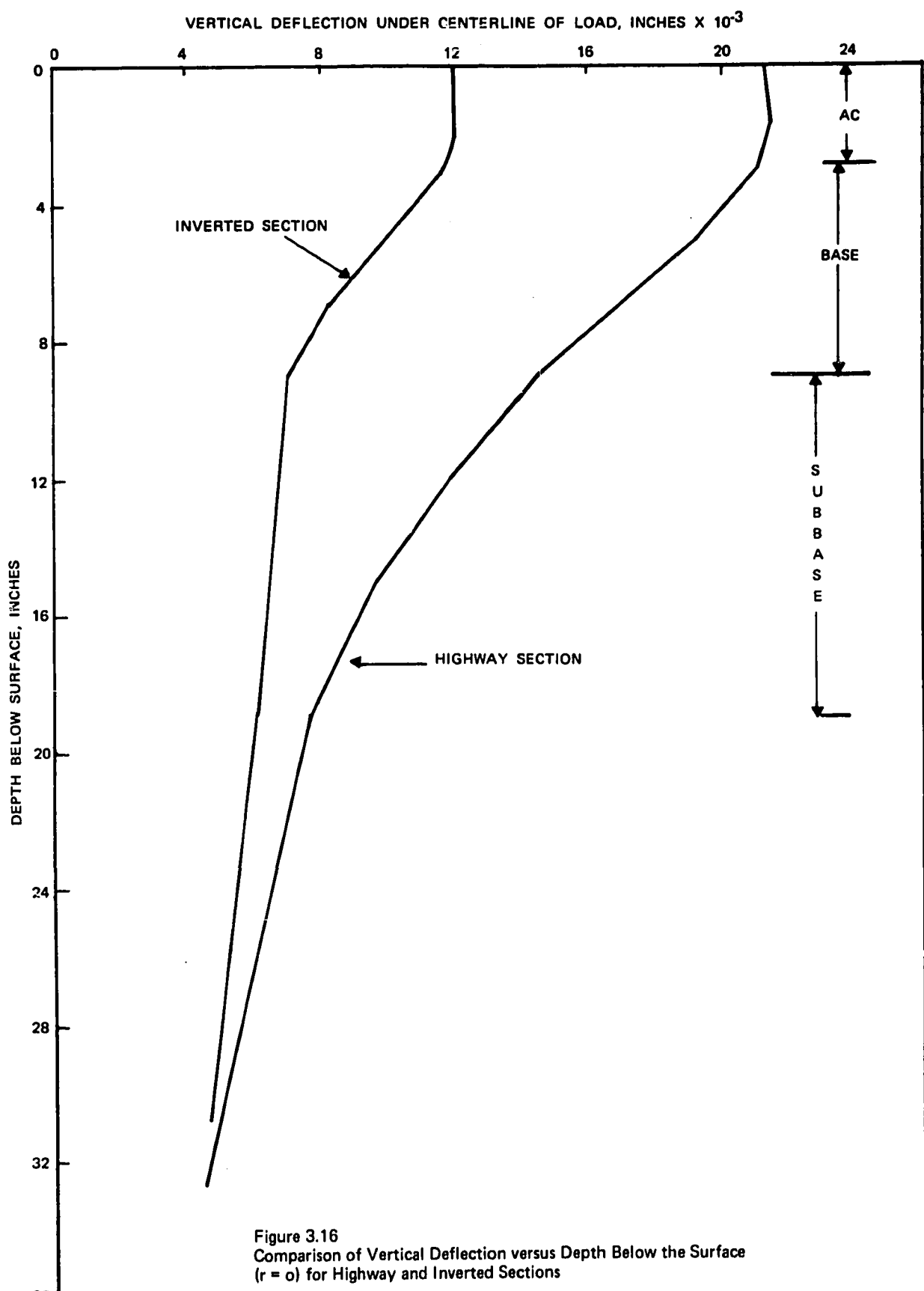
Analysis of the inverted section revealed that the stress dependent properties of granular layers may be exploited to the designer's advantage by utilizing a stiffer stabilized layer below the granular material; thereby increasing the confining pressure in the base course, increasing its modulus, and reducing surface deflections.

In the preliminary analysis of a proposed flexible pavement design three factors have been studied as quantitative indicators of the performance of the proposed structural section: (1) vertical stress on the subgrade, (2) surface deflection, and (3) horizontal strains at the bottom of the asphalt concrete layer. Combinations of these factors have often been used in pavement analyses (Monismith, et al., 49). In a sensitivity analysis Smith and Nair (64) utilized the fatigue failure characteristics of asphalt concrete developed by Monismith, et al., at the University of California at Berkeley, relating fatigue life to tensile strain in the asphalt concrete layer. Therefore, it is felt that the beneficial aspects of the stiffer stabilized layer and greater base-course modulus in the inverted section can best be studied by comparing the variations in these three parameters.

Figure 3.15 compares vertical stresses plotted as a function of depth for the highway and inverted sections. These stresses are computed at a 0.75 inch radial displacement from the centerline of the load because the finite element solution yields stresses at the centers of elements. The load-spreading effects of the stabilized layer result in a 13 per cent reduction in vertical stress at the top of the subgrade. This reduction in vertical stress combines



**Figure 3.15**  
Comparison of Vertical Stresses versus Depth Below the  
Surface for Highway and Inverted Sections



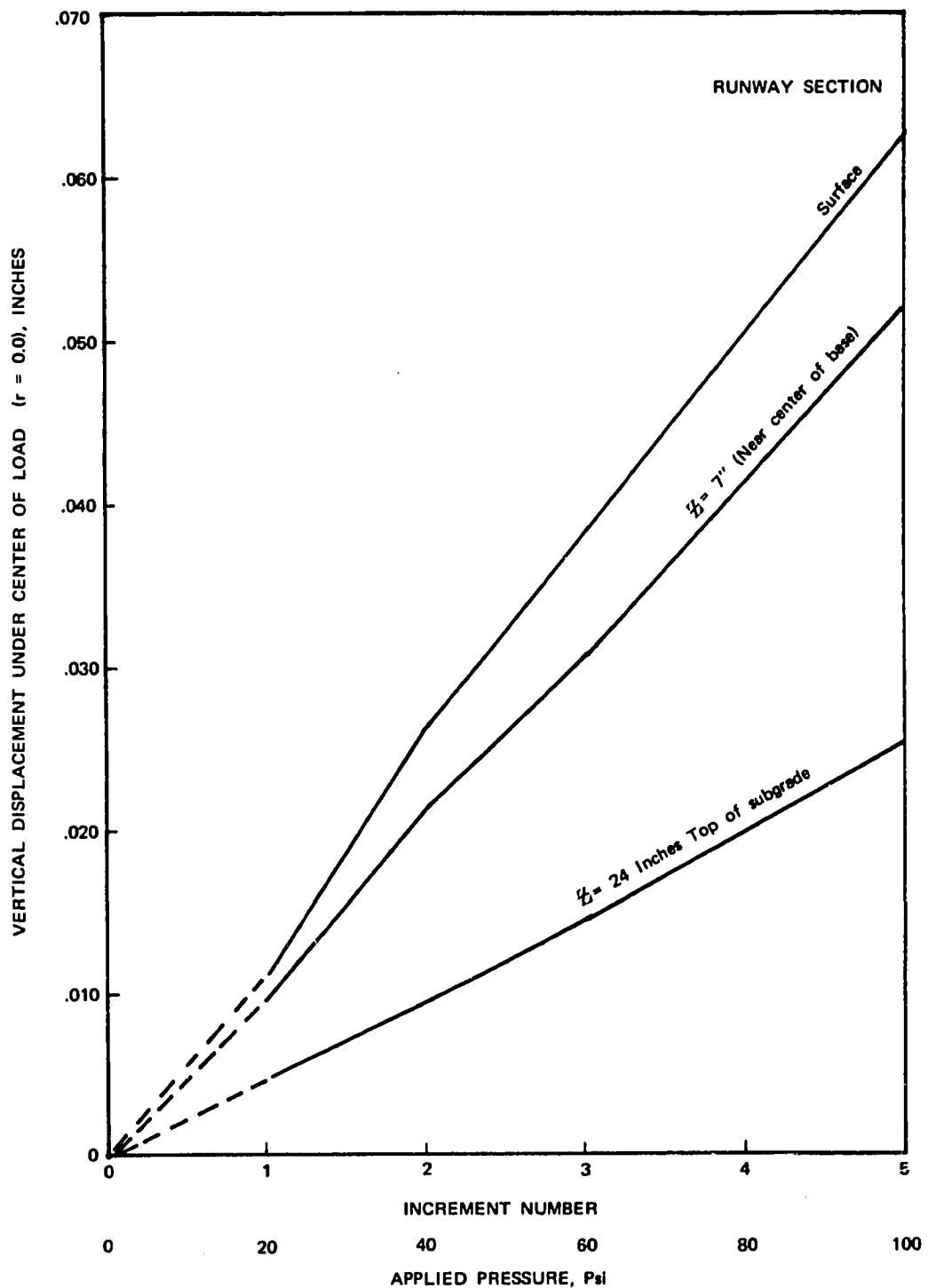
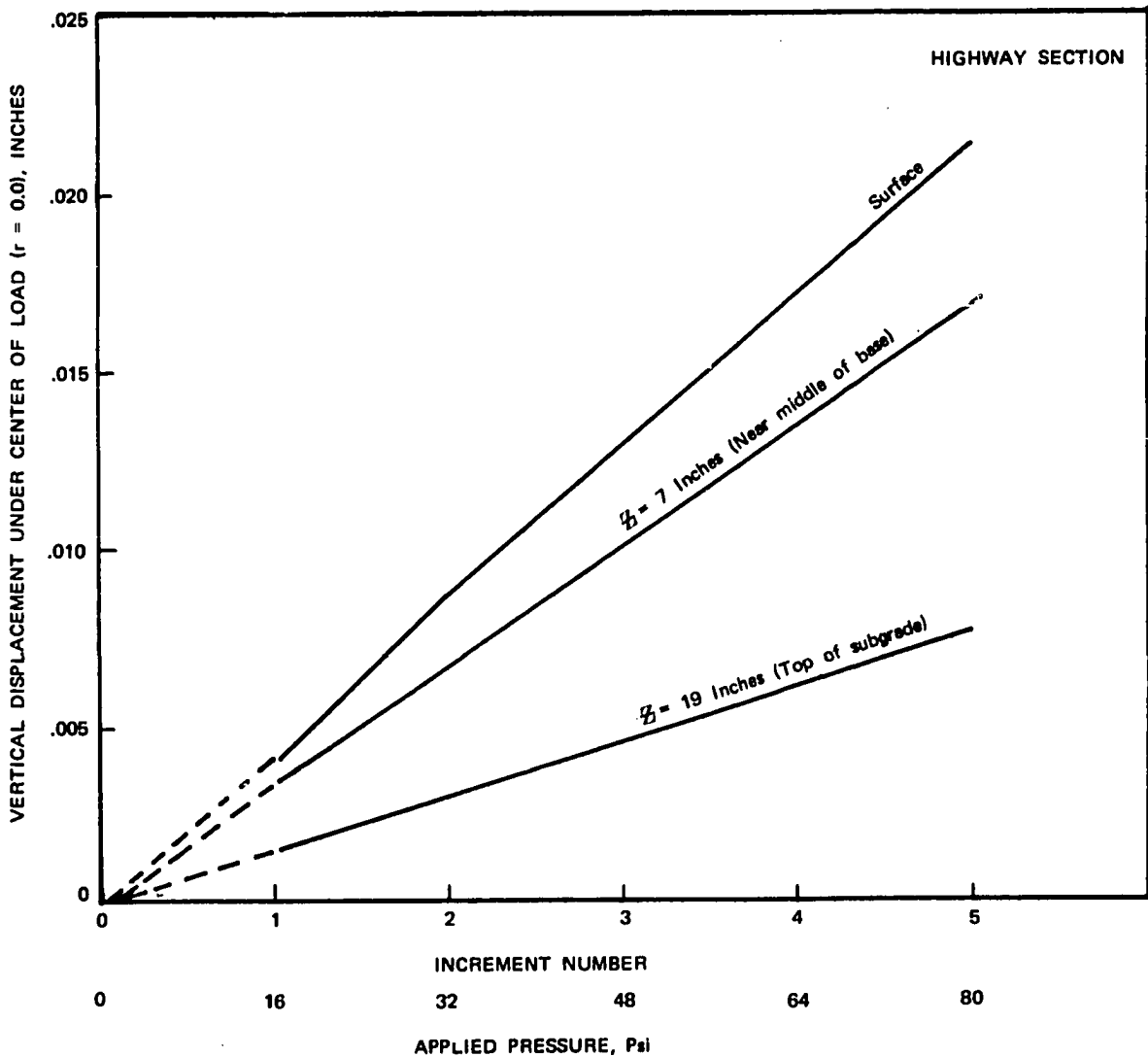
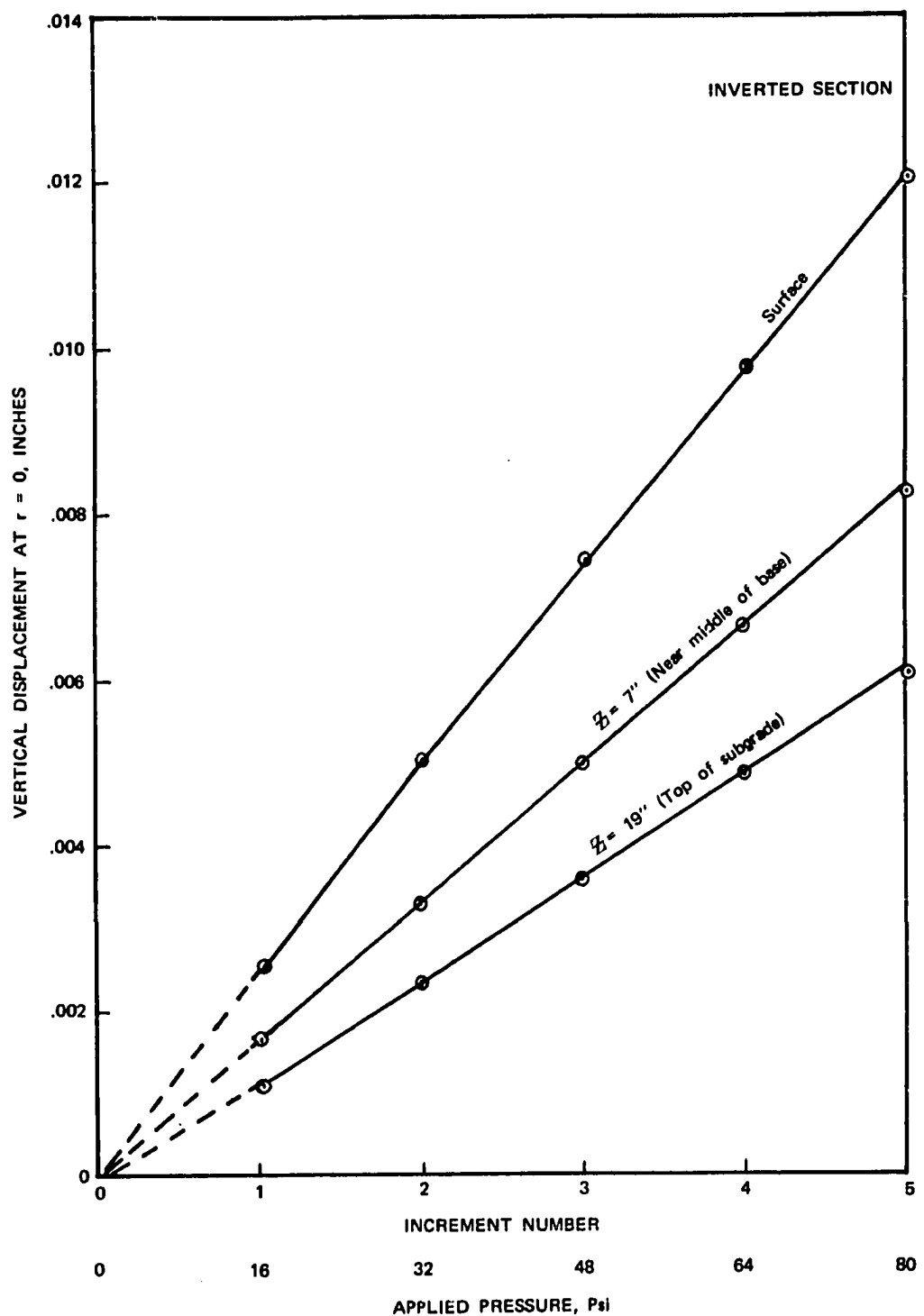


Figure 3.17  
Vertical Displacement ( $r = 0$ ) versus Surface Pressure for  
Runway Section



**Figure 3.18**  
Vertical Displacement ( $r = 0$ ) versus Surface Pressure for  
Highway Section



**Figure 3.19**  
Vertical Displacement ( $r = 0$ ) versus Surface Pressure for  
Inverted Section

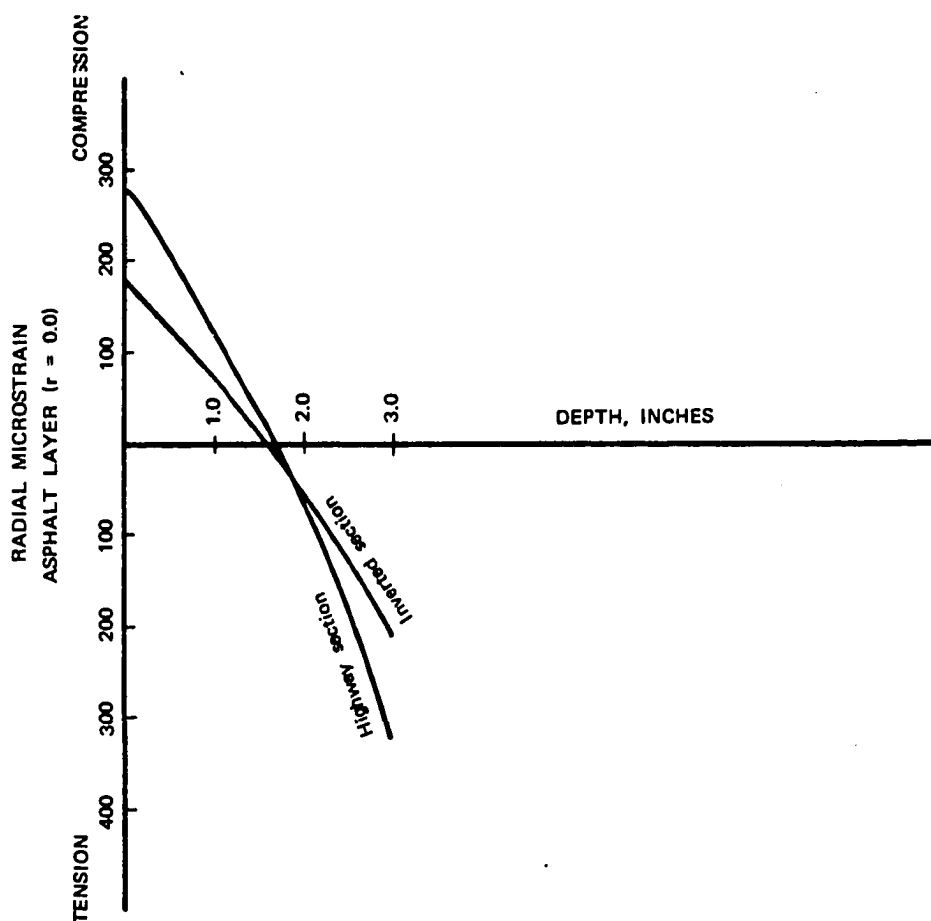


Figure 3.20  
Radial (Horizontal) Microstrain Distribution with Depth  
in Asphalt Concrete Layer of Highway and Inverted Sections

with the resulting slight increase in subgrade modulus to decrease the vertical deflection at the top of the subgrade by about 20 per cent (Figure 3.16).

Vertical deflections versus depth for the two sections are compared in Figure 3.16. The net effect of the stabilized layer is to reduce the maximum surface deflection by about 43 per cent. Although the deflection within the subgrade decreased from 0.0077 inch to 0.0061 inch, the greatest effects were noticed in the granular layers. The 0.0134 inch deflection contributed by the granular layers in the highway section reduced to 0.0059 inch for the stabilized and granular layers in the inverted sections. Two factors account for this drastic reduction. Replacement of the gravel subbase by the stabilized layer provided a reduction of 0.0059 inch in subbase deflection. In addition, despite the 100 per cent increase in vertical stresses within the granular base, the effect of the drastic increase in  $\sigma_3$  and in the resilient modulus was a reduction in vertical deflection within the layer of 0.0018 inch, a decrease of 28 per cent.

Also of interest regarding surface deflection was its nearly linear relationship with surface load. Figures 3.17, 3.18, and 3.19 show that, despite the nonlinear material properties, the load-deflection curve is nearly linear for all three sections. A similar relationship was reported by Dehlen for a full depth asphalt pavement(18).

The stabilized layer in the inverted section also accounted for a 35 per cent reduction in maximum tensile strain in the asphalt layer as compared to the highway section. Radial strains within the asphalt concrete layer are compared for the two sections in Figure 3.20.

The beneficial influence of the stabilized layer in the inverted section is also evident if plastic strains, or rutting are considered. On the basis of a hyperbolic stress-strain law proposed by Kondner, et al., (43), and extended by Duncan and Chang (21), Barksdale (10) presented a method of predicting plastic

strains in a pavement section based on data developed from laboratory repeated-load triaxial tests. He showed that, after 100,000 load repetitions, plastic axial strains were related to confining pressure and deviator stress by the following expression:

$$\varepsilon_a = \frac{(\sigma_1 - \sigma_3)/(K \sigma_3^n)}{1 - \left\{ \frac{(\sigma_1 - \sigma_3) R_f}{2(C \cdot \cos \phi + \sigma_3 \sin \phi)} \right\} \frac{(1 - \sin \phi)}{(1 - \sin \phi)}} \quad (3.23)$$

where,  $\varepsilon_a$  = permanent axial strain

$K \sigma_3^n$  = initial tangent modulus

$C, \phi$  = Coulomb shear strength parameters

$R_f$  = constant relating compressive strength to asymptotic stress difference

Details of the method used to compute the constants in Equation 3.23 are described by Duncan and Chang (21) and the procedure whereby this hyperbolic law is used to predict rut depth in a pavement is detailed by Barksdale (10). Of interest here is the importance of the variables  $\sigma_3$  and  $\sigma_1 - \sigma_3$ . The decrease in deviator stress and increase in confining pressure within the granular base course caused by the underlying stiffer layer would greatly reduce permanent vertical strains within the layer. Because Equation 3.23 has been applied to fine-grained as well as granular materials, it can be inferred that the decrease in deviator stress in the subgrade of the inverted section would indicate smaller plastic strains and, hence, reduced rutting.

Also of importance in the study of pavement performance is the behavior of unstabilized granular layers when subjected to lateral tensile stresses. Such a situation normally exists at the bottom of the granular layer, but it can also be observed near the base-asphalt interface when the modulus of the asphalt concrete is very low. Duncan, Monismith, and Wilson (23) found in

their analysis of a flexible pavement simulating summer conditions (i.e., high temperatures and low asphalt concrete stiffness modulus) that the portion of the base directly under the load was subjected to zero or tensile radial stresses. Most likely this behavior is caused by the large tensile strains in the underside of the asphalt. However, for winter conditions (i.e., lower surface temperature and greater asphalt concrete stiffness modulus) this phenomenon did not develop.

Cognizant of the anisotropic nature of granular materials, Barksdale's (9) approach to the problem involved specifying an angle of shearing resistance,  $\phi$ , for the base course. He reasoned that the material could withstand a certain amount of lateral tension before slip would occur because the tensile stresses would be resisted by a frictional stress equal to the product of the vertical compressive stress and the coefficient of friction,  $\tan \phi$ . Accordingly, for the case where tensile stresses were present but of smaller magnitude than the potential maximum frictional stresses, he specified constant values of vertical and horizontal moduli. He suggested values of 10,000 psi and 8,000 psi, respectively. For the case where slip did occur, he used a vertical modulus of 6,000 psi and a horizontal modulus of 600 psi. It is felt that once slip occurs the passive earth pressures built up in the material at greater radial distances would increase the horizontal modulus and render these latter values conservative. Such an approach, at least, is a step in the right direction in that it considers the anisotropic nature of the material, which has been documented by Moore, Britton, and Schrivner (51) and which was observed during this study, as reported in Chapter 5.

The finite elements solution used in this study sets a lower limit to the resilient modulus of the granular material. The input was specified in such a way that, whenever  $\sigma_3$  was less than 0.1 psi or tensile, the modulus was calculated from  $\sigma_3 = 0.1$  psi. It is felt that this lower limit was not

unconservative since there are indications that the modulus of unstabilized granular materials in the unconfined condition may exceed 5,000 psi. Gray (28) presented results of static triaxial compression tests on granular materials. The data collected for materials tested in the unconfined condition suggest that a modulus of 5,000 psi or more is an entirely reasonable assumption.

Of significance here is the fact that the stiffer underlying layer in the inverted section completely eliminated the tendency for the base course to go into tension, and thus the modulus of the material directly under the center of the load never reached the lower limit.

In summary, the finite elements solution technique as applied to pavement analysis is advantageous in that pavement components may be more realistically characterized. This fact makes possible a more thorough evaluation of the beneficial aspects derived from varying the layered configuration of flexible pavement systems so as to exploit the stress-dependent properties of pavement components.

For these reasons the finite elements solution was used in the sensitivity analysis in Chapter 6. In this analysis the predictive equations for the resilient modulus and Poisson's ratio of granular layers were varied and the ensuing effects on various indicators of pavement performance were observed.

**Chapter 4**  
**LABORATORY TESTING PROGRAM**

**4.1 Description of Materials**

Three materials were tested during this study, a well-graded crushed limestone obtained from a quarry about 30 miles south of Champaign, Illinois, a well-graded siliceous gravel obtained at Mahomet, Illinois, and a blend of the gravel and limestone. The blend was obtained by adding equal percentages of the crushed stone and gravel retained on the number 4 sieve to the gravel material passing the number 4. All three materials met CA-6 gradation requirements as specified by the Illinois Department of Transportation (Figure 4.1). All specimens were prepared from this one gradation.

Atterberg Limits Tests (ASTM D424-59, ASTM D423-66) were performed on the minus number 40 portions of each material. The results are presented in Table 4.1, as are the specific gravity data (ASTM D854-58) for each material. As would be expected, the crushed stone fines had the lower plasticity index, 5, as opposed to a plasticity index of 9 for the gravel fines.

Table 4.1  
 Atterberg Limits and Specific Gravity

Material	Liquid Limit	Plastic Limit	Plasticity Index	Specific Gravity
Crushed Limestone	19	14	5	2.63
Gravel	25	16	9	2.64

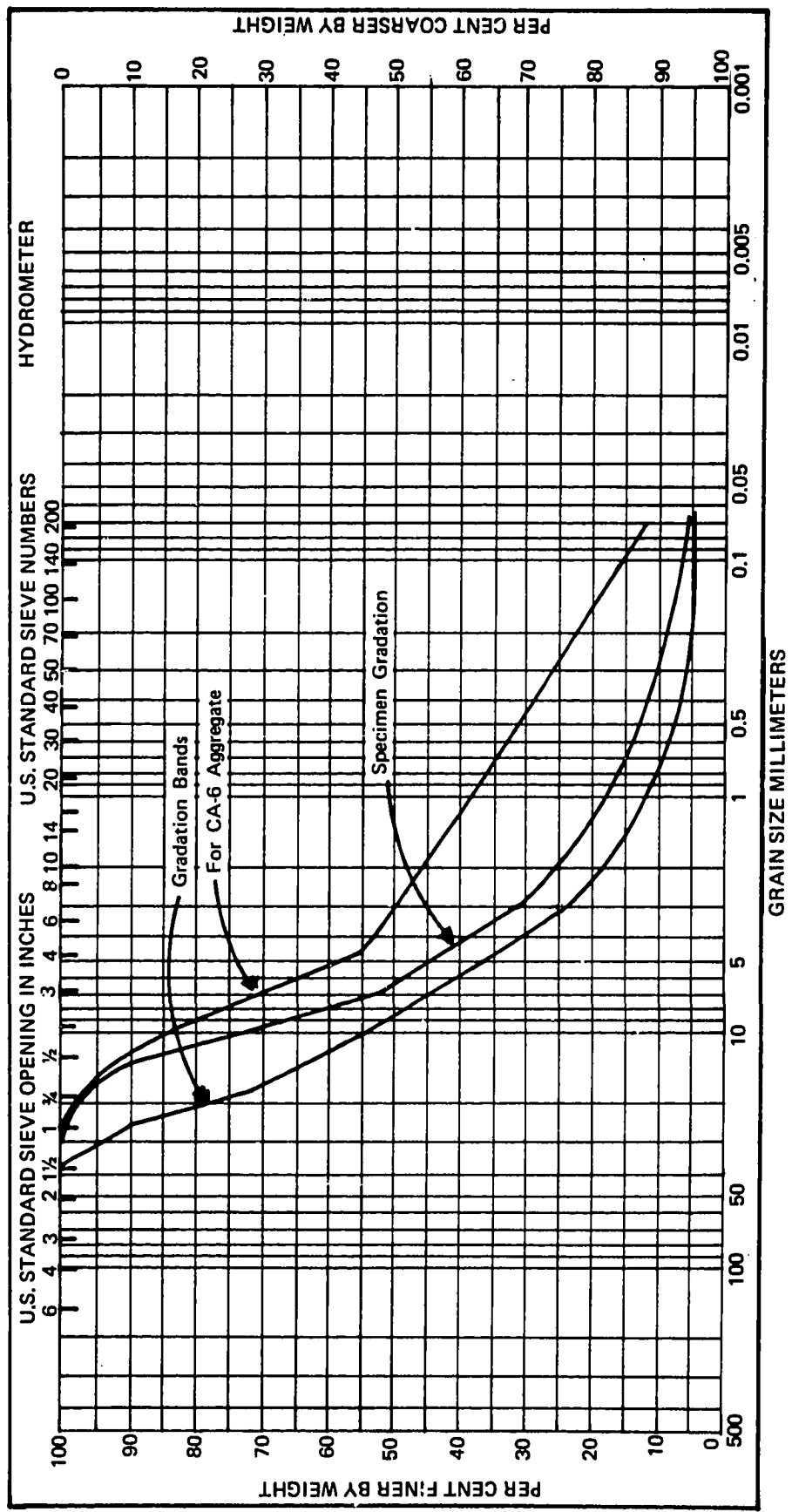


Figure 4.1  
Specimen Gradation and Gradation Bands for CA-6 Aggregate

Compaction control tests were run on the crushed stone and gravel in accordance with ASTM D698-66T and ASTM D 1557-66T. The results are presented in Figures 4.2 and 4.3. For the ASTM D698 test the maximum dry density for the crushed stone was 99.5% of that obtained for the gravel. The optimum moisture content for the crushed stone was only slightly greater than that for the gravel.

The results for the ASTM D1557 test also show only slight differences in maximum dry density and optimum moisture for the two materials. Again, the maximum dry density for the crushed stone was about 99.5% of that for the gravel. Because of this similarity in compaction characteristics, the compaction control tests were not performed on the blend material.

The overall purpose of this study was to observe the behavior of granular materials in conditions closely approximating those found in in-service pavements. Because the ASTM compaction tests referred to above have been widely used as compaction standards in the field, it was decided to test each material at three levels of density determined from these tests. Two of these density levels and the associated water contents were chosen from the peaks of the moisture-density curve for each type of test and the third level was chosen as a density and moisture content about halfway between the peaks.

In summary, three types of materials at each of three density levels were tested in the repeated load triaxial test apparatus, whereby the effects of density and material type on the resilient characteristics of the specimens could be ascertained. These material characteristics are summarized in Table 4.2

#### 4.2 Specimen Preparation

All specimens were 6 inches in diameter and 12 inches in height. The larger diameter was chosen so that the full range of aggregate size could be

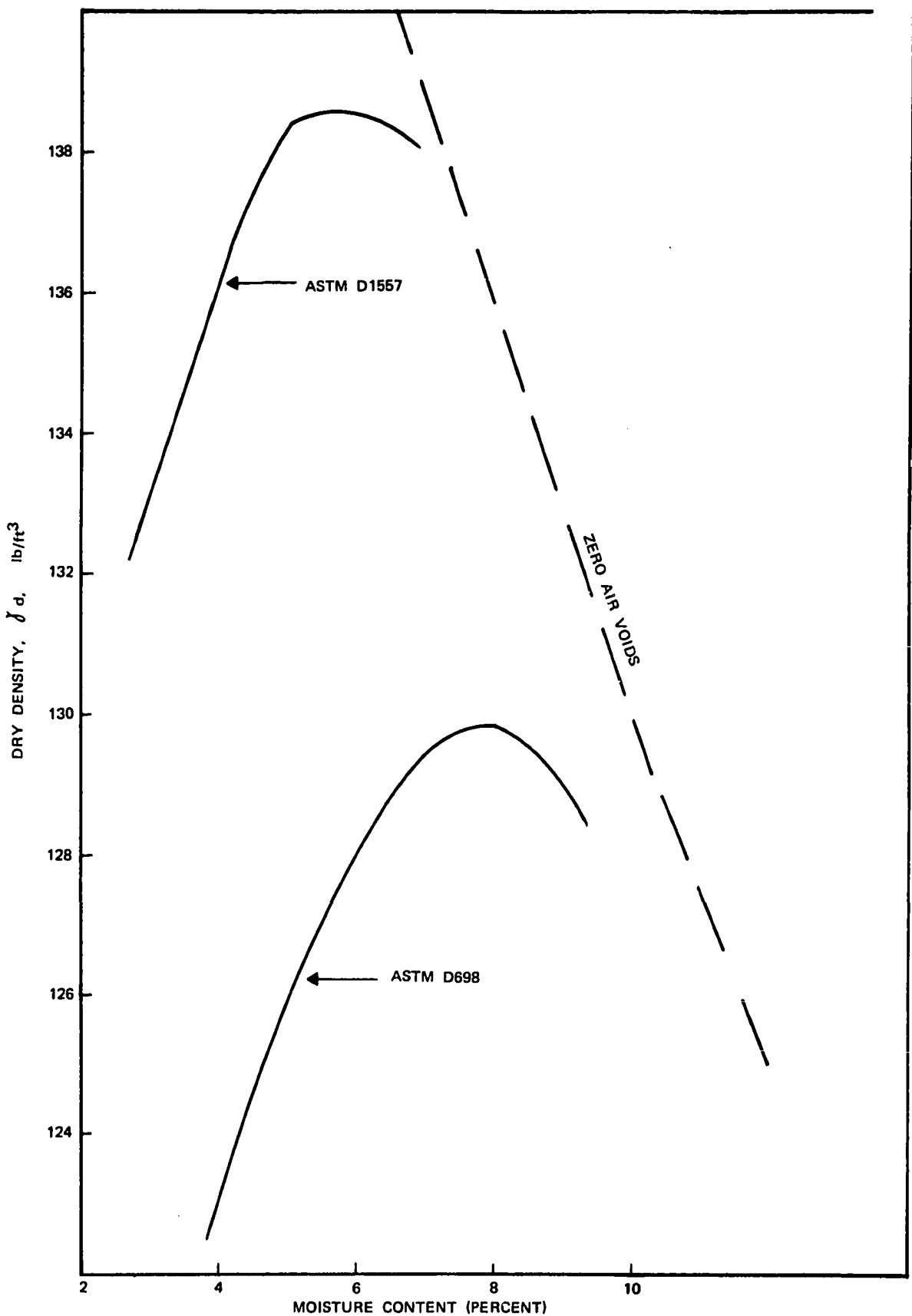


Figure 4.2  
Moisture-Density Curves for Crushed Stone Material

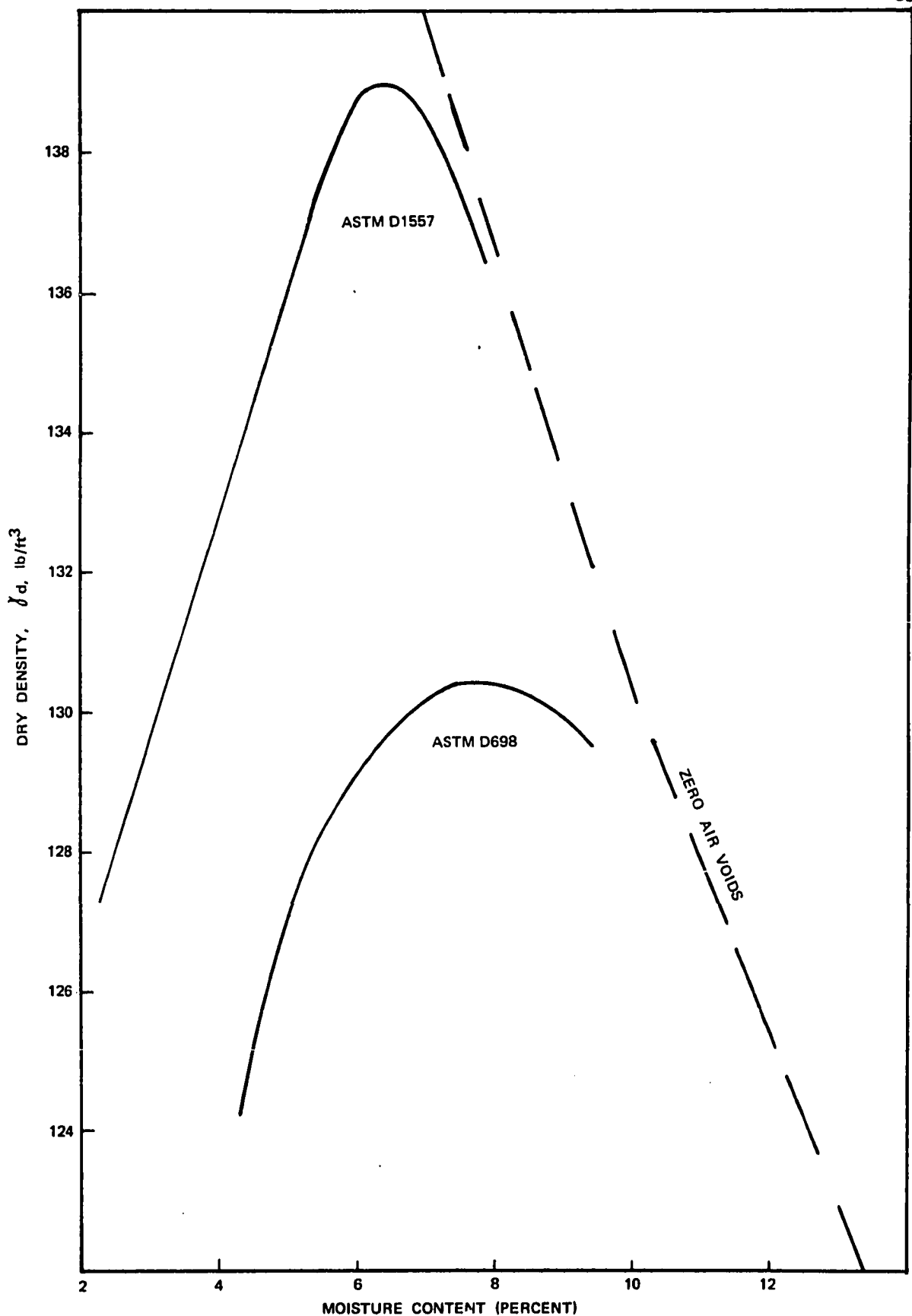


Figure 4.3  
Moisture-Density Curves for Gravel

used (maximum particle size for CA-6 is in excess of 1.0 inch). The standard 2:1 height to diameter ratio was necessary in order to minimize the end effects on deformations measured at the center of each specimen (22)(39).

Table 4.2  
Test Specimens

Specimen	Material	Density, lb/ft <sup>3</sup>	% Moisture	% Saturation
HD-1	Crushed Stone	138.0	High	5.7
MD-1	Crushed Stone	134.0	Intermediate	6.3
LD-1	Crushed Stone	130.0	Low	7.0
HD-2	Gravel	139.4	High	6.3
MD-2	Gravel	134.0	Intermediate	6.5
LD-2	Gravel	131.0	Low	6.7
HD-3	Blend	139.5	High	6.3
MD-3	Blend	134.5	Intermediate	6.8
LD-3	Blend	131.0	Low	7.2

All specimens were prepared directly on the chamber base plate by drop-hammer compaction in a 6 x 12 inch split mold which attached to the base plate by tie rods and wing nuts. The hammer had a 2.0 inch diameter striking face, a weight of 10 pounds, and a fall of 18 inches. Specified densities were attained by varying the number of layers per specimen and the number of blows per layer. The compaction equipment is pictured in Figure 4.4. It should be noted that the ports on either side of the mold were necessary so that a rubber membrane could be placed in the mold prior to compaction. A vacuum was applied through the ports, which held the membrane tightly against the inside of the mold; thereby preventing the membrane from being pinched into the specimen. After compaction the mold was removed, a thin film of silicone grease placed over the inevitable punctures in the membrane, and a second membrane dropped into

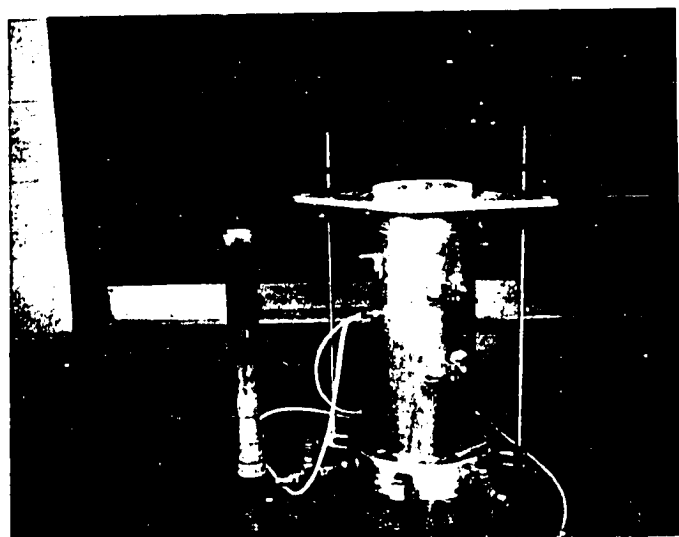


**Figure 4.4**  
**Compaction Mold and Drop Hammer**

place by means of the membrane jacket. The double membrane thickness was deemed necessary to prevent leakage and to maintain a stable moisture regime during the course of the test. The efficiency of the double membrane is verified by the fact that moisture contents determined for each specimen after testing differed by less than 0.5 to 0.6 percent from the original values.

Determination of the number of layers and blows per layer necessary to acquire a given specimen density was predicated on the compaction energy per inch of specimen height delivered in the compaction control test. The compaction energy was computed as the product of the weight of the hammer and the height of fall divided by the layer thickness. Then the total energy input for the 12-inch high test specimens was computed, the number of layers selected, the energy per layer computed, and the number of blows per layer determined as the quotient of the compaction energy for the layer and the energy per blow (10-lb hammer x 18-inch drop = 180 inch pounds). With these figures as starting points, several specimens were prepared in which the numbers of blows per layer and number of layers were varied. These tests revealed that preparing the high density specimens in 5 layers with 90 blows per layer would yield densities very close to the maximum dry density obtained from the ASTM D1157 method. The low density specimens were compacted in 4 layers with 40 blows per layer, a process which produced densities closely approximating the maximum dry density from the ASTM D698 method. Furthermore, specimens compacted in 4 layers with 60 to 65 blows per layer yielded the intermediate level of density shown in Table 4.2.

Early in the program there was concern that the drop hammer method of compaction might cause unacceptable particle degradation. Gradation analysis of the specimens after testing in the triaxial apparatus indicated that only insignificant changes in aggregate grading had occurred. Figure 4.5 shows

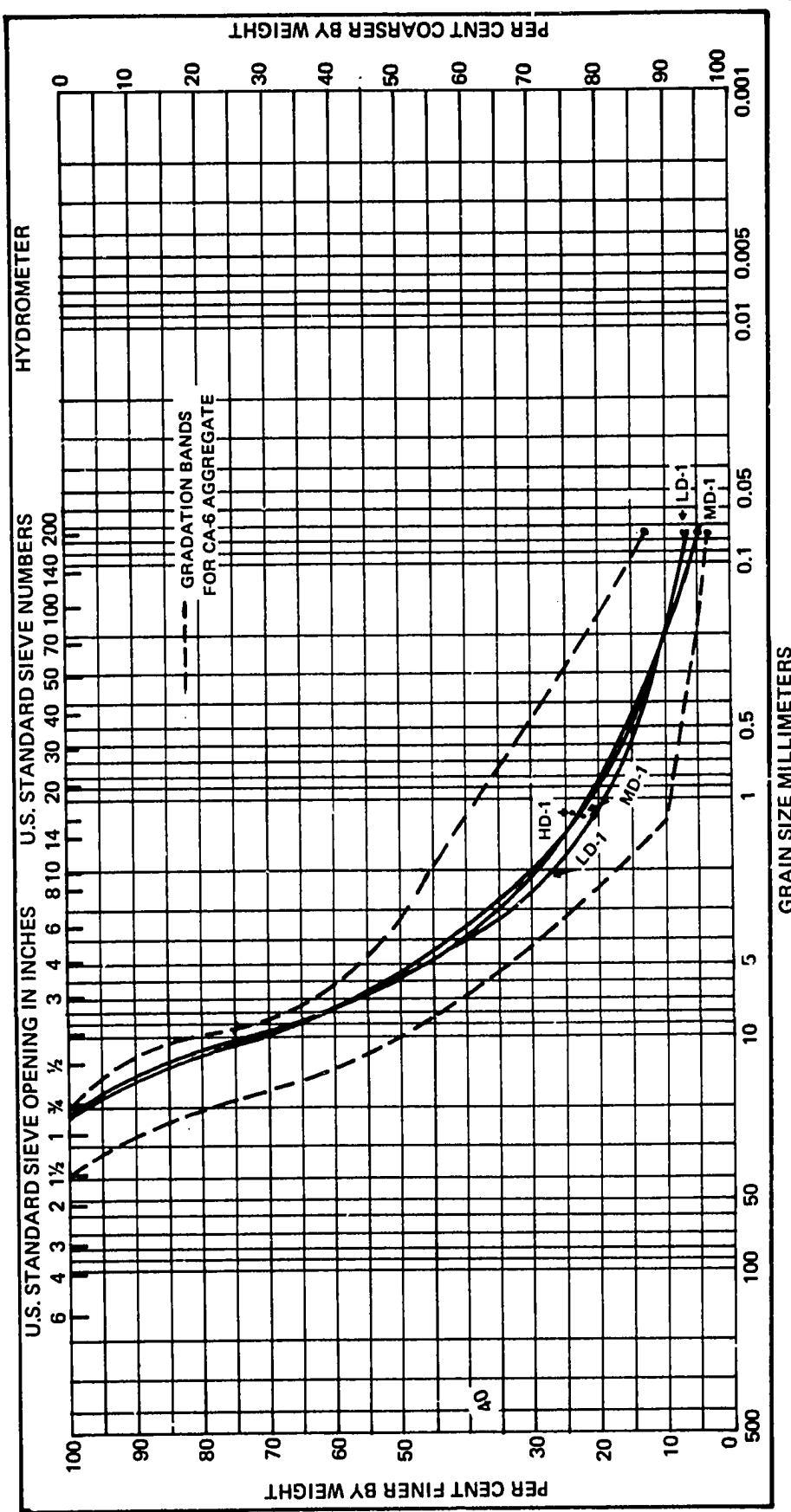


Figure 4.5  
Final Gradation of Crushed Stone Specimens after Testing

the final grain size distribution for the crushed stone specimens and the gradation bands for CA-6 aggregate.

#### 4.3 Testing Equipment and Instrumentation

##### 4.3.1 Testing Equipment

The laboratory investigation portion of this study was conducted at the U. S. Army, Corps of Engineers, Construction Engineering Research Laboratory, USA CERL, at Champaign, Illinois. The unique aspect of this study (i.e., the requirement that the triaxial chamber confining pressure be varied simultaneously with the axial load) was satisfied by a closed-loop testing system built by MTS Systems Corporation and shown schematically in the block diagram of Figure 4.6. The axial stress was applied to the specimen through a hydraulic-actuated piston. The chamber pressure was varied by means of a hydraulic-actuated piston which reacted directly on the chamber fluid, water in this case. Program input was provided by two function generators, one connected to the axial load controller and the other connected to the confining pressure controller. It was necessary to use two function generators to allow for a slight delay in the confining pressure pulse which was caused by compressibility of the chamber fluid and friction loss in the line connecting the chamber and the chamber pressure supply. This procedure made it possible to apply lateral and axial stress pulses to the specimen simultaneously.

##### 4.3.2 Instrumentation

The axial load was monitored by a load cell mounted on the test frame above the triaxial chamber. The maximum capacity for the load cell was 2,000 pounds. Chamber pressure was monitored by a 100 psi maximum pressure transducer installed at the base of the chamber. Axial deformation was measured by two

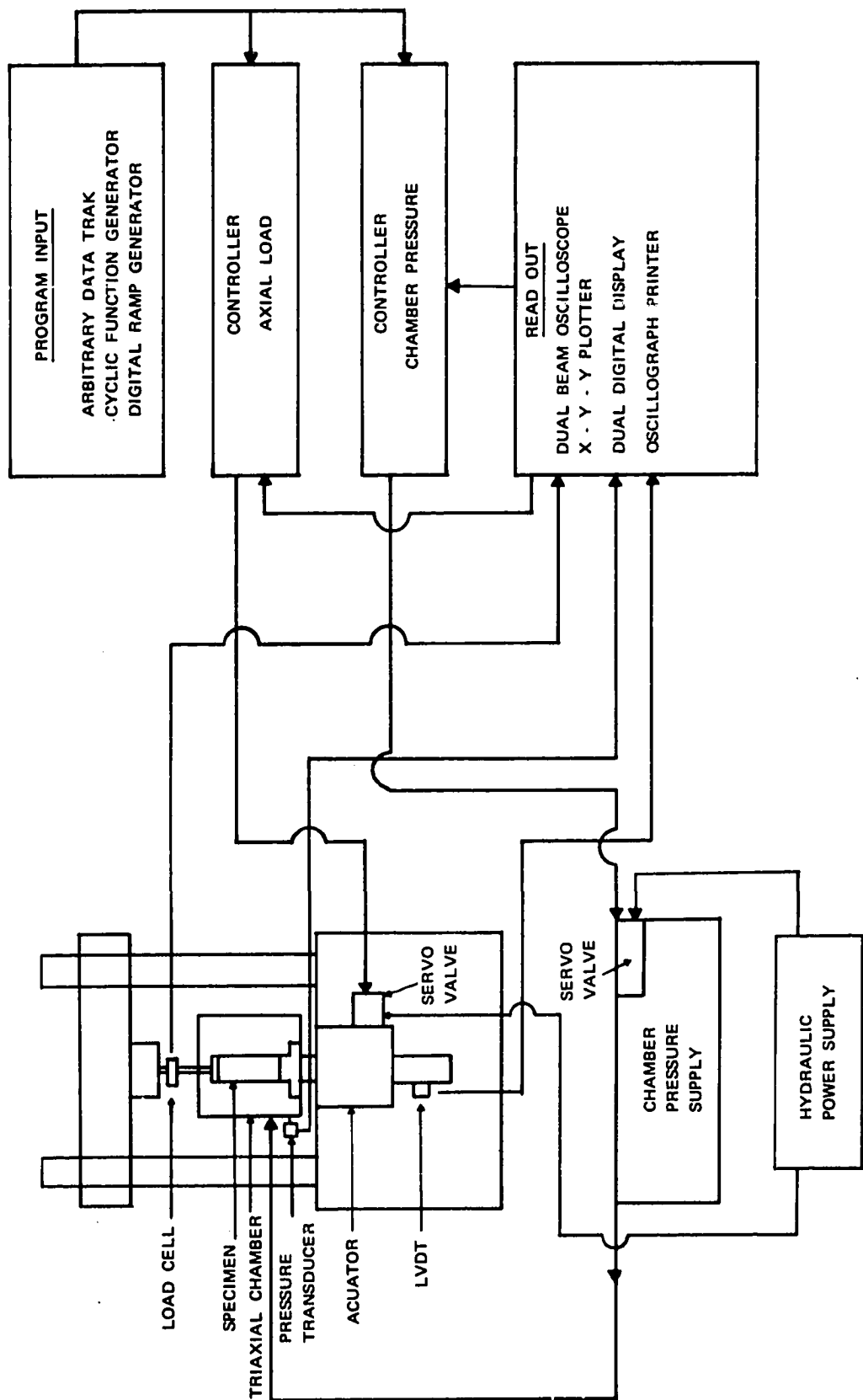
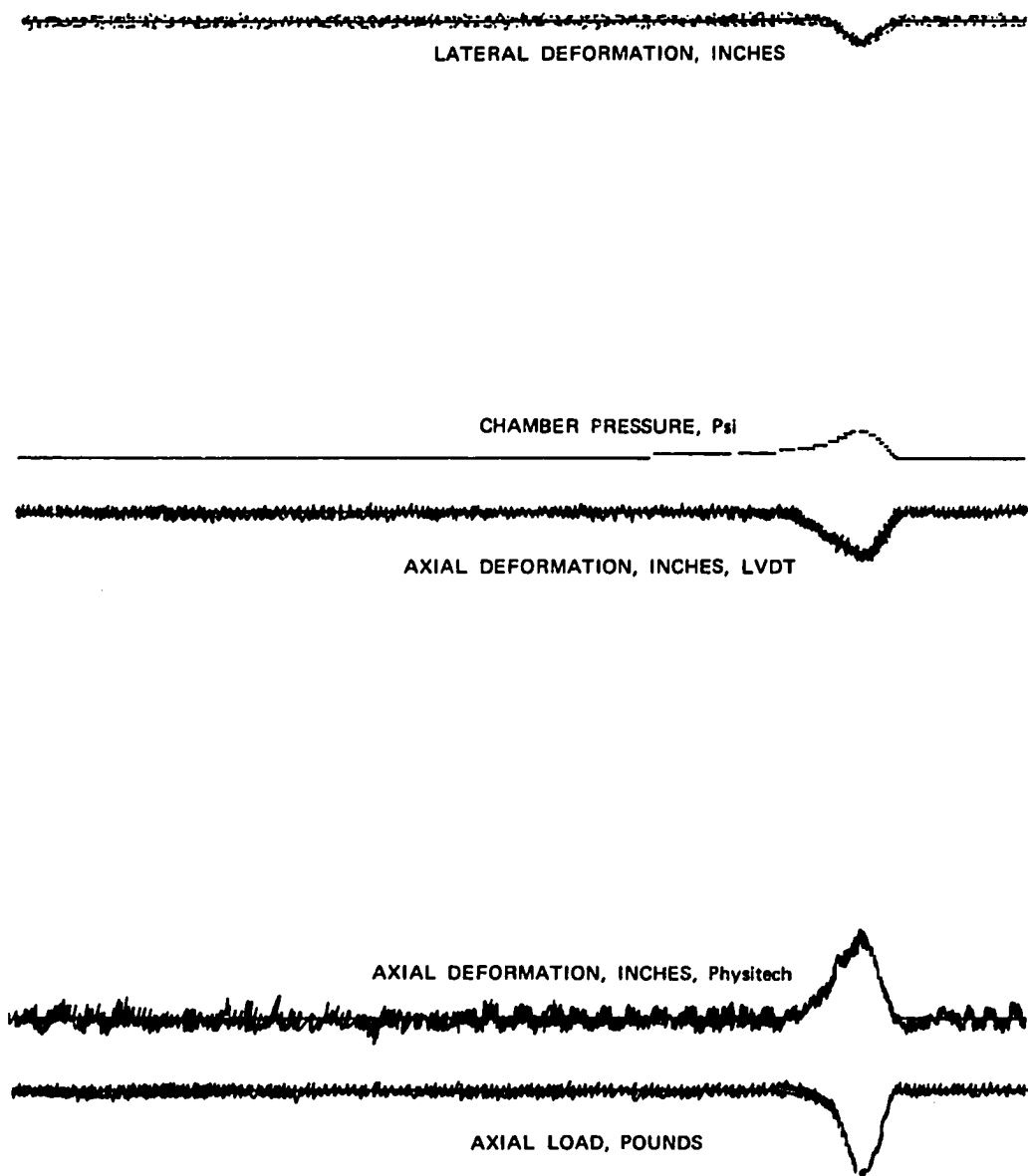


Figure 4.5  
Schematic of Closed-Loop Testing System

Physitech optical trackers. Targets for the trackers consisted of two one and one-half inch long strips of tape, one black and one white, mounted next to each other to provide a contrast for the tracker to sense. One target was three inches below the top of the specimen and the other was three inches above the bottom. Thus, axial deformations were measured over the central half of the specimen. The tape targets were held to the outer membrane by rubber cement. It was observed that the membrane was firmly molded to the specimen surface by the chamber pressure; so little or no error was induced in the observed displacements by mounting the targets on the membrane. This method also had the advantage of eliminating any local stiffening effects that might be brought about by rigid LVDT mounts, as discussed by Barksdale and Hicks (11).

Radial deformation was measured by Bison sensors (4-inch diameter, disk-shaped coils of wire) which were mounted at specimen mid-height and held in place by a two inch wide rubber strip cut from a triaxial membrane. The separation of the sensors affects the electro-magnetic coupling between them. A change in the sensor spacing results in a bridge unbalance; so an inductance bridge may be used to obtain output voltage as a function of displacement. Moisture and temperature effects are negligible provided the sensor leads are waterproofed. In addition, the effects of nearby metal objects can be accounted for by proper calibration procedures.

A dial gage mounted on top of the triaxial chamber and an LVDT on the actuator of the test frame were used to monitor non-recoverable deformations and provided a backup system for obtaining resilient strain data. All stress and deformation data were recorded on a Varian 8-track oscillograph printer. Figure 4.7 is a sample of typical output.



**Figure 4.7**  
Typical Output from Oscillograph Printer

#### 4.3.3 Triaxial Chamber

Certain requirements of this study necessitated the fabrication of a special cylindrical triaxial test chamber. The optical tracker required that the cylinder be made of clear plexiglass so that the targets could be viewed unobstructed. A port was placed on the base plate for attachment of the chamber pressure transducer. Two large ports were placed on the upper plate of the chamber. The first accommodated the 1.1 inch diameter chamber pressure line, and the second was fitted with a hermetic seal to allow egress of the two Bison sensor cables. Figures 4.8 and 4.9 show the triaxial chamber, specimen, and instrumentation.

#### 4.4 Test Sequence

##### 4.4.1 Preliminary Tests

Hicks (31) reported that the resilient stress-strain characteristics of granular materials were virtually the same after 50 to 100 load repetitions as after 25,000 repetitions. He also found that different stress levels could be applied in any sequence without significantly affecting the results and that there was little or no effect of load duration for pulse times between 0.10 and 0.25 seconds. To verify these results for the variable confining pressure condition it was necessary to perform a series of preliminary tests on the crushed stone and gravel specimens.

Specimens of each material were subjected to 10,000 stress repetitions at each of two stress levels. Stress duration was 0.15 seconds. The purpose of these tests was to determine if the resilient response would undergo significant changes as the number of stress repetitions increased. Test results indicated that the response measured after 10 to 20 stress repetitions was representative of the response after several thousand repetitions, provided the specimen had



**Figure 4.8**  
**Triaxial Chamber, Specimen, and Instrumentation**

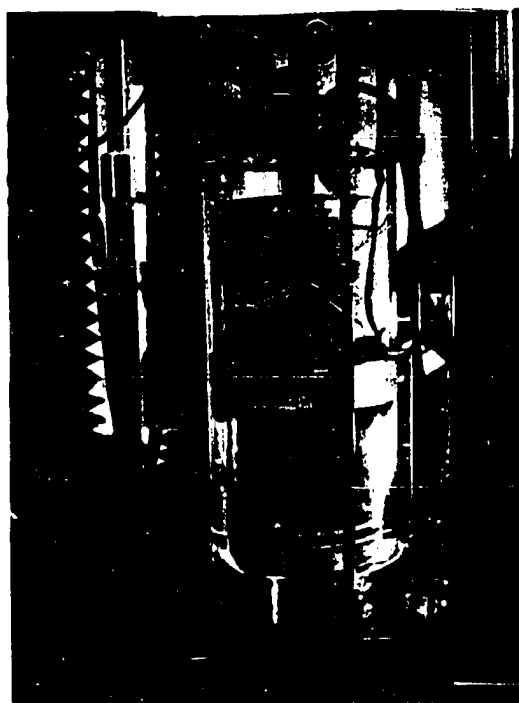


**Figure 4.9**  
**Close-up View of Specimen in Triaxial Chamber**

been conditioned for approximately 1,000 repetitions to eliminate any seating problems between the load platens and the specimen.

The effects of stress duration were investigated by subjecting specimens of each material to 100 stress repetitions each at pulse durations varying from 0.10 second to 1.0 second for the variable confining pressure condition and durations varying from 0.04 second to 1.0 second with constant confining pressure. It was found that the test equipment was unable to cycle the confining pressure in pulses shorter than about 0.10 second, and the optimum pulse time was about 0.15 second for the range of confining pressures used in the primary tests. However, both types of tests yielded data that showed the resilient response to be virtually constant for all pulse times utilized.

Because various levels of confining pressure and axial stress were to be applied to the specimens during the primary test phase, it was deemed necessary to determine whether the order in which the stresses were applied would significantly affect the results. To do this, a stress sequence test was accomplished in which 100 repetitions each of various stress levels were applied in increasing and decreasing sequences. In each case, the axial stress was maintained at one level, and the peak value of  $\sigma_3$  was changed to give different stress ratios. For example, in the increasing sequence the first stress level was  $\sigma_3 = 7$  psi and  $\sigma_1 = 28$  psi. The next level was  $\sigma_3 = 4$  psi and  $\sigma_1 = 28$  psi. Then the specimen was retested at the initial stress level. The decreasing stress sequence had the same initial and final levels, but the intermediate level was  $\sigma_3 = 11$  psi and  $\sigma_1 = 28$  psi. The stress sequence test revealed that the order in which the stress levels were applied to the specimens was of little significance in determining the resilient responses of crushed stone or gravel.

#### 4.4.2 Primary Tests

On the basis of results of the preliminary tests, it was decided to subject each of the 9 specimens (3 materials, 3 density levels) to 100 stress repetitions at each of a range of stress levels. A stress pulse duration of 0.15 seconds was chosen since the test equipment could most efficiently apply the entire range of confining pressure pulses at this duration. In addition, the stress duration tests showed that there was negligible change in the resilient response of unbound granular materials with variations in stress duration. The range of stress levels was chosen to most closely approximate those found in typical pavement sections. At each stress level, each specimen was tested at constant confinement and with variable confining pressure. The stress analysis, as reported in Chapter 3, revealed that one stress pulse shape, the half-sinusoid, could be used to adequately simulate both the major and minor principal stresses. Accordingly, all specimens were subjected to axial and confining pressure pulses of this shape. Moreover, since the literature survey indicated that load frequencies of 20 to 30 repetitions per minute were common (30)(61), one frequency, 20 repetitions per minute, was utilized throughout this study. Details of all tests are summarized in Table 4.3. Tests results are discussed in Chapter 5.

Table 4.3

## TEST SCHEDULE

Specimen	Material	Density Level	Load Duration, Second	Number Repetitions	$\sigma_3$ psi	$\sigma_1$ psi	$\sigma_1/\sigma_3$
<b>I. Preliminary Tests</b>							
<b>a. Stress History</b>							
SH-1	Crushed Stone	High	0.15	10000 10000	7 10	28 30	4 3
SH-2	Gravel	High	0.15	10000 10000	10 5	30 30	3 6
<b>b. Stress Sequence</b>							
SH-1	Crushed Stone	High	0.15	100 100 100 100 100	8 12 8 4 8	24 24 24 24 24	3 2 3 6 3
SH-2	Gravel	High	0.15	100 100 100 100 100	7 11 7 4 7	28 28 28 28 28	4 2.5 4 7 4
<b>c. Load Duration</b>							
Constant confining pressure				0.04, 0.07 0.10	100 ea.	7	28
SH-2				0.15, 0.25, 0.5, 1.0			
Variable confining pressure SH-1 and SH-2				0.1, 0.15, 0.25, 0.5, 1.0	100 ea.	7	28

Table 4.3 (con't.)

## TEST SCHEDULE

<u>II Primary Tests</u>		$\sigma_3$ , psi	$\sigma_1$ , psi	$\sigma_1/\sigma_3$	Confining Pressure
All Specimens	0.15 sec	100 repetitions			
		2	8	4	Variable
		2	12	6	Variable
		2	16	8	Variable
		2	8	4	Constant
		2	12	6	Constant
		2	16	8	Constant
		5	10	2	Constant
		5	15	3	Constant
		5	25	5	Constant
		5	35	7	Constant
		5	45	9	Constant
		5	10	2	Variable
		5	15	3	Variable
		5	25	5	Variable
		5	35	7	Variable
		5	45	9	Variable
		8	12	1.5	Variable
		8	24	3	Variable
		8	40	5	Variable
		8	56	7	Variable
		8	12	1.5	Constant
		8	24	3	Constant
		8	40	5	Constant
		8	56	7	Constant
		11	22	2	Constant
		11	44	4	Constant
		11	66	6	Constant
		11	22	2	Variable
		11	44	4	Variable
		11	66	6	Variable
		15	25	1.6	Variable
		15	45	3	Variable
		15	60	4	Variable
		15	75	5	Variable
		15	25	1.6	Constant
		15	45	3	Constant
		15	60	4	Constant
		15	70	4.7	Constant

## CHAPTER 5

### PRESENTATION AND DISCUSSION OF RESULTS

#### 5.1 Methods of Computing the Resilient Modulus, $E_r$ , and Resilient Poisson's Ratio, $\nu_r$

---

Figure 4.7, page 91, shows the form of the raw data output from the oscillograph printer. The instrumentation was calibrated to yield displacements in inches, chamber pressure in pounds per square inch, and axial load in pounds. It was necessary to convert the displacements, axial and radial, to strains by dividing the peak value of the displacement pulse by the gage length. Gage lengths for axial strains corresponded to the Physitech target spacing, and for radial strains the gage length was equal to the specimen diameter since the Bison sensors were placed 180 degrees apart on the specimen circumference. Axial load was transformed to stress by dividing the peak value of the load pulse by the cross sectional area of the specimen.

The resilient modulus, as computed from results of constant confining pressure triaxial tests (hereafter referred to as the CCP test) is defined as the ratio of the repeated deviator stress,  $\sigma_1 - \sigma_3$ , to recoverable axial strain,  $\epsilon_a$ . The resilient Poisson's ratio is defined as the ratio of recoverable lateral strain,  $\epsilon_\ell$ , to recoverable axial strain,  $\epsilon_a$ . This method of computation is the same as would apply to an isotropic, linear elastic material under uniaxial stress conditions. The nature of the CCP test, in which the specimen is allowed to consolidate under a constant chamber pressure before the dynamic increment of stress is applied only in the axial direction, has led to general acceptance of this method of determining the resilient parameters.

However, the nature of the variable confining pressure triaxial test (hereafter referred to as the VCP test), in which the lateral stress is applied dynamically

and simultaneously with the axial stress, is such that to compute the resilient modulus as described above would be to ignore the effect of Poisson's ratio on axial strains and would tend to overestimate the modulus. Therefore, it was necessary to use the three dimensional stress-strain relations for isotropic, linear elastic material, Equations 5.1:

$$\epsilon_a = \frac{1}{E_r} (\sigma_a - 2 v_r \sigma_r) \quad (5.1)$$

$$\epsilon_l = \frac{1}{E_r} (\sigma_r - v_r (\sigma_a + \sigma_r))$$

where,  $\sigma_a$  = axial stress

$\sigma_r$  = radial stress

$\epsilon_a$  = recoverable axial strain

$\epsilon_l$  = recoverable lateral (radial) strain

$E_r$  = resilient modulus

$v_r$  = resilient Poisson's ratio

It should be noted that, under the assumed condition of axial symmetry of the triaxial test, tangential stresses and strains are equal to radial stresses and strains. On this basis, the resilient parameters,  $E_r$  and  $v_r$ , were calculated for any individual combination of stresses applied during the VCP test by substituting the peak values of applied stresses and resulting strains into Equations 5.1, a procedure which obviously yields secant values of the parameters. It should also be noted that, for a given stress state, stresses and strains in granular media may be related by the psuedo-elastic constants of Equation 5.1. This approach is consistent with the concept of resilient behavior of such materials. In effect, the assumption is made that for any individual state of stress the material behaves linearly and elastically. The assumption of

elastic behavior is verified by the fact that the observed deformations during the VCP test as well as the CCP test were almost completely recoverable and instantaneous.

As discussed in Chapter 2, when the stress-deformation relations for granular materials are compared for a range of stress levels it is obvious that  $E_r$  is not constant but varies with the state of stress. Therefore, this nonlinear, stress dependent behavior can be characterized by the regression line developed from statistical analysis of the values of  $E_r$  calculated for a range of stresses. In such an analysis  $E_r$  is the dependent variable and the independent variable is some appropriate stress parameter,  $\sigma_3$  or  $\theta$ , the sum of the principal stresses. The stress dependent nature of  $E_r$  was confirmed by the results of the statistical analysis, discussed in Section 5.2

As an illustration of the necessity of applying the above mentioned procedure for calculating  $E_r$ , consider the following data taken from the VCP test on specimen HD-1.

$$\sigma_r = 8.0 \text{ psi} \quad \epsilon_l = .000290 \text{ in/in}$$

$$\sigma_a = 39.37 \text{ psi} \quad \epsilon_a = .001100 \text{ in/in}$$

Use of the uniaxial stress-strain relation results in the following calculated values of  $E_r$  and  $v_r$ :

$$E_r = \frac{\sigma_a}{\epsilon_a} = \frac{39.37}{.001100} = 35,800 \text{ psi}$$

$$v_r = \frac{\epsilon_l}{\epsilon_a} = \frac{.000290}{.001100} = 0.26$$

However, Equations 5.1 yield:

$$E_r = 30,600 \text{ psi}$$

$$v_r = 0.36$$

In this case, by ignoring the three dimensional state of stress the modulus is overestimated by 17 per cent and Poisson's ratio is underestimated by 28 per cent. On the basis of the foregoing discussion it was decided to compute the resilient parameters for the CCP test from the uniaxial relations and those for the VCP test from Equations 5.1.

### 5.2 Statistical Analysis of Data

No statistical analysis was applied to the results of the preliminary tests because the purpose of these tests was to aid in establishing procedures for the primary test series by observing changes in the material parameters as induced by such factors as stress duration, numbers of repetitions, and stress sequence rather than to develop predictive equations.

However, statistical analysis of the data gathered during the primary test series was necessary in order to develop predictive equations for the resilient parameters. The statistical procedures included linear and nonlinear regression analysis and were conducted using computer programs available at USACERL. The first step was to attempt to correlate the calculated values of  $E_r$  and  $\nu_r$  from each specimen with various stress parameters. Regression constants, correlation coefficients and standard errors were determined for several models in which  $E_r$  was the dependent variable and the independent variables ranged from  $\sigma_3$ , to  $\sigma_1 - \sigma_3$ , to  $\sigma_1/\sigma_3$ , to  $\theta$  and combinations of these. Similar models were attempted for  $\nu_r$ . The results for each specimen for each model were tabulated so that correlation coefficients and standard errors could be compared.

All of these models in which both principal stresses were considered yielded very similar correlation coefficients and standard errors. For example the model  $E_r = b_0 + b_1 \sigma_3 + b_2 (\sigma_1 - \sigma_3)$  had a range of correlation coefficients

from 0.866 to 0.991. The model  $E_r = b_0 + b_1 \sigma_3 + b_2 (\sigma_1/\sigma_3)$  had a very similar range of correlation coefficients. The standard errors of the two models were also of like magnitude. However, the model  $\ln E_r = b_0 + b_1 \ln \sigma_3$  had a considerably larger range of correlation coefficients, 0.490 to 0.933, and considerably higher standard errors.

It was apparent that the model in which the natural log of  $E_r$  is related to the log of  $\theta$ , the sum of the principal stresses, was superior to the other models for several reasons. First, the correlation coefficients and standard errors were comparable to those of the models consisting of more than one independent variable. Second, it is considerably easier to graphically present and compare the results of tests on more than one specimen if only one independent variable is present. In addition, this model will account for all three principal stresses when used in pavement analyses. It should also be noted that the correlation between  $\ln E_r$  and  $\ln \theta$  was significant at the 99.9 per cent level ( $\alpha = 0.001$ ) for all specimens, both CCP and VCP test data. The form of this model is as follows:

$$\ln E_r = b_0 + b_1 \ln \theta \quad (5.2)$$

where,  $b_0$  and  $b_1$  are the constants from linear regression analysis and  $\theta$  is the sum of the principal stresses,  $\sigma_1 + 2\sigma_3$ . One other model was selected, since  $E_r$  has been presented as a function of  $\sigma_3$  by other investigators (10)(31)(61):

$$\ln E_r = b_0 + b_1 \ln \sigma_3 \quad (5.3)$$

where,  $b_0$  and  $b_1$  are as defined above, and  $\sigma_3$  is the minor principal stress.

Since a rather wide range of axial stresses were applied at each value of  $\sigma_3$  in the triaxial tests and since the granular materials were affected by changes in the major principal stress, it was not surprising that the model of Equation 5.3 had consistently lower correlation coefficients and higher

standard errors than the previous model.

In a similar manner a model for Poisson's ratio was selected:

$$\nu_r = b_0 + b_1 (\sigma_1/\sigma_3) + b_2 (\sigma_1/\sigma_3)^2 + b_3 (\sigma_1/\sigma_3)^3 \quad (5.4)$$

where, the b coefficients are regression constants and  $\sigma_1/\sigma_3$  is the principal stress ratio.

It was desired to present the models for the resilient modulus in a form that has been proposed by other investigators. Accordingly the linear logarithmic relations of Equations 5.2 and 5.3 were transformed by nonlinear regression techniques into the following models:

$$E_r = K\theta^n \quad (5.5a)$$

and

$$E_r = K' \sigma_3^{n'} \quad (5.5b)$$

where, K, n, K' and n' are constants from nonlinear regression analysis and  $\theta$  and  $\sigma_3$  are as previously defined. The final results are presented later in this chapter. Standard errors and correlation coefficients for each specimen are summarized in Table 5.3. Furthermore, the raw data from the primary test series are included in Appendix A.

### 5.3 Results of the Preliminary Test Series

As a guide in planning the primary test series it was necessary to first investigate the influence of such factors as stress history, stress duration, and stress sequence on the resilient response of granular materials. A knowledge of these effects was required as a first step in determining the numbers of repetitions of each stress level to be applied, the number of specimens to be tested, the order in which stresses should be applied, and the duration

of the applied stress pulses.

### 5.3.1 Stress History Effects

As discussed in Chapter 2, Hicks (31) found that the resilient response of granular materials measured after 50 to 100 stress repetitions was indicative of the response after 25,000 stress repetitions. Consequently, it was decided that, for sake of completeness, a limited test series should be conducted to verify his results for the materials used in this program. Table 4.3, page 96, summarizes the stress levels and numbers of repetitions utilized. Figure 5.1 shows the variation in recoverable axial strains as a function of stress repetitions for the crushed stone specimen SH-1. Note that nowhere does the variation in axial strain exceed about 10 per cent. Also, if the specimens are initially conditioned with 1000 stress repetitions to eliminate poor seating between the specimen and load platens the maximum variation is about 5 per cent.

Figure 5.2 shows the variation in resilient modulus with stress repetitions for the gravel specimen, SH-2. Again, the effects of number of stress repetitions would appear to be minimal, at least for the range of repetitions applied in this study. It should be mentioned that the primary purpose of this study was to assess the effects of non-constant lateral stresses on granular materials at specified conditions of moisture content and density rather than to determine the long term effects of large numbers of stress repetitions. Hence, the results of the stress history tests were accepted as verification of Hick's findings, and for subsequent tests the resilient response at each stress level was measured after 100 stress repetitions. Each specimen was initially conditioned for 1000 stress repetitions to minimize the seating effects mentioned previously.

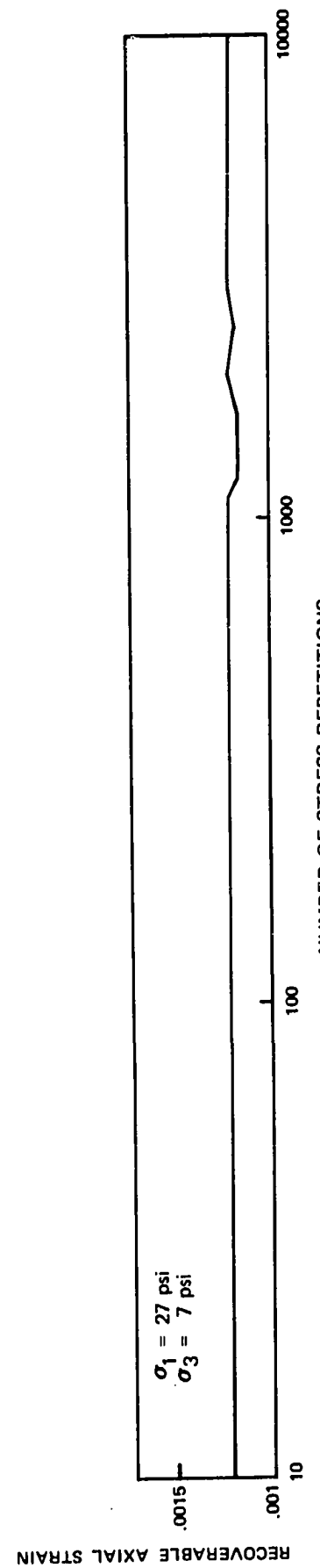


Figure 5.1  
Variation in Recoverable Axial Strain with Number of Stress  
Repetitions, Crushed Stone Specimen SH-1

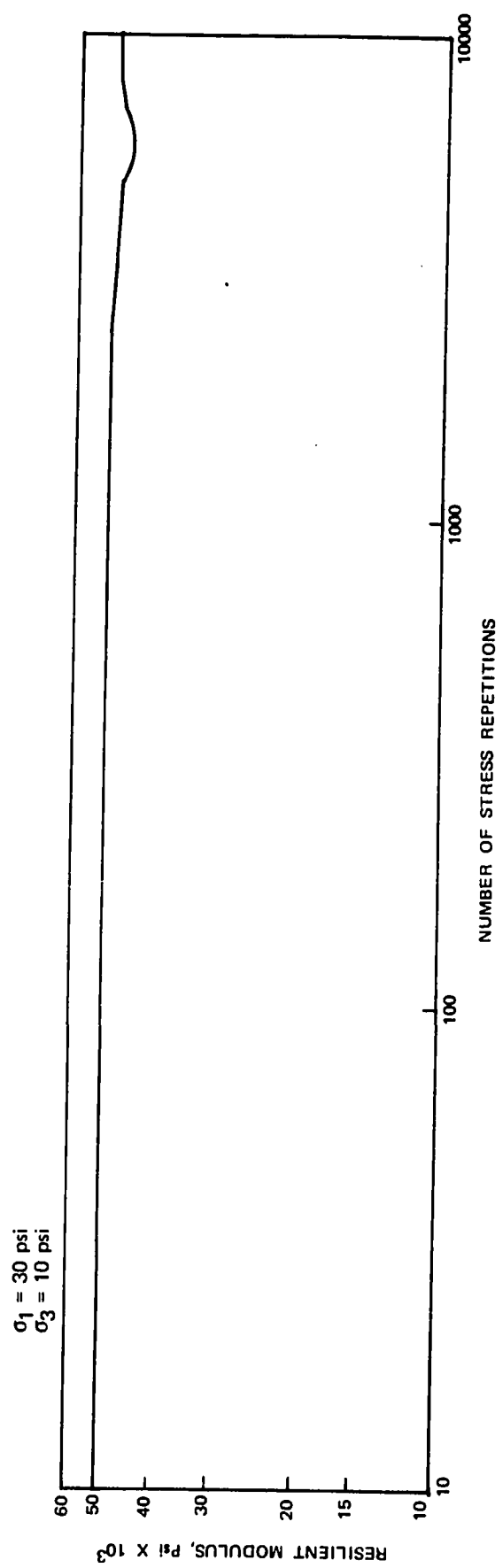


Figure 5.2  
Variation in Resilient Modulus with Number of Stress Repetitions,  
Gravel Specimen SH-2

### 5.3.2 Stress Pulse Duration Effects

Because a pavement structure will be used by vehicles traveling at a range of speeds, and because limitations of time and expense dictated that one pulse duration be used for the primary test series, it was deemed necessary to subject specimens of the crushed stone and gravel to a range of stress pulse durations in order to ascertain if appreciable errors would be introduced by the use of only one pulse time.

Table 5.1 shows the variation in resilient modulus and resilient Poisson's ratio for VCP test stress durations varying from 0.10 second to 1.0 second. Note that for the crushed stone specimen the resilient modulus decreased by about 2 per cent as pulse time increased to 1.0 second, and the maximum variation in Poisson's ratio was about 5 per cent. Also, only slight changes were observed in the response of the gravel specimen.

To observe the effects of even shorter stress durations, the gravel specimen was tested under CCP test conditions with stress durations varying from 0.04 second to 1.0 second. The results are included in Table 5.1. Here again the negligible effects of pulse length are obvious.

On the basis of the data in Table 5.1 it was concluded that a stress pulse duration of 0.15 second could be used throughout the primary test series without incurring significant testing errors.

### 5.3.3 Stress Sequence Effects

Because of the non-destructive nature of the repeated load triaxial test conducted at the stress levels applied in this study it was possible to measure the response of a single specimen to all stress levels; thereby eliminating specimen-to-specimen variations in density, moisture content, and dimensions, except for those variations planned as part of the study. It was necessary,

TABLE 5.1  
RESULTS OF STRESS PULSE DURATION TESTS

Material Type	$\sigma_3$ , psi	$\sigma_1$ , psi	Test Type	Pulse Duration, Sec.	$E_r$ , psi	$v_r$
Crushed Stone	7.0	27.6	VCP	0.10	24346	.36
Crushed Stone	7.0	27.6	VCP	0.15	24258	.35
Crushed Stone	7.0	27.6	VCP	0.25	23942	.34
Crushed Stone	7.0	27.6	VCP	0.50	23942	.34
Crushed Stone	7.0	27.6	VCP	1.00	23819	.35
Gravel	7.2	27.8	VCP	0.10	57018	0.27
Gravel	7.2	27.8	VCP	0.15	57018	0.27
Gravel	7.2	27.8	VCP	0.25	54917	0.27
Gravel	7.2	27.8	VCP	0.50	54917	0.27
Gravel	7.2	27.8	VCP	1.00	54917	0.27
Gravel	7.0	27.5	CCP	0.04	50800	0.47
Gravel	7.0	27.5	CCP	0.07	50800	0.47
Gravel	7.0	27.5	CCP	0.10	50800	0.47
Gravel	7.0	27.5	CCP	0.15	50800	0.47
Gravel	7.0	27.5	CCP	0.25	49100	0.47
Gravel	7.0	27.5	CCP	0.50	49100	0.47
Gravel	7.0	27.5	CCP	1.00	49100	0.47

therefore, to determine if the order in which the stresses were applied would significantly affect the resilient response of a specimen. The results of the stress sequence test, described in Chapter 4, are tabulated in Table 5.2 for the crushed stone and gravel specimens. It should be noted that the term "increasing sequence" refers to the test in which the second applied principal stress ratio was greater than the initial and final ratio. The initial and final stress ratios are identical since the specimen is retested at the original stress level after the intermediate state of stress is applied. The decreasing sequence refers to a lower intermediate stress ratio.

Table 5.2 shows that for the crushed stone specimen, the resilient modulus and Poisson's ratio remained unchanged after the decreasing sequence test. After the increasing sequence test Poisson's ratio was unchanged, but the resilient modulus had decreased by less than 2 per cent. Similar results were obtained for the gravel specimens. Poisson's ratio remained unchanged after each sequence. The resilient modulus increased about 1.5 per cent after the decreasing sequence test and decreased about 3 per cent after the increasing sequence test.

On the basis of the data in Table 5.2 it was concluded that one test sequence could be used for each specimen during the primary test series with little error involved. Accordingly, the stress states shown in Table 4.3, page 96, were applied to each specimen in the order shown, which constituted an increasing test sequence for each level of peak confining pressure. Periodically throughout the test series specimens were retested at previous stress levels, and negligible changes in response were observed.

#### 5.3.4 Summary of Preliminary Test Results

With the completion of the preliminary test series it was possible to design the primary test series so as to incorporate into the results only minimal

TABLE 5.2  
RESULTS OF STRESS SEQUENCE TESTS

Material Type	Stress Level No.	$\sigma_1$ , psi	$\sigma_3$ , psi	$\sigma_1/\sigma_3$	$E_r$ , psi	$v_r$	Sequence
Crushed Stone	1	23.6	8.0	3	22766	0.34	Decreasing
Crushed Stone	2	23.9	12.0	2	28643	0.28	Decreasing
Crushed Stone	3	23.6	8.0	3	22766	0.34	Decreasing
Crushed Stone	1	23.6	8.0	3	22766	0.34	Increasing
Crushed Stone	2	23.8	4.0	6	21940	0.38	Increasing
Crushed Stone	3	23.6	8.0	3	22325	0.34	Increasing
Gravel	1	28.0	7.0	4.0	47280	0.25	Decreasing
Gravel	2	28.0	11.0	2.5	52032	0.12	Decreasing
Gravel	3	28.0	7.0	4.0	48000	0.25	Decreasing
Gravel	1	28.0	7.0	4.0	48000	0.25	Increasing
Gravel	2	27.5	4.0	6.9	40135	0.33	Increasing
Gravel	3	28.0	7.0	4.0	46494	0.25	Increasing

errors due to testing procedures. The conclusions drawn from the preliminary test results were strengthened inasmuch as they confirmed Hicks' (31) conclusions based on similar laboratory tests. In summary, it was decided that any one specimen could be tested over the entire range of stress levels, both VCP and CCP. Also, the resilient material parameters, as determined after 50 to 100 stress repetitions, were known to be indicative of those determined after several thousand repetitions. Furthermore, the stress sequence test confirmed that the various stress states could be applied in any order without introducing significant error into the results, and the stress duration test revealed that one pulse time, 0.15 second, could be used throughout the primary test series. The resilient response of granular materials thus determined would be representative of that of similar materials in a pavement subjected to various vehicular speeds.

#### 5.4 Results of the Primary Test Series

The general purpose of this study was to evaluate the effects of non-constant lateral pressures on the resilient response of granular materials. In addition, the effects of such factors as material type and density were investigated. Furthermore, observations were made concerning plastic (non-recoverable) deformations and anisotropic material behavior.

##### 5.4.1 Effects of State of Stress

The predictive equations for the resilient moduli and resilient Poisson's ratios of the materials tested are summarized in Table 5.3. The resilient modulus is presented as a function of the sum of the principal stresses, (Equation 5.5a), and as a function of  $\sigma_3$ , (Equation 5.5b). Poisson's ratio is presented as a function of the principal stress ratio (Equation 5.4).

TABLE 5.3(a)  
REGRESSION EQUATIONS FOR  $E_r$  FROM PRIMARY TEST DATA

Specimen	Material Type	Test Type	$E_r = f(\theta)$	Correlation Coefficient	Standard Error	$E_r = f(\sigma_3)$	Correlation Coefficient	Standard Error
HD-1	Crushed Stone	VCP	6635 $\theta$ .40	.930**	3144	18010 $\sigma_3$ .28	.669*	6338
MD-1	Crushed Stone	VCP	1793 $\theta$ .70	.992**	1463	8556 $\sigma_3$ .57	.794**	7014
LD-1	Crushed Stone	VCP	2113 $\theta$ .65	.982**	2058	8410 $\sigma_3$ .57	.819**	6227
HD-2	Gravel	VCP	7766 $\theta$ .32	.767**	3996	18480 $\sigma_3$ .19	.515(a)	5338
MD-2	Gravel	VCP	6995 $\theta$ .33	.906**	2202	15738 $\sigma_3$ .23	.664*	3897
LD-2	Gravel	VCP	1613 $\theta$ .69	.973**	2033	7924 $\sigma_3$ .51	.781**	5473
HD-3	Blend	VCP	6891 $\theta$ .45	.980**	2035	18951 $\sigma_3$ .35	.832**	5638
MD-3	Blend	VCP	7725 $\theta$ .33	.981**	1042	15806 $\sigma_3$ .26	.841**	2890
LD-3	Blend	VCP	4562 $\theta$ .43	.856**	3367	14516 $\sigma_3$ .24	.498(a)	5648
HD-1	Crushed Stone	CCP	2376 $\theta$ .69	.997**	1149	12454 $\sigma_3$ .55	.845**	7896
MD-1	Crushed Stone	CCP	4928 $\theta$ .46	.973**	1950	14254 $\sigma_3$ .39	.872**	4115
LD-1	Crushed Stone	CCP	3083 $\theta$ .59	.962**	3132	11068 $\sigma_3$ .53	.909**	4813
HD-2	Gravel	CCP	4596 $\theta$ .50	.741**	8063	11128 $\sigma_3$ .54	.803**	7157
MD-2	Gravel	CCP	8016 $\theta$ .31	.803**	3551	14729 $\sigma_3$ .31	.838**	3247
LD-2	Gravel	CCP	2849 $\theta$ .56	.882**	4289	8517 $\sigma_3$ .55	.916**	3641
HD-3	Blend	CCP	5989 $\theta$ .48	.932**	4254	16433 $\sigma_3$ .45	.922**	4542
MD-3	Blend	CCP	6459 $\theta$ .37	.829**	3977	13379 $\sigma_3$ .37	.873**	3471
LD-3	Blend	CCP	2966 $\theta$ .60	.882**	4962	9079 $\sigma_3$ .58	.914**	4260

(a) Significant at  $\alpha = .05$   
 \* Significant at  $\alpha = .01$   
 \*\* Significant at  $\alpha = .001$

TABLE 5.3(b)  
REGRESSION EQUATIONS FOR  $v_r$  FROM PRIMARY TEST DATA

Specimen	Material Type	Test Type	$v_r = f(\sigma_1/\sigma_3)$	Correlation Coefficient	Standard Error
HD-1	Crushed Stone	VCP	.62 - .19 $(\sigma_1/\sigma_3)$ + .04 $(\sigma_1/\sigma_3)^2$ - .002 $(\sigma_1/\sigma_3)^3$	.907**	.026
MD-1	Crushed Stone	VCP	.47 - .07 $(\sigma_1/\sigma_3)$ + .02 $(\sigma_1/\sigma_3)^2$ - .001 $(\sigma_1/\sigma_3)^3$	.838***	.045
LD-1	Crushed Stone	VCP	.60 - .14 $(\sigma_1/\sigma_3)$ + .02 $(\sigma_1/\sigma_3)^2$ - .0007 $(\sigma_1/\sigma_3)^3$	.881***	.036
HD-2	Gravel	VCP	-.12 + .45 $(\sigma_1/\sigma_3)$ - .09 $(\sigma_1/\sigma_3)^2$ + .005 $(\sigma_1/\sigma_3)^3$	.645**	.085
MD-2	Gravel	VCP	.46 + .01 $(\sigma_1/\sigma_3)$ - .01 $(\sigma_1/\sigma_3)^2$ + .002 $(\sigma_1/\sigma_3)^3$	.889***	.026
LD-2	Gravel	VCP	.70 - .22 $(\sigma_1/\sigma_3)$ + .04 $(\sigma_1/\sigma_3)^2$ - .002 $(\sigma_1/\sigma_3)^3$	.925***	.027
HD-3	Blend	VCP	.49 + .01 $(\sigma_1/\sigma_3)$ - .01 $(\sigma_1/\sigma_3)^2$ + .001 $(\sigma_1/\sigma_3)^3$	.766***	.037
MD-3	Blend	VCP	.50 - .02 $(\sigma_1/\sigma_3)$ - .003 $(\sigma_1/\sigma_3)^2$ + .0006 $(\sigma_1/\sigma_3)^3$	.561*	.048
LD-3	Blend	VCP	.52 - .07 $(\sigma_1/\sigma_3)$ + .006 $(\sigma_1/\sigma_3)^2$ + .0002 $(\sigma_1/\sigma_3)^3$	.840***	.026
HD-1	Crushed Stone	CCP	-.17 + .30 $(\sigma_1/\sigma_3)$ - .04 $(\sigma_1/\sigma_3)^2$ + .002 $(\sigma_1/\sigma_3)^3$	.895***	.047
MD-1	Crushed Stone	CCP	.29 + .12 $(\sigma_1/\sigma_3)$ - .01 $(\sigma_1/\sigma_3)^2$ + .0006 $(\sigma_1/\sigma_3)^3$	.746***	.060
LD-1	Crushed Stone	CCP	-.01 + .28 $(\sigma_1/\sigma_3)$ - .04 $(\sigma_1/\sigma_3)^2$ + .002 $(\sigma_1/\sigma_3)^3$	.723***	.096
HD-2	Gravel	CCP	-.14 + .46 $(\sigma_1/\sigma_3)$ - .06 $(\sigma_1/\sigma_3)^2$ + .003 $(\sigma_1/\sigma_3)^3$	.429(a)	.208
MD-2	Gravel	CCP	.25 - .22 $(\sigma_1/\sigma_3)$ + .04 $(\sigma_1/\sigma_3)^2$ - .002 $(\sigma_1/\sigma_3)^3$	.654**	.144
LD-2	Gravel	CCP	-.04 + .32 $(\sigma_1/\sigma_3)$ - .05 $(\sigma_1/\sigma_3)^2$ + .003 $(\sigma_1/\sigma_3)^3$	.953***	.056
HD-3	Blend	CCP	-.16 + .37 $(\sigma_1/\sigma_3)$ - .05 $(\sigma_1/\sigma_3)^2$ + .003 $(\sigma_1/\sigma_3)^3$	.868***	.073
MD-3	Blend	CCP	-.02 + .27 $(\sigma_1/\sigma_3)$ - .03 $(\sigma_1/\sigma_3)^2$ + .001 $(\sigma_1/\sigma_3)^3$	.828***	.091
LD-3	Blend	CCP	-.09 + .36 $(\sigma_1/\sigma_3)$ - .05 $(\sigma_1/\sigma_3)^2$ + .003 $(\sigma_1/\sigma_3)^3$	.729***	.121

(a) Significant at  $\alpha = 0.1$   
 \* Significant at  $\alpha = .02$   
 \*\* Significant at  $\alpha = .01$   
 \*\*\* Significant at  $\alpha = .001$

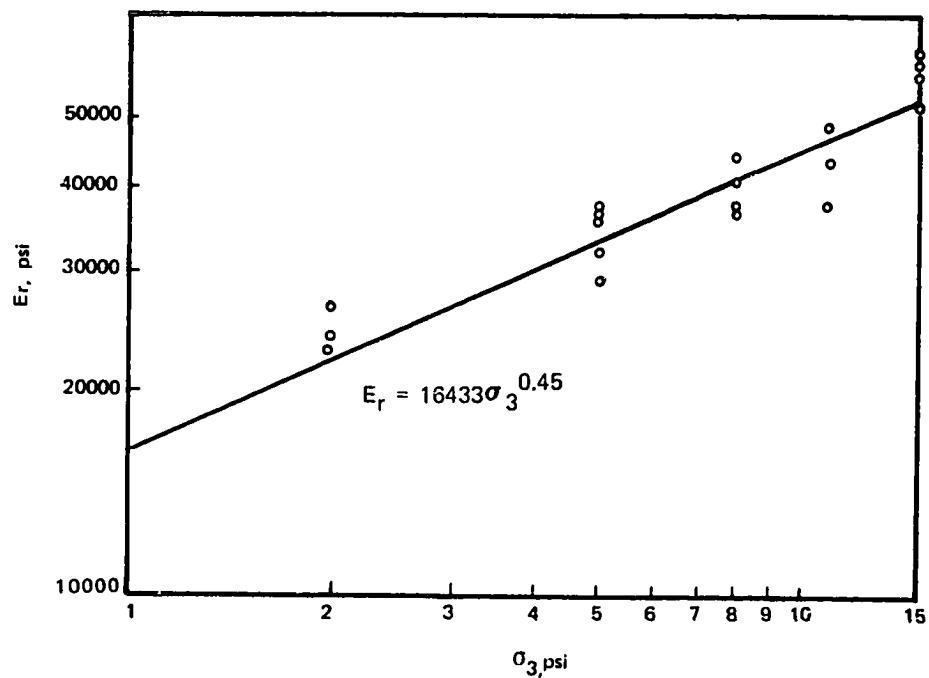


**Figure 5.3**  
Resilient Modulus ( $E_r$ ) as a Function of  $\sigma_3$ ,  
CCP Results, High Density Blend Specimen (HD-3)

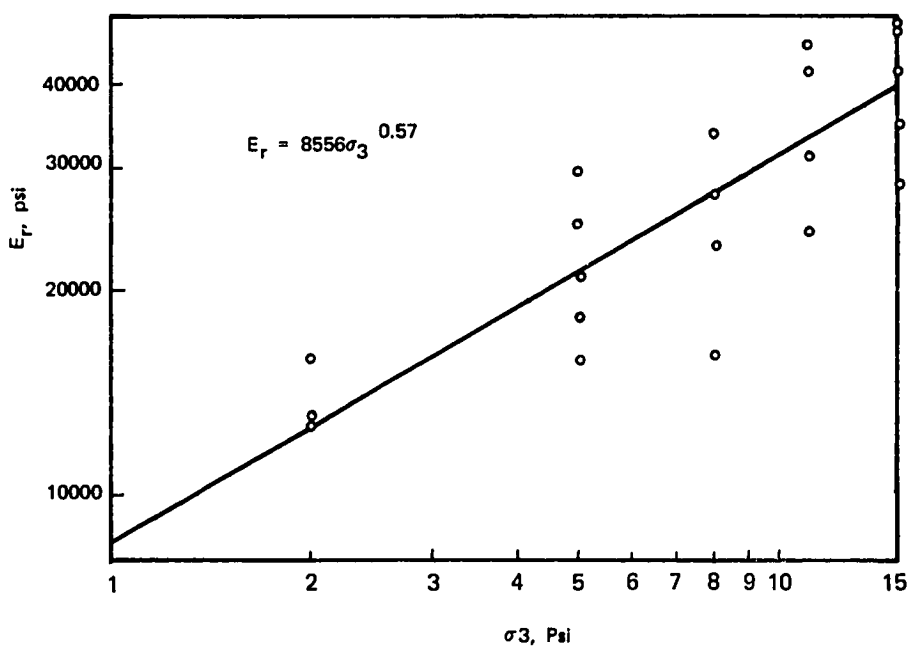


Figure 5.4  
Resilient Modulus ( $E_r$ ) as a Function of  $\sigma_3$ , VCP Results,  
Intermediate Density Crushed Stone Specimen (MD-1)

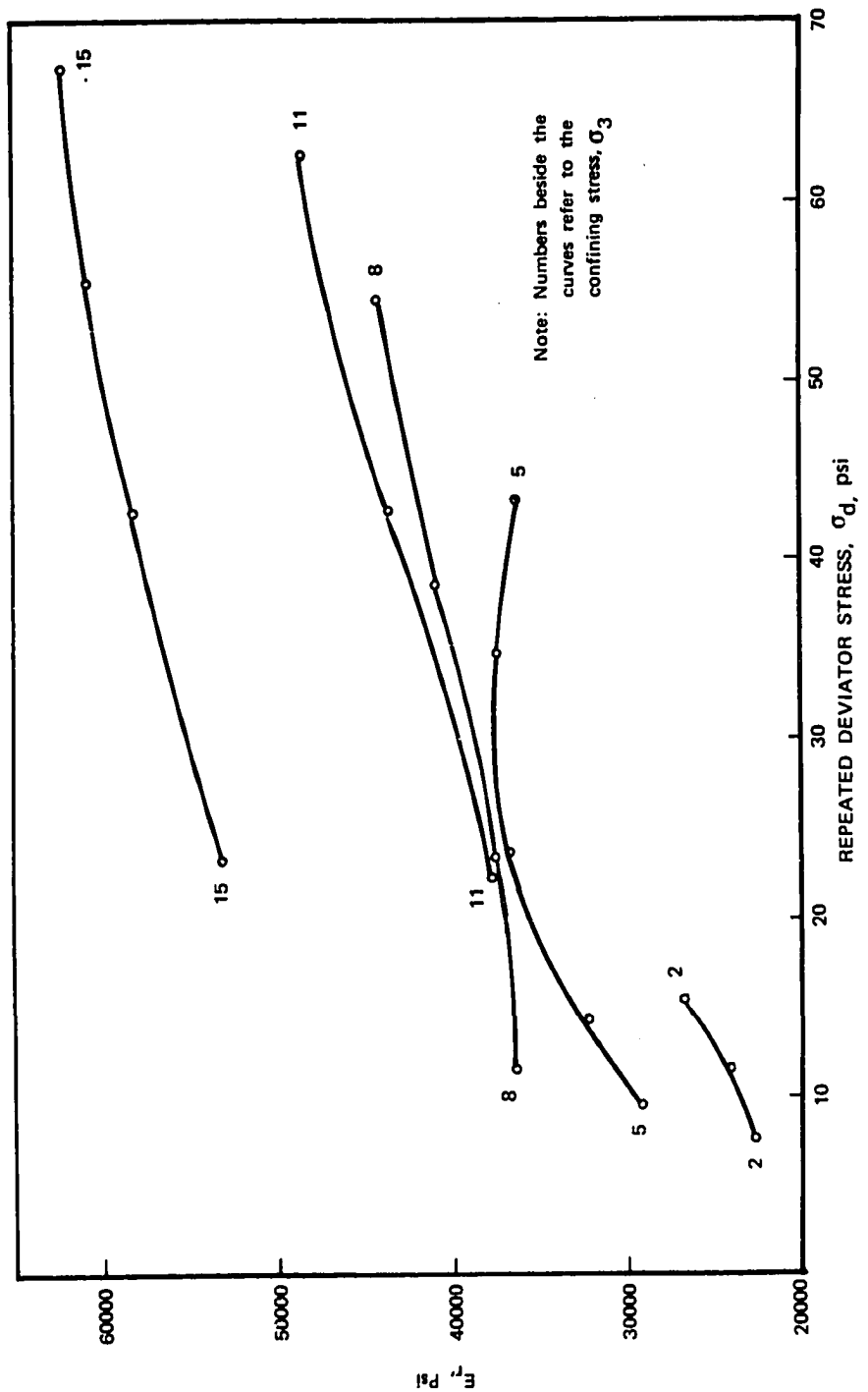


Figure 5.5  
Effect of Repeated Axial Deviator Stress ( $\sigma_d$ ) on the Resilient Modulus ( $E_r$ ), CCP Results, High Density Blend Specimen (HD-3)

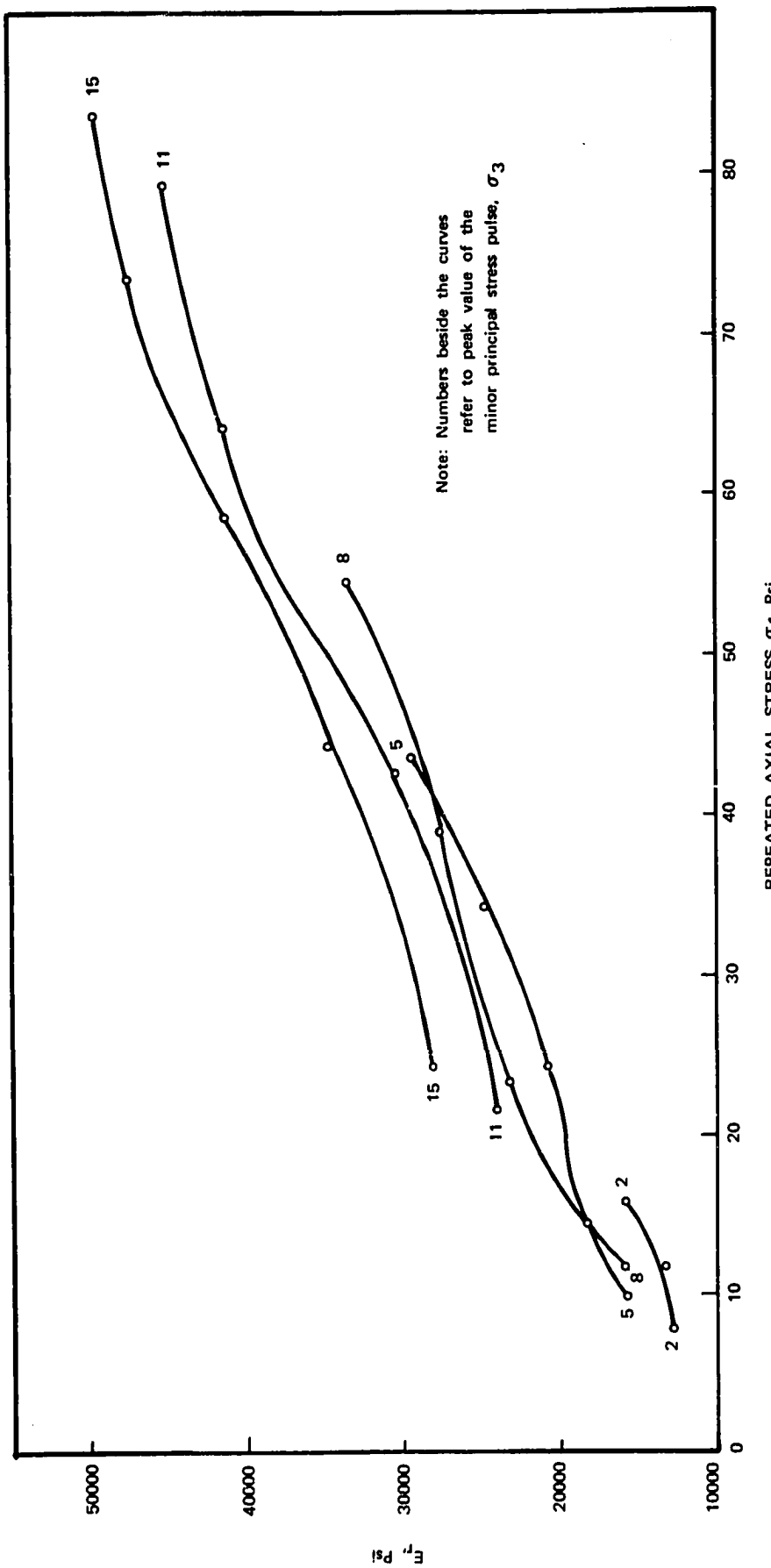


Figure 5.6  
Effect of Repeated Axial Stress ( $\sigma_1$ ) on the Resilient Modulus ( $E_r$ ),  
VCP Results, Intermediate Density Crushed Stone Specimen (MD-1)

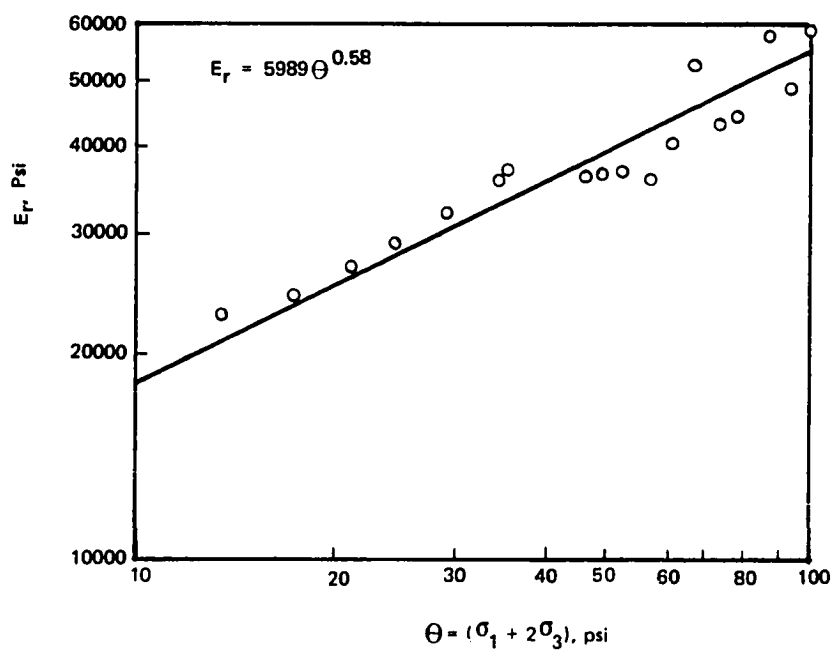
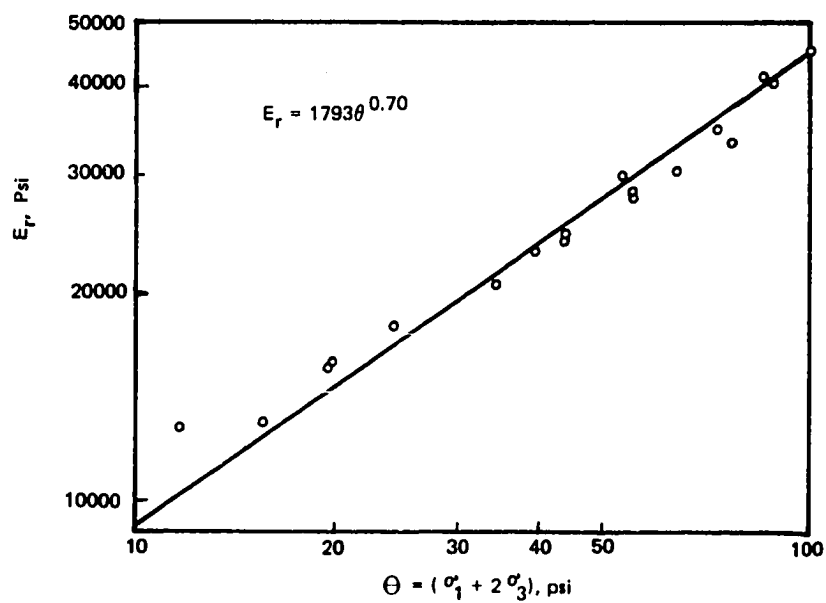


Figure 5.7  
Resilient Modulus ( $E_r$ ) as a Function of the Sum of the Principal Stresses ( $\Theta$ ), CCP Results, High Density Blend Specimen (HD-3)



**Figure 5.8**  
Resilient Modulus ( $E_r$ ) as a Function of the Sum of the Principal Stresses ( $\Theta$ ), VCP Results, Intermediate Density Crushed Stone Specimen (MD-1)

The primary test series results clearly demonstrate that the resilient material parameters are much more significantly affected by changes in the state of stress than by changes in any other factors investigated in this study. For example, the resilient modulus may change by as much as 400 per cent over the range of stress states encountered in a typical pavement system.

The effects of confining pressure on the resilient modulus are illustrated in Figures 5.3 and 5.4. These figures are typical of the entries in Table 5.3. Figure 5.3 shows the data extracted from the CCP test results of the high density blend specimen. It should be noted that  $\sigma_3$  increases from 1 to 10 psi the resilient modulus increases by almost 300 per cent. Figure 5.4, VCP test results for the intermediate density crushed stone specimen, shows a similar increase in the resilient modulus. It should be pointed out that a range in  $\sigma_3$  values of 1 to 10 psi is not atypical of confining stresses thought to exist in actual pavement sections.

The variations in the resilient modulus at each value of  $\sigma_3$  in Figures 5.3 and 5.4 are indicative of the effects of the axial stress,  $\sigma_1$ , on the resilient response. Figures 5.5 and 5.6 show the modulus versus  $\sigma_1$  at various levels of  $\sigma_3$  for the same two specimens illustrated in Figures 5.3 and 5.4. It can be seen that the major principal stress can exert a significant influence on the resilient modulus. In addition, the influence of  $\sigma_1$  helps to explain the scatter in the data shown in Figures 5.3 and 5.4.

The model relating  $E_r$  to the first invariant of the stress tensor,  $\theta$ , reduces the scatter in the data by accounting for the effects of all three principal stresses. Figures 5.7 and 5.8 show this relation for the same two specimens just discussed. The higher correlation coefficients and lower standard errors associated with the  $\theta$  models as compared with  $\sigma_3$  models (Figures 5.3, 5.4, 5.7, 5.8) were also obtained for the other specimens. Again, the increase

in  $E_r$  as  $\theta$  increases is evident, with Figure 5.8 indicating a 400 per cent increase in  $E_r$  as  $\theta$  increases from 10 psi to 80 psi. While the data from only two specimens are presented in Figures 5.3 through 5.8, the same trends were evident from the results obtained for all specimens.

The stress-dependent nature of the resilient Poisson's ratio is illustrated in Figure 5.9. The best fit to the laboratory data was obtained for all specimens by expressing  $v_r$  as a function of  $\sigma_1/\sigma_3$  (Equation 5.4). Figure 5.9 shows this relationship for the VCP test data from the low density gravel specimen. Of interest is the relatively flat slope of the curve through the range of  $\sigma_1/\sigma_3$  of 2 to 7. This observation indicates that, since this range of stress ratios is typical of that found in pavement systems, pavement analyses based on a representative constant value of Poisson's ratio for the granular layers might be appropriate. The validity of this observation is strengthened by the fact that the VCP test results for all specimens yielded values of Poisson's ratio very close to those shown in Figure 5.9 for the same range of  $\sigma_1/\sigma_3$ . This topic is discussed further in Chapter 6.

Figure 5.10 shows  $v_r$  values from the CCP test on the same specimen as Figure 5.9. This figure, typical of the CCP results for all specimens, differs in two respects from the typical VCP results shown in Figure 5.9. First, the curve is concave downward throughout the range of  $\sigma_1/\sigma_3$  of interest, as opposed to the upward concavity evident in Figure 5.9. Second, the values of  $v_r$  are much higher (>.50) throughout the same range of  $\sigma_1/\sigma_3$  for the CCP results than for the VCP test data. This contrast in behavior may indicate that the CCP test conditions cause the specimen to undergo more volume change than the VCP test. The results of the two test types are compared in detail later in this chapter.

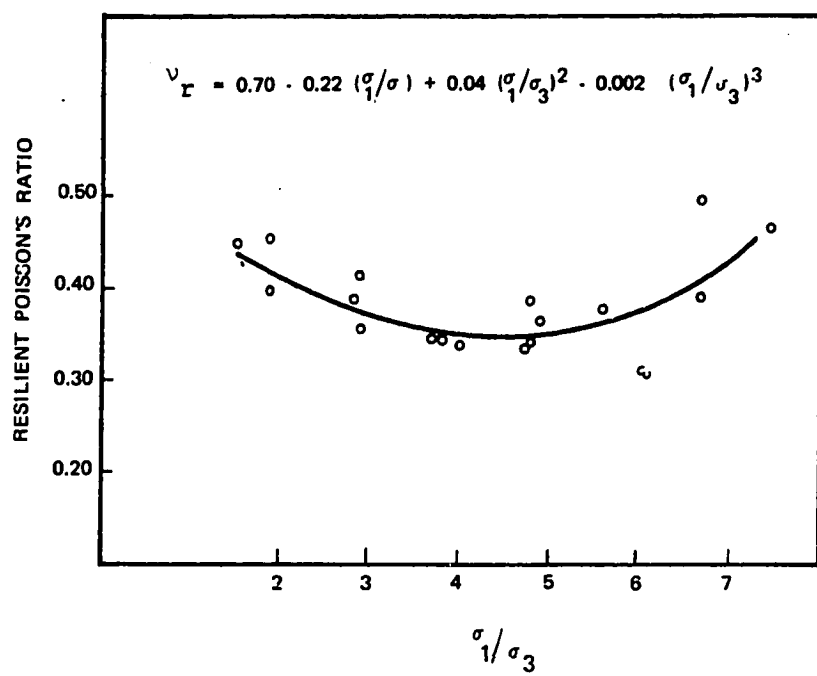
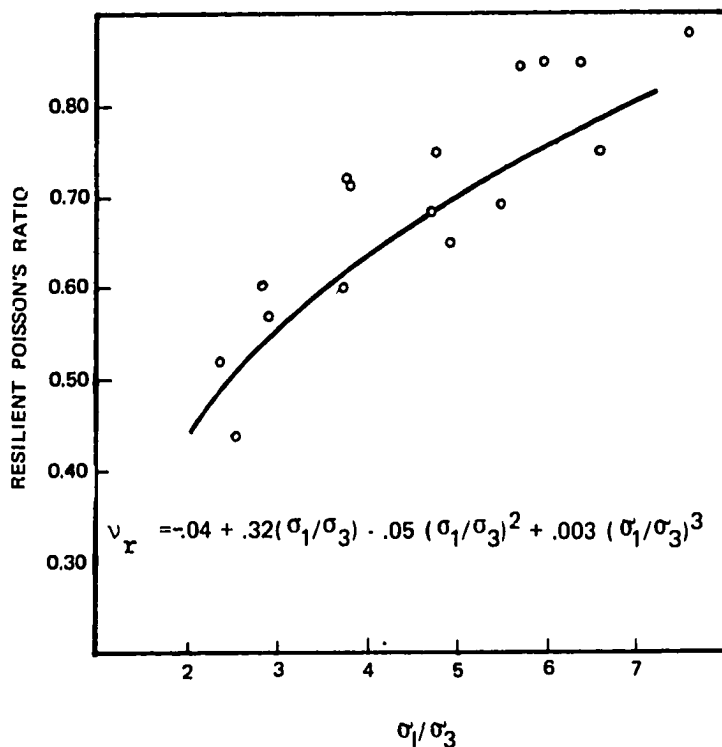


Figure 5.9  
Resilient Poisson's Ratio ( $v_r$ ) as a Function of Principal Stress Ratio ( $\sigma_1/\sigma_3$ ), VCP Results, Low Density Gravel Specimen (LD-2)



**Figure 5.10**  
Resilient Poisson's Ratio ( $v_r$ ) as a Function of Principal Stress Ratio ( $\sigma_1/\sigma_3$ ), CCP Results, Low Density Gravel Specimen (LD-2)

#### 5.4.2 Effects of Density

The effects of variations in dry density,  $\gamma_d$ , on  $E_r$  are shown in Figures 5.11 through 5.13 for the VCP tests and in Figures 5.14 through 5.16 for the CCP test data. In general, it would appear that density effect is more pronounced at lower values of  $\theta$  than for higher values. As Figures 5.11 through 5.16 indicate, there is a general trend of increasing values of  $E_r$  as  $\gamma_d$  increases, although this relation was not without exception. Notably, Figure 5.14 (CCP results - crushed stone specimens) shows the intermediate density specimen to have a higher  $E_r$  for values of from 10 to 22 psi. Thereafter, for larger values of  $\theta$  the high density specimen had the higher  $E_r$ . This intersection of  $E_r$  curves was also exhibited by the VCP test results from the gravel specimens, except that the point of intersection was near the high extremity of  $\theta$  values. Below the point of intersection, the higher density specimens had larger values of  $E_r$  than did the lower density specimens.

The effects of dry density on the degree of stress dependency of the resilient parameters can be examined by looking at the slope of the regression line, the exponent n. Figure 5.17 shows the variation of the constants K and n with density for the VCP test results. The somewhat erratic nature of the density relation for each constant would appear to render the data inconclusive in that respect. However, one very important observation may be made concerning the interaction of the constants K and n. In almost every case, curves computed for a specimen of density level so as to yield the minimum value of K also show a maximum value of n. Similarly, maximum K values have an accompanying minimum n, and intermediate values of K and n appear together. This observation is true of the CCP test results in Figure 5.18. This observation of interaction of the constants explains why it is possible to see the general trend of higher values of  $E_r$  for higher density specimens when the regression lines for  $E_r$

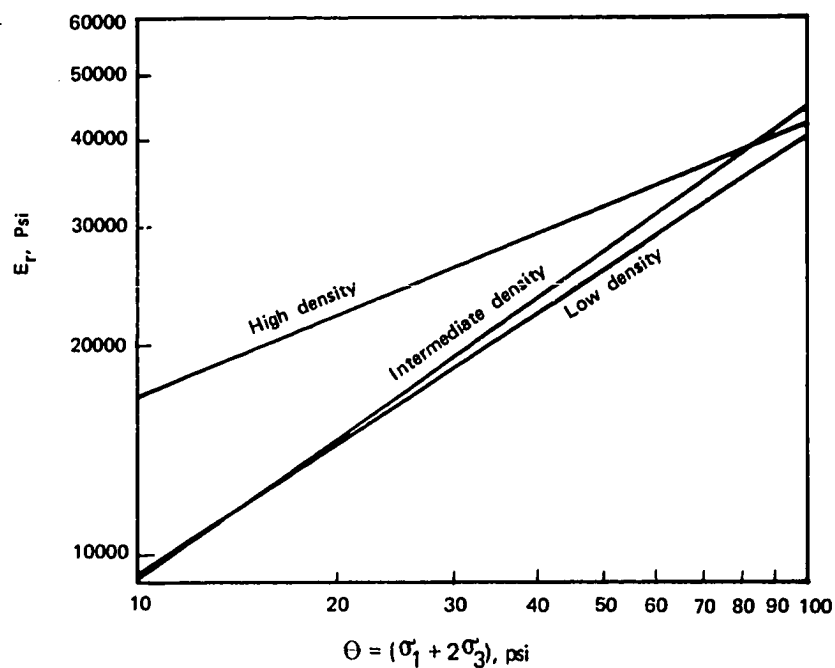


**Figure 5.11**  
Effect of Density on Relationship between  $E_r$  and  $\Theta$ , VCP Results,  
Crushed Stone Specimens

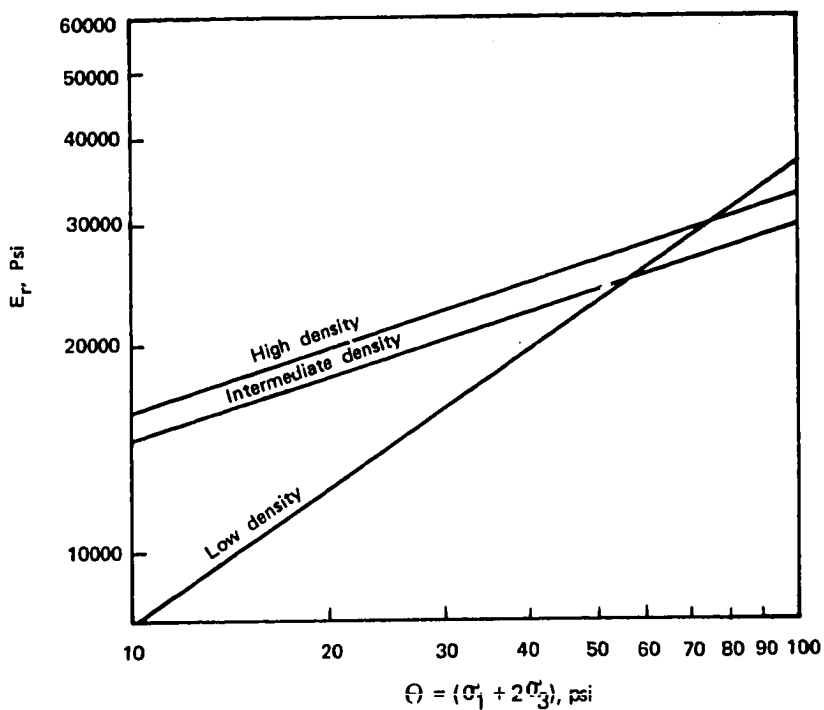


**Figure 5.12**  
**Effect of Density on the Relationship between  $E_r$  and  $\Theta$ , VCP Results,**  
**Gravel Specimens**

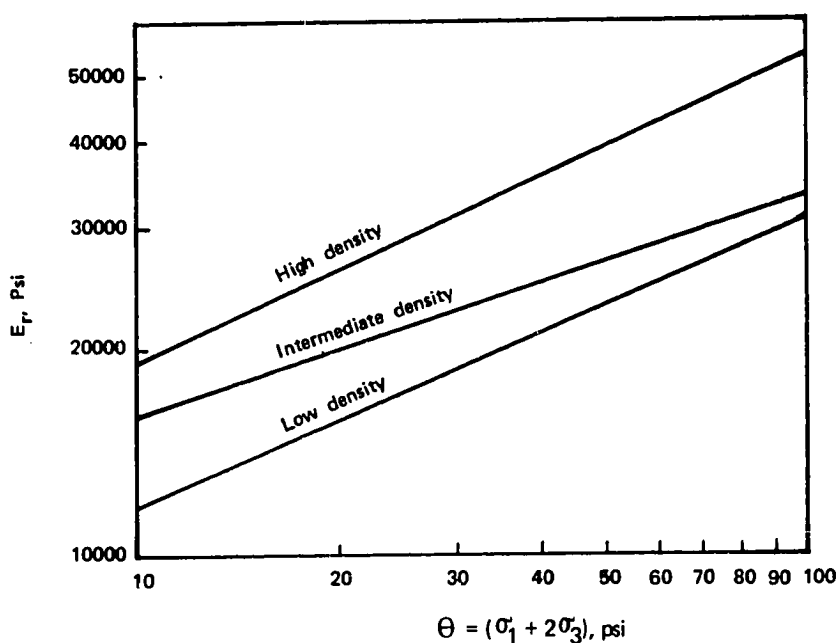


**Figure 5.13**  
Effect of Density on the Relationship between  $E_r$  and  $\Theta$ , VCP Results,  
Blend Specimens

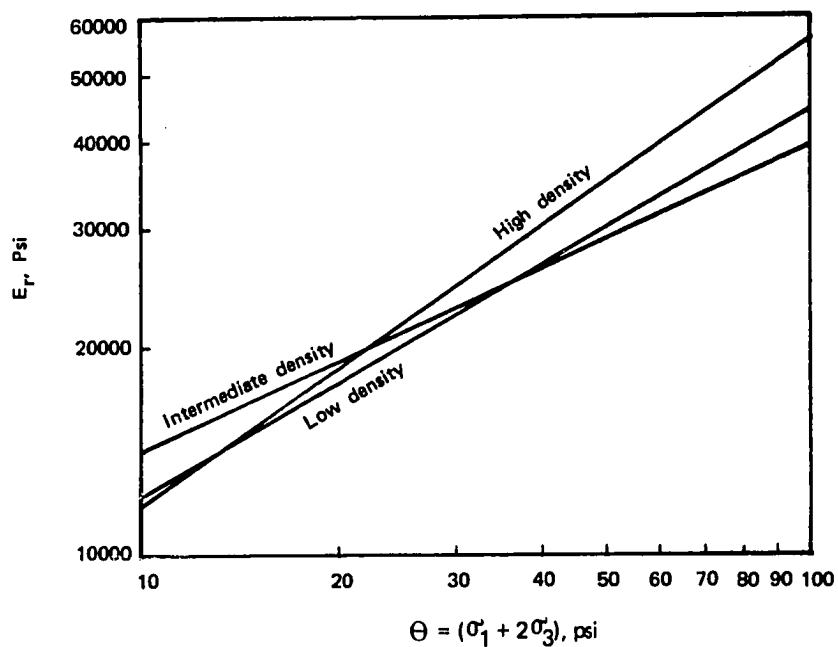


**Figure 5.14**  
Effect of Density on the Relationship between  $E_r$  and  $\Theta$ , CCP Results,  
Crushed Stone Specimens

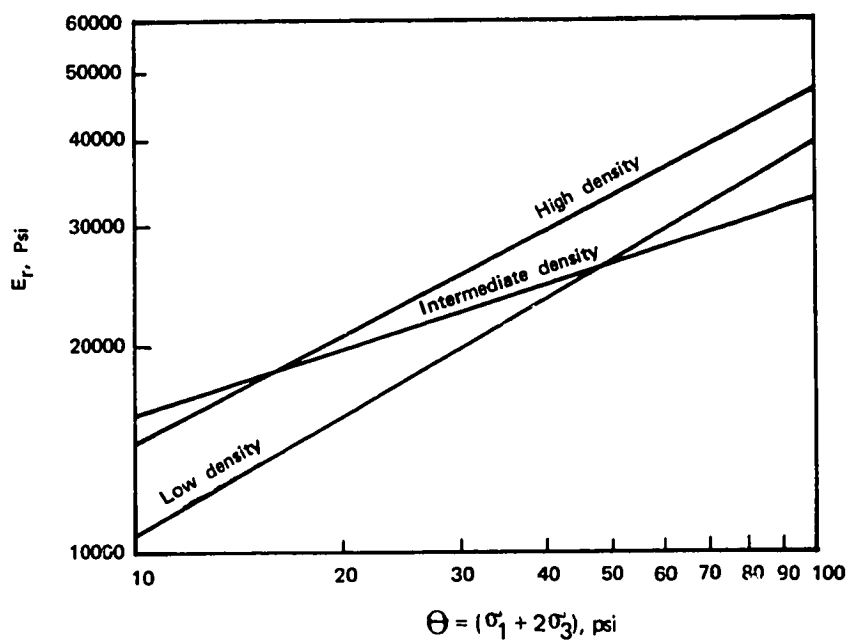


**Figure 5.15**  
Effect of Density on the Relationship between  $E_r$  and  $\Theta$ , CCP Results,  
Gravel Specimens

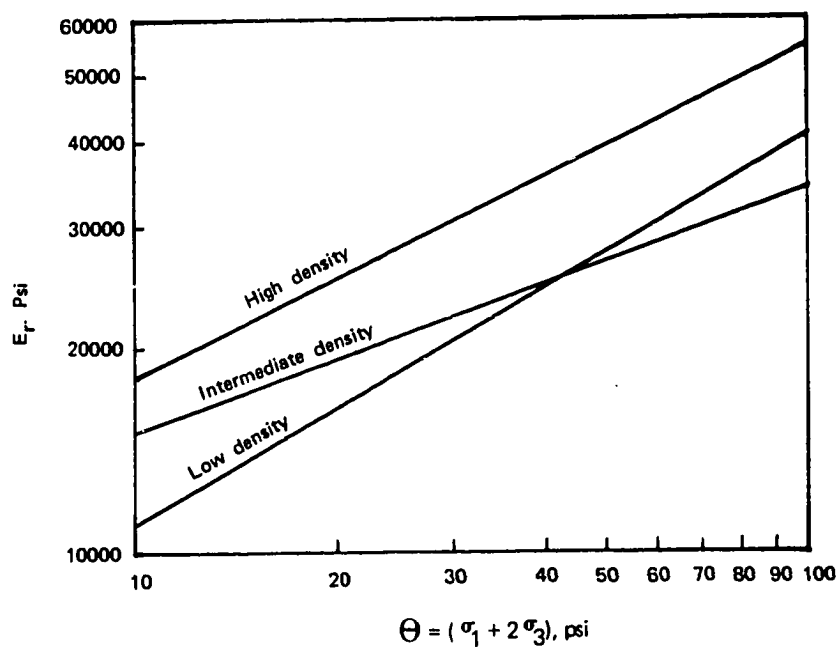


**Figure 5.16**  
Effect of Density on the Relationship between  $E_r$  and  $\Theta$ , CCP Results,  
Blend Specimens

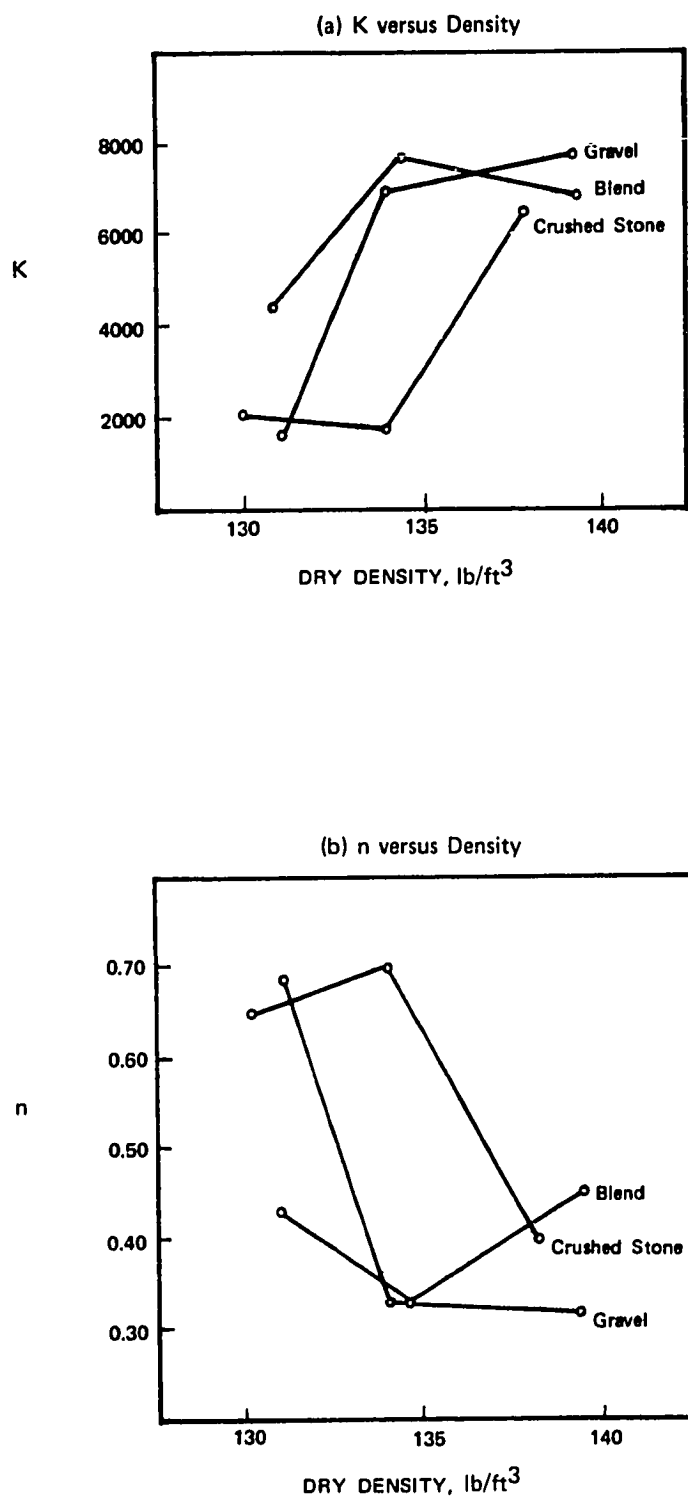


**Figure 5.17**  
Variation in the Resilient Parameters  $K$  and  $n$  ( $E_r = K \cdot \Theta^n$ ) with Density, VCP Results

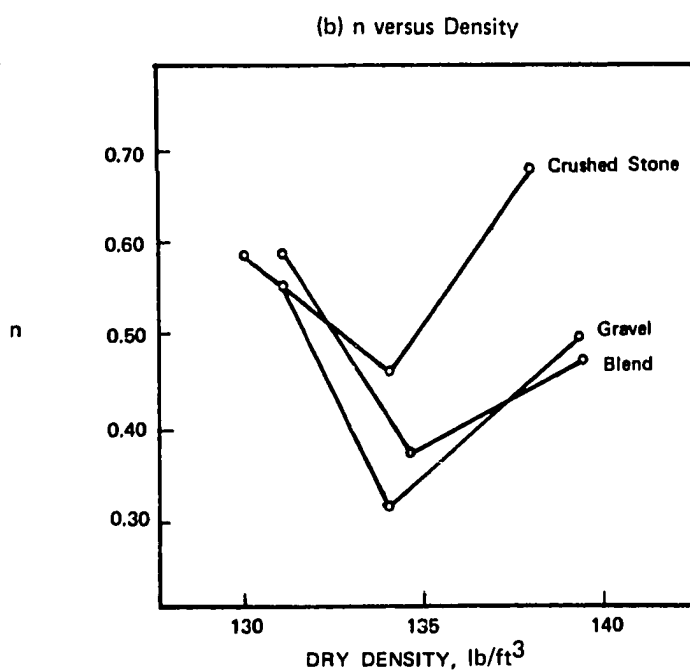
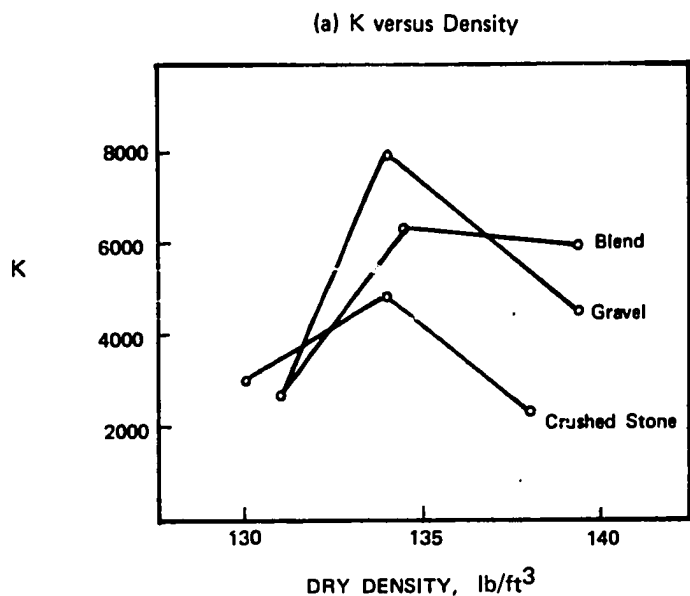


**Figure 5.18**  
Variation in the Resilient Parameters K and n ( $E_r = K \cdot \Theta^n$ ) with Density, CCP Results

versus  $\theta$  are plotted on a log-log scale even though the K or n values taken singularly do not support such a trend. This concept is discussed in greater detail in Chapter 6.

The effects of density on the resilient Poisson's ratio are shown in Figure 5.19 for the VCP test results and in Figure 5.20 for the CCP test data. Of interest concerning the VCP data are the very slight differences in  $v_r$  values for various density levels. In general it appears that the high density specimens had somewhat lower values of  $v_r$  than the lower density specimens, although there were exceptions. For the gravel and blend specimens the low density specimens showed lower  $v_r$  values except at the upper extreme of  $\sigma_1/\sigma_3$  values. No trends are evident from the CCP data, except that  $v_r$  obtained from the CCP test is everywhere greater than that obtained from the VCP test data. Again, this fact would seem to indicate that greater amounts of volume change are induced by the CCP test conditions.

It should be mentioned that the effects of density variations and material type on the resilient parameters are undoubtedly influenced by the differences in degree of saturation from specimen to specimen (Table 4.2). Hicks (31) found that the resilient modulus and Poisson's ratio decreased as the degree of saturation increased from zero to 100 per cent. However, these effects were slight as compared with the influence of the state of stress. For this study efforts were made to achieve desired specimen densities by controlling the moisture content and compactive effort. Therefore, variations in degree of saturation are inevitable. It is felt that these variations exert only minimal influence on the measured parameters.

#### 5.4.3 Effects of Material Type

Figures 5.21 through 5.26 show the effects of material type on the resilient

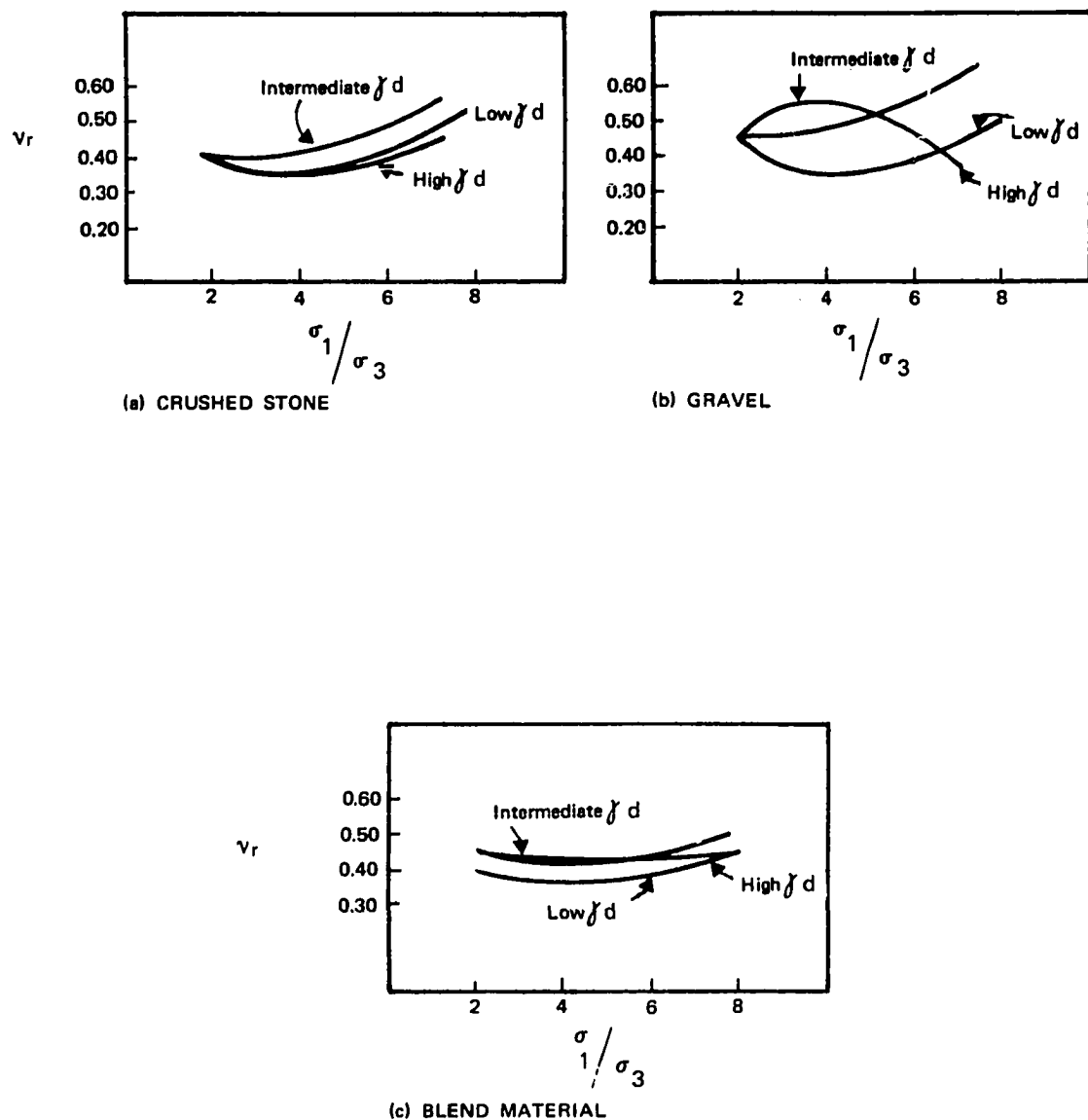
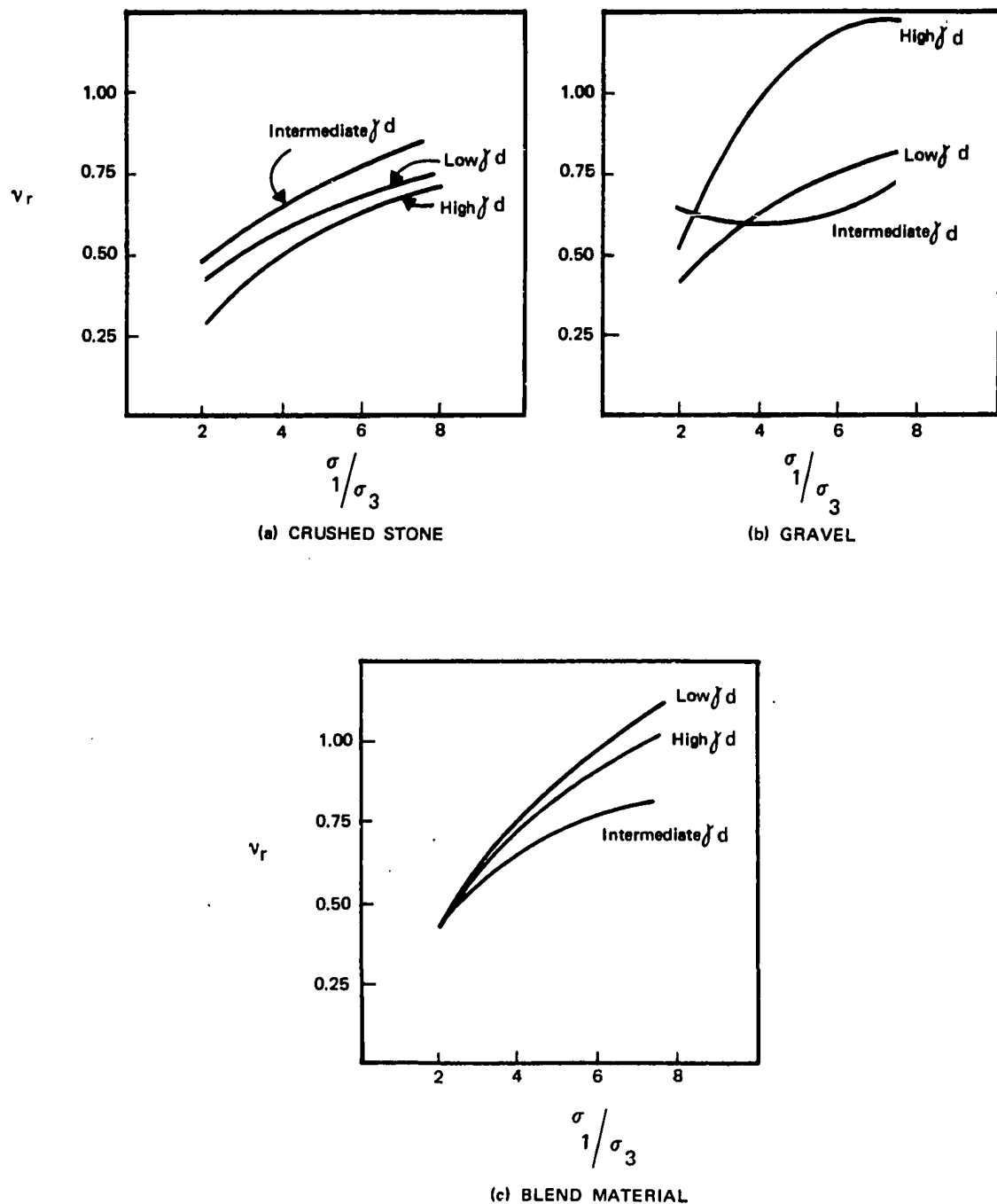


Figure 5.19  
Effect of Density on the Relationship between  $v_r$  and  $\sigma_1 / \sigma_3$   
VCP Results



**Figure 5.20**  
Effect of Density on the Relationship between  $v_r$  and  $\sigma_1/\sigma_3$   
CCP Results

modulus of the granular specimens. For the VCP test data, Figures 5.21 through 5.23, in general the crushed stone was stiffer than the gravel. However, for the intermediate density specimens the gravel exhibited higher values of  $E_r$  for a range of  $\theta$  from 10 to 30 psi. For values of  $\theta$  greater than 30 psi the crushed stone had greater stiffness. For the high density specimens, the blend material showed higher values of  $E_r$  throughout the range of  $\theta$  than did either the crushed stone or gravel. However, for the intermediate density specimens, the curves for the blend and crushed stone intersected at  $\theta$  equal to 49 psi with the blend showing higher stiffness at lower  $\theta$  and the the crushed stone yielding greater values of  $E_r$  for higher  $\theta$  values. The regression lines for the low density specimens show the same trend, except that the point of intersection is at  $\theta$  equal to 27 psi. It should be noted that in most cases where the regression lines for specimens of different materials intersect, the point of intersection is near the mid-range of values for the first invariant that would be expected to occur in a typical pavement section subjected to mixed traffic loads.

Similar observations may be made regarding the CCP test data shown in Figures 5.24 through 5.26. For the high density specimens, Figure 5.24, the regression curves for the crushed stone and gravel specimens intersect at a value of 28 psi. The blend material yielded consistently higher values of  $E_r$  except for values of  $\theta$  greater than 65 psi. Thereafter, the crushed stone showed greater stiffness. Figure 5.25, for the intermediate density specimens, shows the crushed stone with higher values of  $E_r$ , the blend with intermediate values, and the gravel with lower values, all for values of  $\theta$  greater than about 22 psi. For smaller  $\theta$  values there is little difference in the stiffness of the three materials. Throughout the entire range of  $\theta$  values in Figure 5.26 (low density specimens) the materials are ranked in order of decreasing stiffness:

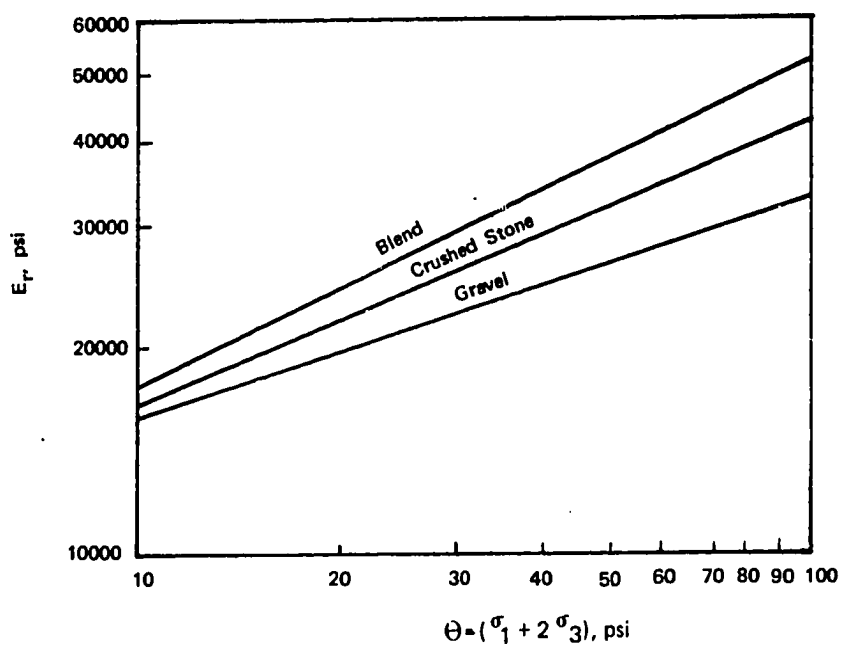


**Figure 5.21**  
Effect of Material Type on the Relationship between  $E_r$  and  $\Theta$   
VCP Results, High Density Specimens

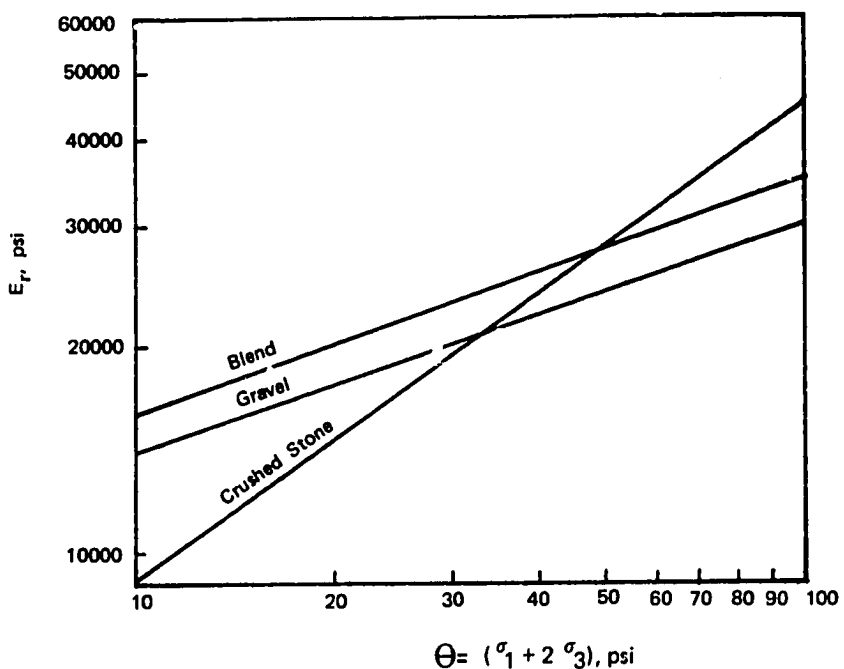


**Figure 5.22**  
Effect of Material Type on the Relationship between  $E_r$  and  $\Theta$ ,  
VCP Results, Intermediate Density Specimens

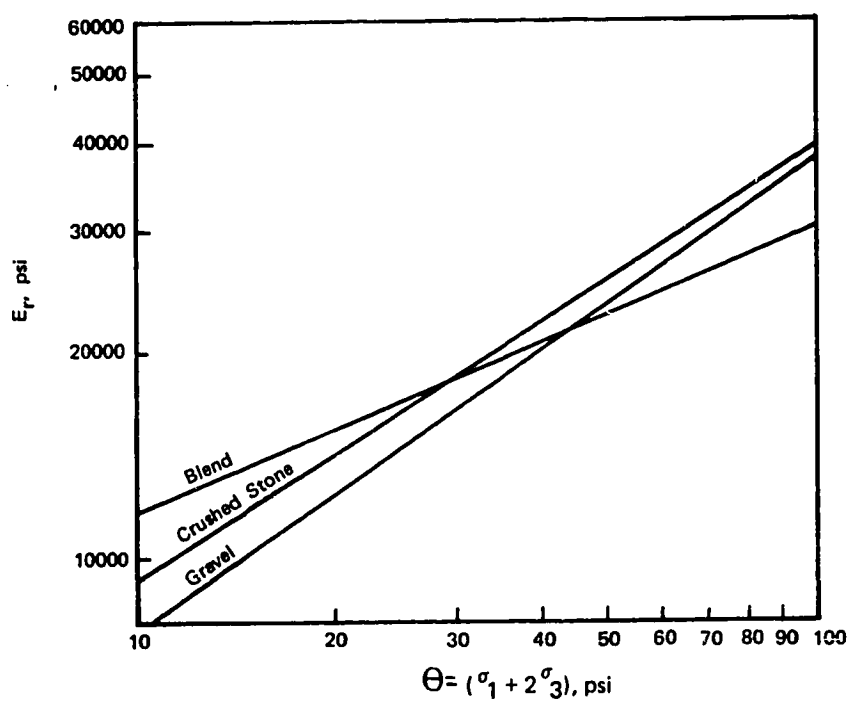


**Figure 5.23**  
Effect of Material Type on the Relationship between  $E_r$  and  $\Theta$ ,  
VCP Results, Low Density Specimens

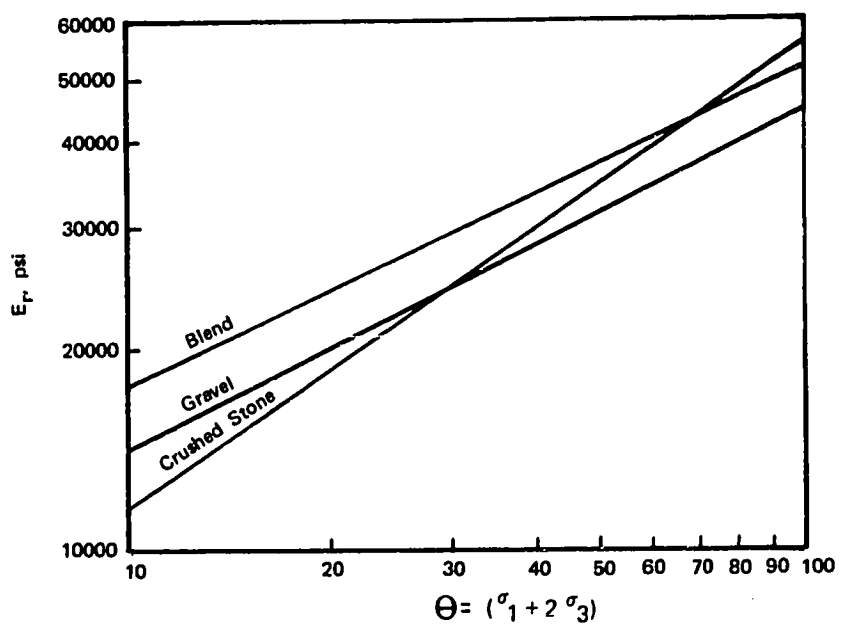


**Figure 5.24**  
Effect of Material Type on the Relationship between  $E_r$  and  $\Theta$ ,  
CCP Results, High Density Specimens

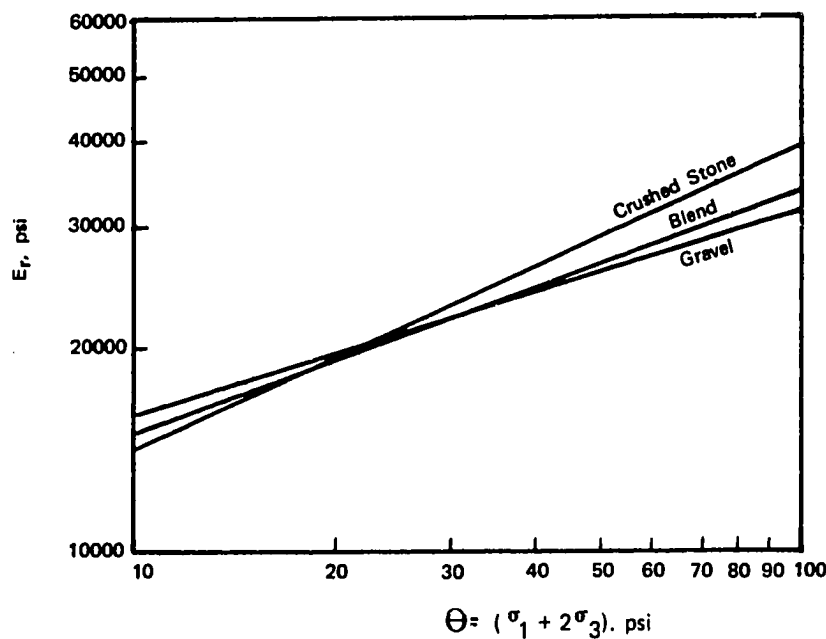


**Figure 5.25**  
Effect of Material Type on the Relationship between  $E_r$  and  $\Theta$ ,  
CCP Results, Intermediate Density Specimens

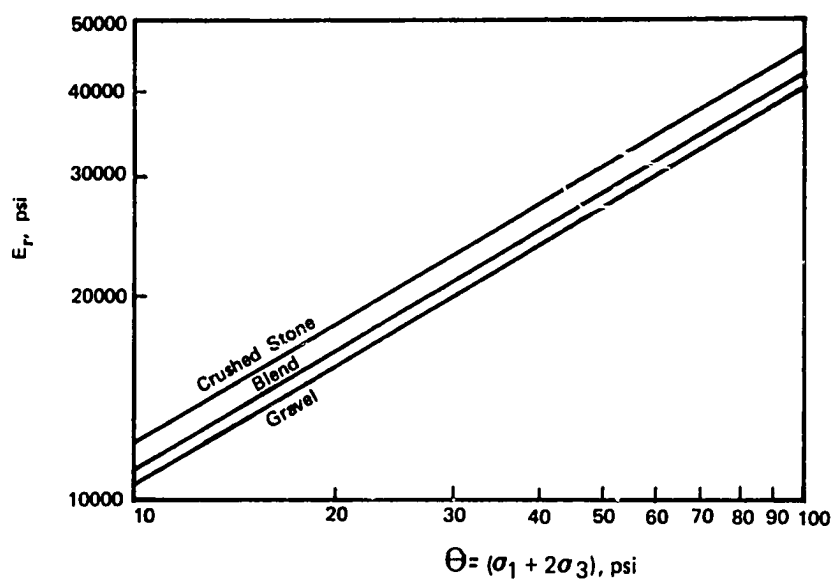


**Figure 5.26**  
Effect of Material Type on the Relationship between  $E_r$  and  $\Theta$ ,  
CCP Results, Low Density Specimens

crushed stone, blend, then gravel.

The effects of material type on the resilient Poisson's ratio are shown in Figures 5.27 and 5.28. The VCP test results (Figure 5.27) indicate almost identical values of  $\nu_r$  for all three materials at the lowest density level. There is not a great deal of difference between the regression lines for the other density level specimens. However, the gravel displayed consistently higher values of Poisson's ratio than the crushed stone or blend material. Again, the relatively flat nature of the regression curves in the region of  $\sigma_1/\sigma_3$  from 2 to 7 should be noted.

The CCP test data shown in Figure 5.28 shows considerably more variation in  $\nu_r$  values for different material types, but no firm conclusions can be reached. For the high and low density specimens, the crushed stone displayed the lowest values of  $\nu_r$ , but the gravel yielded the highest values for the high density specimens, the intermediate values of  $\nu_r$  for the low density specimens, and the lowest Poisson's ratio for the intermediate density specimens. Here, too, it is seen that the CCP test results yield consistently higher values of Poisson's ratio than do the VCP results. The implications of this observation are discussed in section 5.4.5.

#### 5.4.4 Plastic Deformations

Although no attempts were made to measure the plastic (nonrecoverable) deformations associated with individual stress pulses, data are available showing total plastic deformations accumulated by each specimen throughout the test series. This total change in specimen length was converted to plastic axial strains by dividing it by the specimen length. Table 5.4 shows the total plastic axial strain for each specimen. The entries in Table 5.4 reflect the sum of plastic strains per specimen occurring during the CCP and VCP test series.

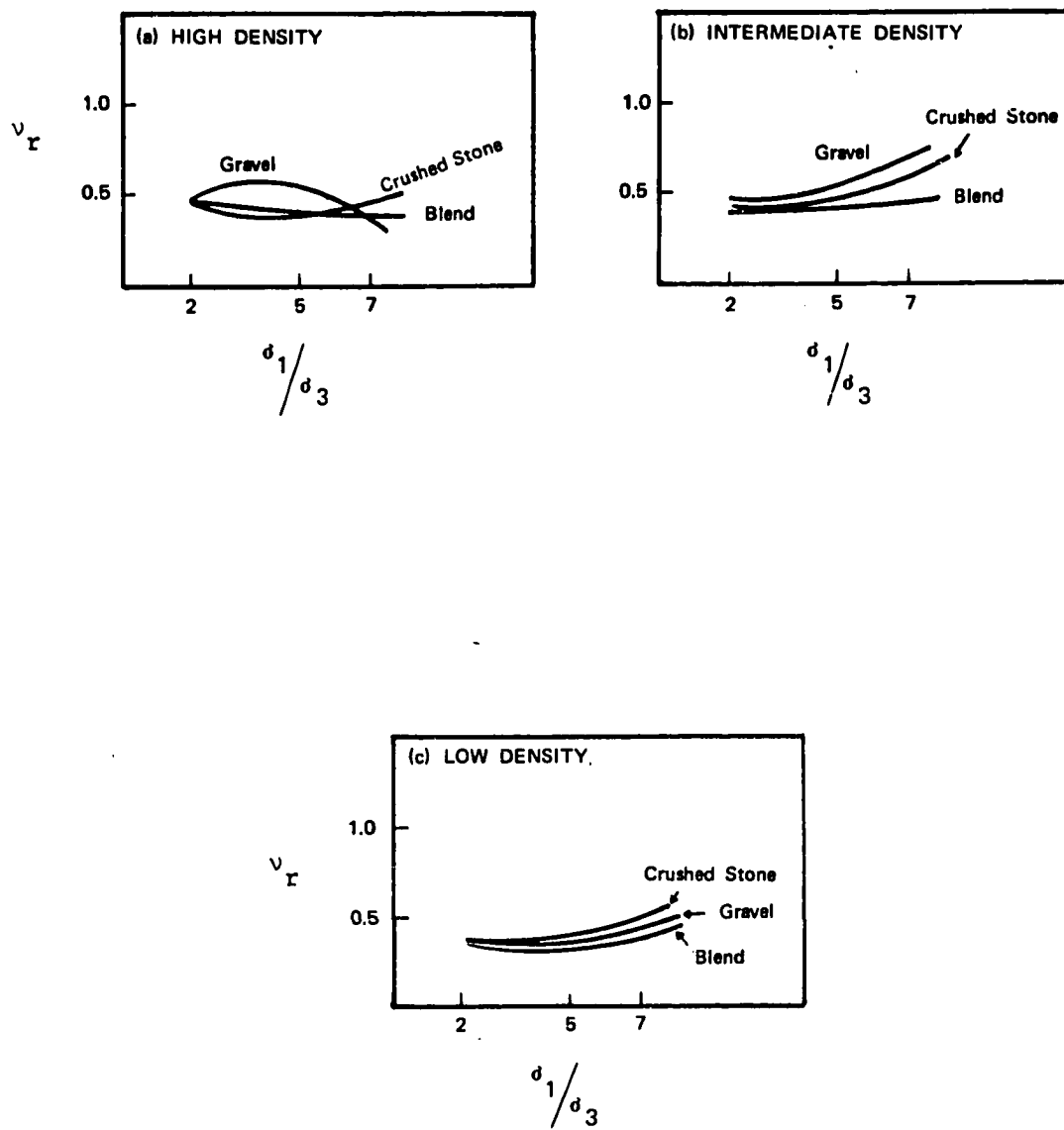


Figure 5.27  
Effect of Material Type on the Relationship between  $v_r$  and  $\sigma_1/\sigma_3$ , VCP Results

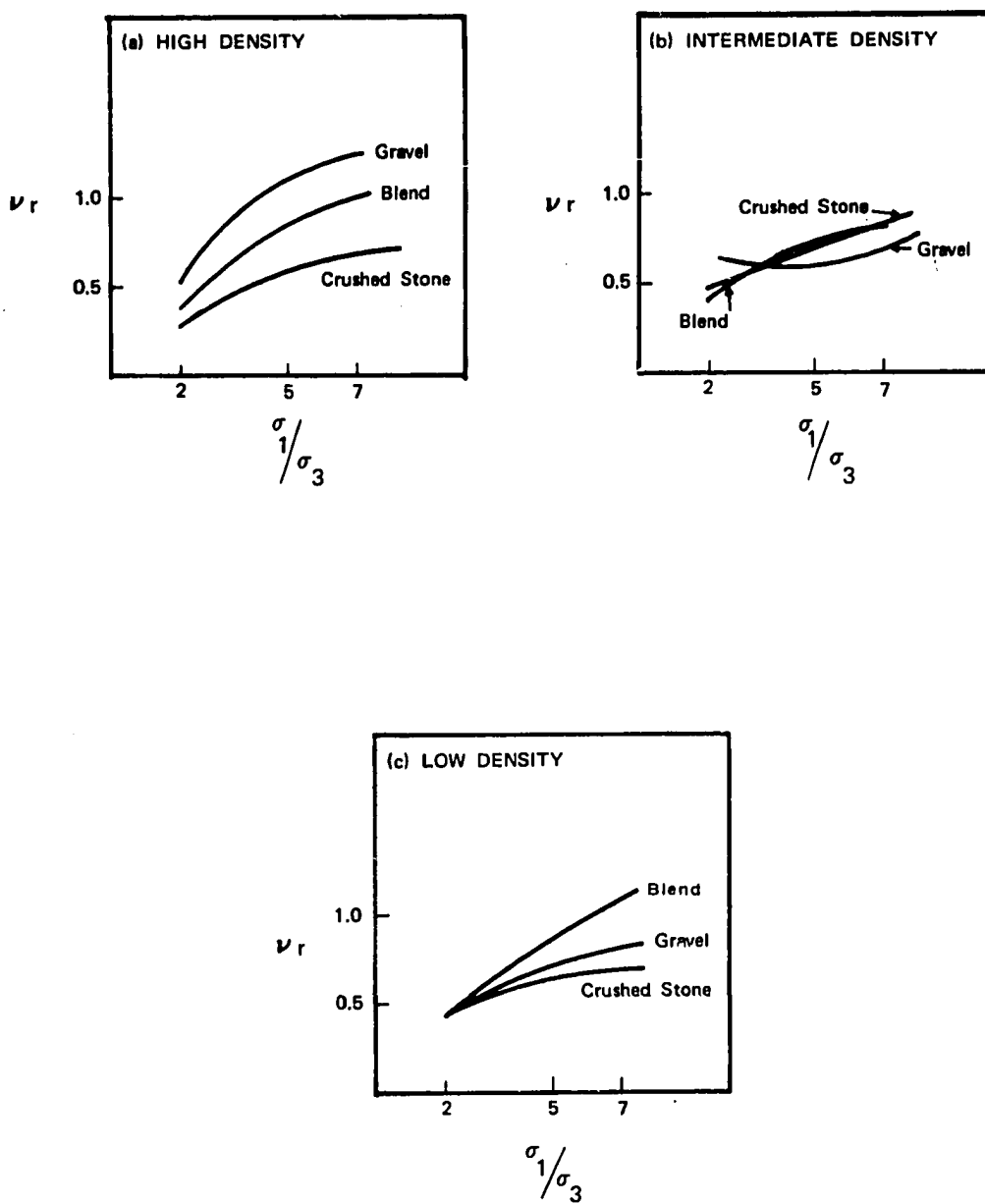


Figure 5.28  
Effect of Material Type on the Relationship between  $V_r$  and  
 $\sigma_1/\sigma_3$ , CCP Results

TABLE 5.4  
TOTAL PLASTIC AXIAL STRAIN

Specimen	Material Type	Density Level	Total Plastic Axial Strain, $\epsilon_p$ , in/in
HD-1	Crushed Stone	High	.0036
MD-1	Crushed Stone	Intermediate	.0149
LD-1	Crushed Stone	Low	.0191
HD-2	Gravel	High	.0158
MD-2	Gravel	Intermediate	.0173
LD-2	Gravel	Low	.0204
HD-3	Blend	High	.0063
MD-3	Blend	Intermediate	.0152
LD-3	Blend	Low	.0193

Since every specimen was subjected to identical stresses and numbers of loads, the ranking in Table 5.4 may be considered indicative of the relative plastic response of the three materials at the three stated density levels. Two trends may be detected from the data of Table 5.4. First, within each material type there is an increase in total plastic strain as the specimen density decreases. Second, for each density level the crushed stone specimens experienced the least plastic strains, the gravel specimens accumulated the greatest plastic strains and the blend materials showed intermediate values of plastic axial strains. The density effects are consistent with those reported by Gray (28) as observed during static triaxial testing and by Barksdale (10) regarding the results of repeated load triaxial tests conducted at constant chamber pressure.

Since all specimens were prepared from one material gradation, the variation in plastic strains shown for different material types at the same density would appear to be related to the surface characteristics of the aggregates. The rougher, more angular nature of the crushed stone as compared to the gravel would indicate that the crushed stone should exhibit a higher angle of shearing resistance,  $\phi$ , for equal densities. Similarly, the blend of the two materials could be expected to possess an intermediate value of  $\phi$ . This observation is supported by Gray (28). Examination of the hyperbolic plastic stress-strain law (Chapter 3) reveals that materials with higher values of  $\phi$  should undergo smaller plastic deformations at any given stress state than materials with smaller angles of shearing resistance, and vice-versa. Therefore, the plastic strain data shown in Table 5.4 are consistent with the theoretical treatment of plastic behavior of granular materials.

One further conclusion may be drawn from consideration of the plastic strain data in conjunction with the resilient strain data. Although a quantitative comparison is not possible, it would appear that the variations in plastic

strain from one type material to another and from one density level to another are more pronounced than the variations observed in  $E_r$ . Therefore, it may be concluded that a greater portion of total deformations are recoverable for the crushed stone than for the gravel and blend materials. In addition, the ratio of recoverable deformations to total deformations would be greater for the blend than for the gravel at a given level of density. This conclusion may be visualized by considering an individual stress pulse. If the recoverable strains experienced by different specimens subjected to the same stress pulse are similar in magnitude, but if the plastic strains vary widely from specimen to specimen, then the ratio of recoverable strains to total strains would be greatest for the specimen with the least plastic strain.

If two materials exhibit similar resilient response to dynamic loading such that either is acceptable for use as a base course for a flexible pavement structure, that is if analysis indicates that the fatigue response of the structure constructed of either material is satisfactory, serious error might result if the rutting potential (plastic response) of each is not examined. Because fatigue cracking is but one pavement distress mechanism, it must be kept in mind that the resilience concept does not directly pertain to other modes of failure and that satisfactory performance in one mode of behavior does not imply satisfactory performance in all modes.

#### 5.4.5 Anisotropic Behavior

Poisson's ratio is a most difficult parameter to determine in the laboratory. The problem of devising instrumentation to accurately measure lateral deformations, while difficult to solve, can be overcome. It is felt that the Bison sensors used in this study possess adequate sensitivity to slight change in axial spacing to provide satisfactory measurements. However, no matter what instrumentation

scheme is utilized, the lateral deformations of the specimen are affected by the nonuniform stress and deformation conditions which inevitably exist in the triaxial specimen. These nonuniform stress-deformation conditions are manifested by the typical bulged shape of the lateral deformation distribution near the mid-height of the specimen and may be minimized by selecting specimen height to diameter ratios of two or greater and by using lubricated end platens. For this study the necessity of compacting the specimens directly on the base load platen was thought to limit the usefulness of lubricating the platens. Therefore, even though the height-diameter ratio was 2:1 it must be assumed that specimen end effects exerted some influence on the lateral deformations observed.

It can be shown that elastic isotropic materials cannot have a value for Poisson's ratio in excess of 0.5. However, as was reported earlier, the CCP test results yielded values of  $\nu$  consistently in excess of 0.5. Certainly, a percentage of the large lateral deformations involved are due to the nonuniform stress and strain states within the specimens; however, it can also be assumed that these results indicate anisotropic behavior on the part of the granular materials. The same conclusion has been reached by Moore, Britton, and Scrivner (51), Barksdale and Hicks (11), and Dehlen (18).

At principal stress ratios,  $\sigma_1/\sigma_3$ , in the range from 2 to 7, typical of those thought to exist in granular layers of flexible pavement systems, the anisotropic behavior mentioned above was not observed in the VCP test series, as evidenced by the consistently lower values of Poisson's ratio. However, at stress ratios approaching hydrostatic conditions, the measured lateral deformations were so large as to be incompatible with isotropic material properties. This behavior was indicative that the stiffness of the material was less in the lateral direction than in the axial direction. Dehlen (18) reported similar

cross-isotropic behavior of sands. Despite the evidence of some degree of anisotropic properties of the materials tested, the VCP test data would seem to indicate that, in the proper range of stress states, such behavior only minimally influences the results.

#### 5.4.6 Comparison of VCP and CCP Test Results

Test results for the crushed stone and gravel materials indicate that the CCP test yields slightly higher values of  $E_r$  throughout the range of  $\theta$  values for the intermediate and low density specimens than does the VCP test. This observation was also true for the low density blend specimen for values of  $\theta > 15$  psi. The difference in  $E_r$  values in each case was maximum for values of  $\theta$  near 10 psi, the lower extreme for  $\theta$ . At this point the CCP test on the intermediate density crushed stone specimen showed  $E_r$  to be approximately 50 per cent greater than the VCP test data indicated. This difference diminished as  $\theta$  increased, since the regression lines converged at higher  $\theta$  values. However, the differences in  $E_r$  for the other specimens mentioned above were considerably less, on the order of 30 per cent at maximum. Figures 5.29 and 5.30 illustrate the variation in  $E_r$  for the CCP and VCP test data derived from specimens MD-1 and MD-2.

Similar results were obtained from the high density crushed stone and gravel specimens, Figures 5.31 and 5.32. Figure 5.31, for the gravel, shows the CCP and VCP test regression lines to intersect at a value of  $\theta$  near 17 psi; so for most of the range of  $\theta$  of interest the CCP test results yield higher values of  $E_r$ . However, for the crushed stone specimen the point of intersection was  $\theta = 35$  psi.

For two specimens, the high and intermediate density blend specimens, the VCP and CCP test data result in almost identical regression lines for  $E_r$ , Figure 5.33.

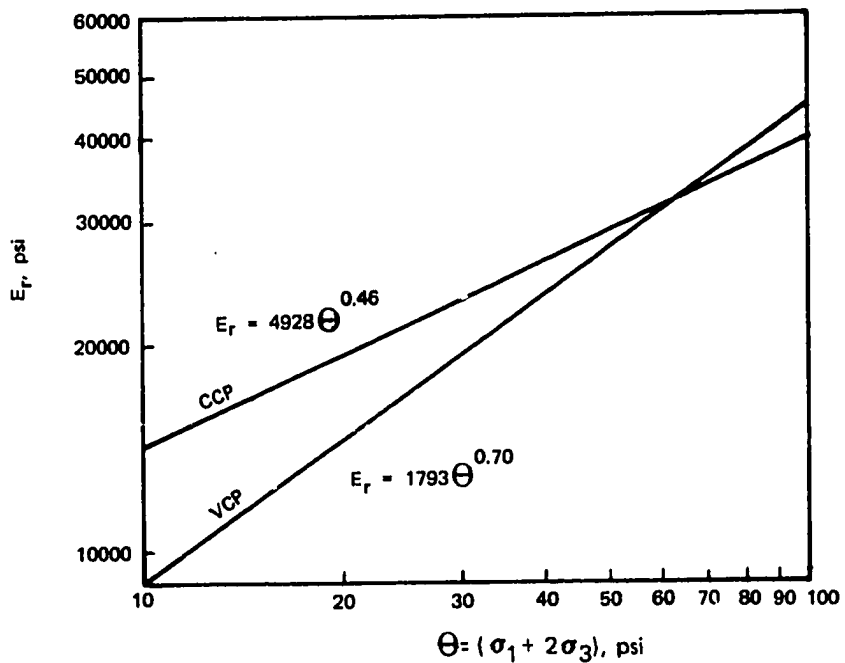
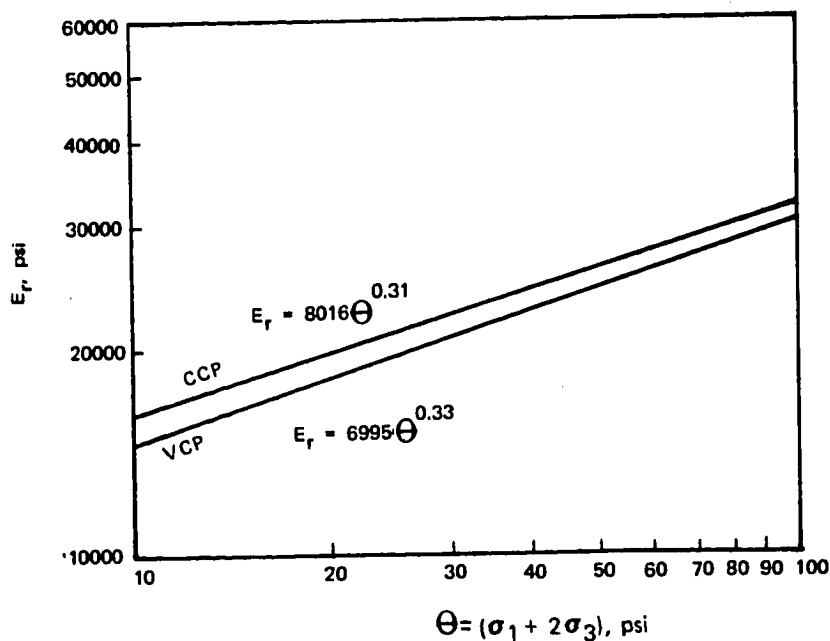
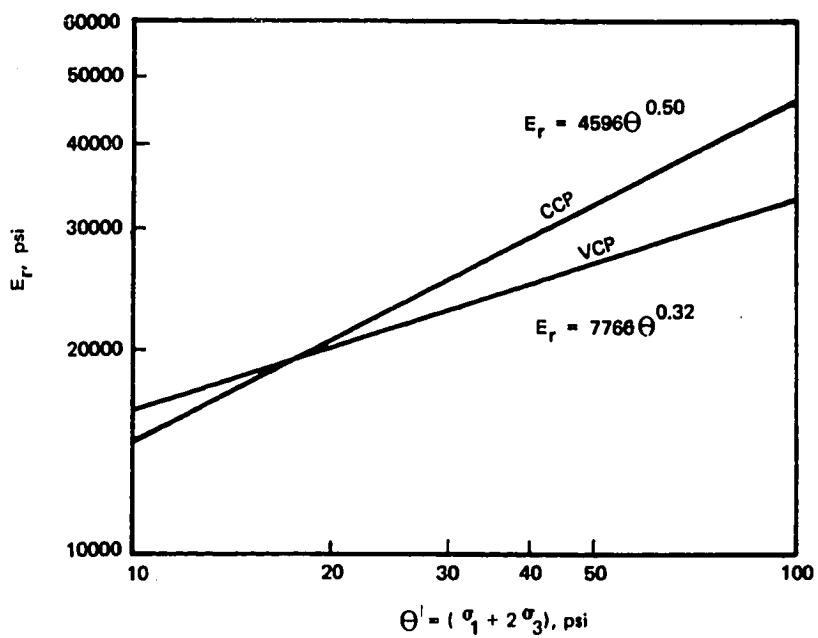


Figure 5.29  
Comparison of VCP and CCP Relationships between  $E_r$  and  $\Theta$ ,  
Intermediate Density Crushed Stone Specimen (MD-1)



**Figure 5.30**  
Comparison of VCP and CCP Relationships between  $E_r$  and  $\Theta$ ,  
Intermediate Density Gravel Specimen (MD-2)



**Figure 5.31**  
Comparison of VCP and CCP Relationships between  $E_r$  and  $\theta$   
High Density Gravel Specimen (HD-2)

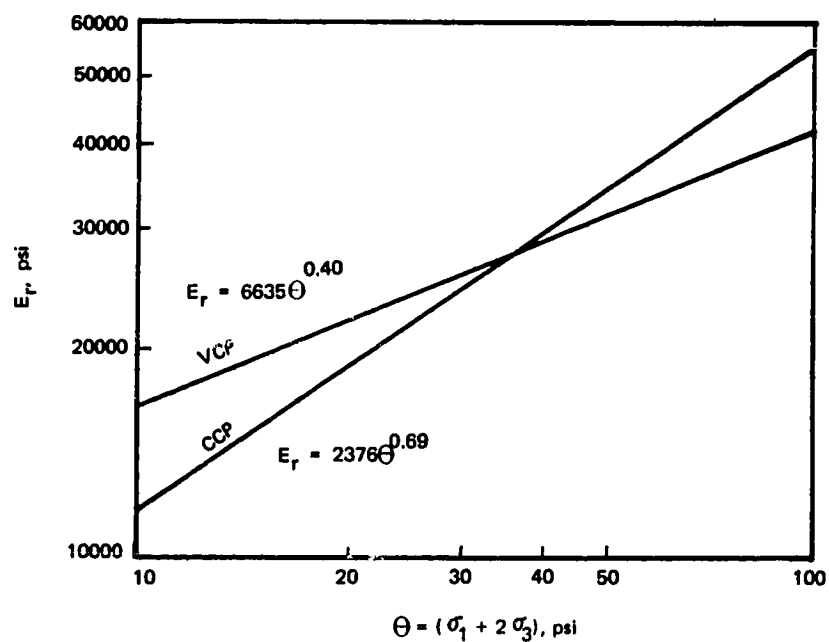
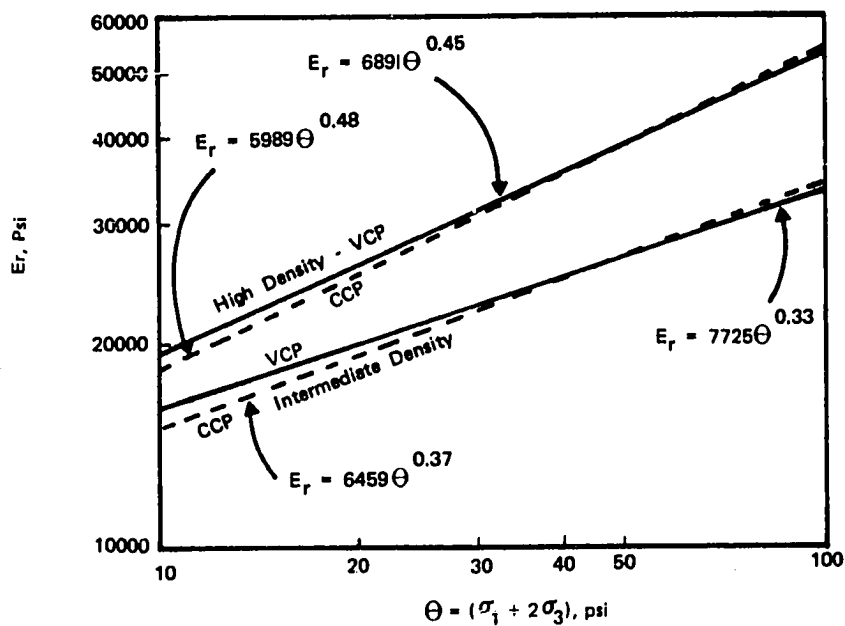


Figure 5.32  
Comparison of VCP and CCP Relationships between  $E_r$  and  $\Theta$   
High Density Crushed Stone Specimen (HD-1)



**Figure 5.33**  
Comparison of VCP and CCP Relationships between  $E_r$  and  $\Theta$   
High Density (HD-3) and Intermediate Density (MD-3) Blend  
Specimens

On the basis of the above discussion, it would appear that, in general, the CCP test data would tend to overestimate the resilient modulus compared to the VCP test. However, two observations should be made. First, this phenomenon was not observed for all specimens. Second, in the cases where it did occur the magnitude of the difference in  $E_r$  is not constant because of the intersecting or convergent nature of the regression lines; therefore, the magnitude of the difference depends upon the value of  $\theta$  for which the values of  $E_r$  are calculated. It follows that the differences in the results of the two types of test may or may not be significant as regards pavement response to load since the modulus throughout the granular layers is determined from the existing state of stress. This point is discussed in greater detail in Chapter 6.

It has been mentioned previously that the CCP test data for all specimens yielded significantly higher values for the resilient Poisson's ratio than the VCP data. That this is indicative of correspondingly greater volume change may be seen from the following.

It can be shown that the volumetric strain of a specimen  $\frac{\Delta v}{v}$ , is equal to the first invariant of the strain tensor,  $\epsilon_1 + 2\epsilon_3$  for the triaxial test specimen. A quick examination of the data in Appendix A will show that at almost all stress levels applied during the CCP test,  $\frac{\Delta v}{v}$  calculated from the sum of the principal strains would indicate that the specimen increased in volume. However, applying the same procedure to the VCP test results would show much lower magnitudes of volume change. Accordingly, it is felt that the conditions of the CCP test are such that inordinate degrees of volume change are imposed on the specimen; thereby yielding results that erroneously overestimate Poisson's ratio.

For all specimens the CCP test caused larger plastic axial strains than did the VCP test. Table 5.5 shows the total plastic axial strain accumulated by each specimen during the entire test series. It also shows the percentage

TABLE 5.5  
PERCENTAGE TOTAL AXIAL STRAIN ACCUMULATED  
DURING VCP AND CCP TESTS

Specimen	Total Plastic Axial Strain, $\epsilon_p$ in/in	% $\epsilon_p$ During VCP test	% $\epsilon_p$ During CCP test
HD-1	.0036	49	51
MD-1	.0149	22	78
LD-1	.0191	48	52
HD-2	.0158	42	58
MD-2	.0173	43	57
LD-2	.0204	43	57
HD-3	.0063	49	51
MD-3	.0152	46	54
LD-3	.0193	43	57

of the total plastic strain accrued during the CCP and VCP portions of each test series. From Table 5.5 it can be seen that the CCP portion of each test series resulted in from 2 per cent to 56 per cent greater plastic axial strains than the VCP test, although for most specimens the difference was around 8 to 10 per cent. Finn (26) has shown that, on the basis of the Mohr-Coulomb yield criteria for soils, plastic strain is accompanied by volume change. From this viewpoint, the greater volume change observed during the CCP test is compatible with the greater resultant plastic strains.

Although for this study no measurements were made relating plastic strain to principal stress ratio, plastic strains appeared to increase as the principal stress ratio increased at all levels of confining pressure. This rate of increase was observed to be greater for the CCP test conditions. Barksdale (10) also reported the increase in plastic strains resulting from increasing stress ratios.

### 5.5 Summary of Laboratory Results

The preliminary test series confirmed the findings of previous investigators that the resilient response of the granular test specimens was only minimally affected by variations in stress pulse duration and that the resilient response determined after a very few stress repetitions was representative of the response after several thousand repetitions. Furthermore, one specimen could be subjected to the entire range of stress levels and these stresses could be applied in any sequence.

The primary test series data indicated that, in general, the resilient modulus of a specimen increased as the dry density increased. Similarly, the crushed stone appeared to exhibit slightly greater values of  $E_r$  than the gravel. Poisson's ratio was less affected by material type and level of density.

Accumulated plastic axial strains decreased as density increased. The crushed stone showed the least plastic strain followed by the blend material and gravel in that order.

Compared to the VCP test data, the CCP data consistently overestimated Poisson's ratio and generally overestimated the  $E_r$  by varying amounts. Also, the CCP test always resulted in slightly greater plastic axial strains.

The most significant findings were that the resilient response of all specimens was drastically affected by stress level. This observation is best illustrated by the forms of the regression equations for  $E_r$  and  $v_r$  (Equations 5.4, 5.5a and 5.5b). As compared with the variations in  $E_r$  induced by changes in the state of stress, density and material-type effects are small. The typically flat appearance of the  $v_r$  curve in the range of  $\sigma_1/\sigma_3$  most likely to occur in in-service pavements would indicate that this parameter would vary only slightly under field conditions.

Before conclusions can be drawn regarding the significance of the variations in resilient parameters induced by variations in material type and density, or obtained by different test procedures, it is first necessary to examine these differences in the context of their effects on the response of a pavement structure to wheel loadings. This is done in Chapter 6.

## CHAPTER 6

## IMPLICATIONS OF THE LABORATORY RESULTS FOR PAVEMENT ANALYSIS

6.1 Introduction

As discussed in Chapter 5, the results of the laboratory investigations yielded predictive equations for the resilient modulus for each specimen that differed for each type of test (VCP and CCP). For two specimens, the high and intermediate density blend materials, there was very little difference in the data derived from the two tests. However, for the other specimens the CCP test appeared to overestimate  $E_r$  throughout most of the range of  $\theta$  values. The magnitude of the difference in each case was seen to be a function of  $\theta$ , because of the intersecting nature of most of the pairs of regression lines. Obviously the difference in calculated values of  $E_r$  would be small for values of  $\theta$  near the point of intersection and would increase for  $\theta$  values progressively less than or greater than  $\theta$  at the point of intersection. Even for the cases where  $E_r$ , as determined by the CCP test, was greater than  $E_r$  from the VCP test throughout the range of  $\theta$ , the difference was not constant because of the different slopes of the regression lines. Therefore, any determination of the significance of the differences in test results must take into account the variable  $\theta$ , the sum of the principal stresses or first invariant. It is obvious that if the range of  $\theta$  occurring in a particular pavement section would yield similar values of  $E_r$  from the predictive equations for either type test, then the use of either model in an analysis would result in only very slight changes in certain computed indicators of pavement response. Conversely, if any analysis is carried out at each of a wide range of resilient material parameters, then the calculated changes in these same indicators would be indicative of the relative influence of each parameter that was varied. Such a procedure, termed sensitivity analysis,

has been used by other investigators to determine the effects of variations in material parameters on various aspects of pavement response to load (49) (64). The sensitivity analysis reported in this chapter was undertaken as an attempt to assay the significance, if any, of the variations in  $E_r$  resulting from the VCP and CCP type triaxial tests.

Four indicators of pavement response were studied--surface deflection, tensile strain in the asphalt layer, vertical stress and vertical strain in the subgrade. The first three indicators were discussed in Chapter 3. The use of vertical strain in the subgrade as a factor to be studied has been suggested by Klomp and Dormon (40). As reported in reference (40), limiting values of vertical subgrade strain constitute part of the basis of the design procedure for flexible pavements developed by the Koninklijke Shell Laboratorium in Amsterdam. It is known that surface deflection and maximum tensile strain at the bottom of the bituminous surface course relate directly to fatigue cracking of the asphalt (64), and vertical stresses and strains in the subgrade can be correlated with subgrade rutting (20). Therefore it is considered that these four indicators of pavement performance are sufficiently comprehensive to provide reliable evidence of the effects of variations in material properties on pavement response to load.

The sensitivity analysis discussed herein consisted of finite elements analysis of one typical flexible pavement section. Twenty one combinations of base and subbase course material parameters were utilized. The computer solution was described in Chapter 3. For this analysis the program was modified to allow the modulus of the granular material to be computed as a function of  $\theta$ ,  $E_r = K\theta^n$ . Poisson's ratio was input as a constant for each layer in the system, but in view of the very slight changes in  $\nu_r$  for the range of  $\sigma_1/\sigma_3$  encountered in a flexible pavement structure the error resulting from

the use of a constant value can be regarded as minimal.

The one pavement structural configuration analyzed is shown in Figure 6.1, and the finite element grid is depicted in Figure 6.2. The 80 psi surface pressure was applied in 8 increments.

To ascertain the significance of changes in  $K$  and  $n$  values ( $E_r = K \theta^n$ ) and Poisson's ratio, each of the three parameters was varied over a wide range of possible values. In addition, an inverted section, similar to Figure 6.1 except that the granular subbase was replaced by an equal thickness of lime-stabilized subgrade, was analyzed. Descriptions of the different combinations of material parameters are listed in Table 6.1. Note that Section 1 is described as the reference section. Changes in the indicators of pavement performance induced by variations in material parameters are compared to the indicators resulting from analysis of section 1. Likewise Section 15, the stabilized reference section, serves as a basis for comparison of the subsequent sections. For section 1  $E_r$  and  $\nu_r$  of the base course were described by the regression line developed from the VCP triaxial test data for specimen HD-1 and the resilient parameters of the subbase were determined by the VCP test on specimen LD-2. For all sections the properties of the asphalt layer and subgrade were as for the section described in Chapter 3. It should be noted that the ranges of values for  $K$ ,  $n$ , and  $\nu_r$  shown in Table 6.1 were determined from analysis of the laboratory data.

#### 6.2 $K$ and $n$ Varied Simultaneously

The results of the sensitivity analysis are shown in Table 6.2. For Section 2 the equations for  $E_r$  for both the base and subbase were replaced with those determined from the CCP test results on the same specimens. The resulting

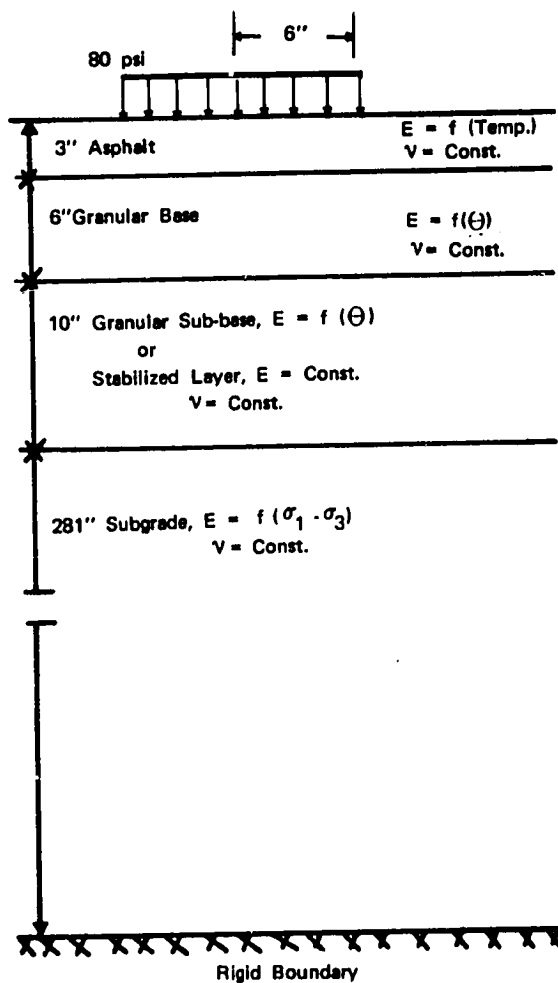
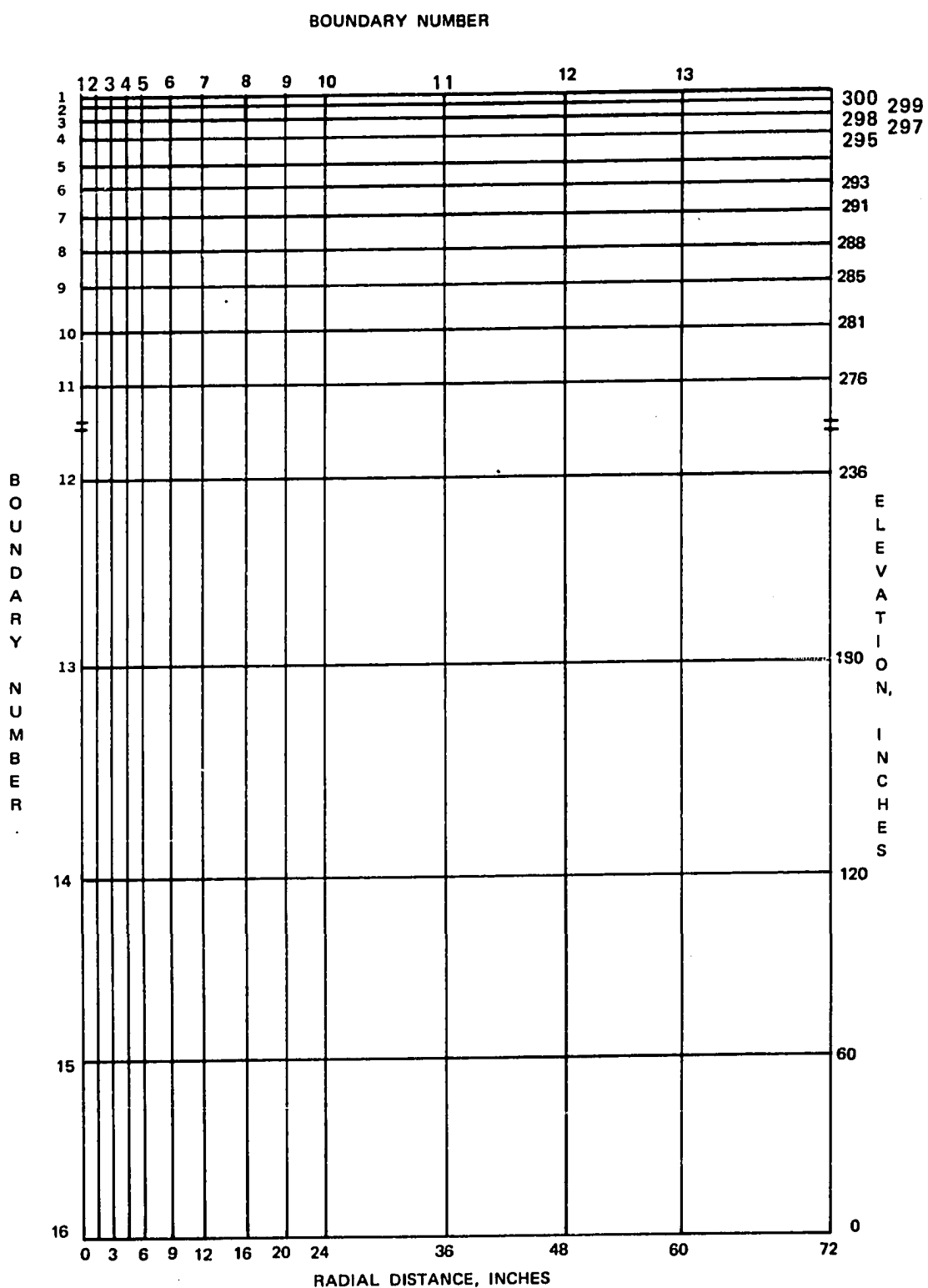


Figure 6.1  
Pavement Structural Configuration Used in Sensitivity Analysis



**Figure 6.2**  
Finite Element Mesh Configuration of Pavement Structure used  
in Sensitivity Analysis

TABLE 6.1

## RESILIENT MATERIAL PARAMETERS USED IN SENSITIVITY ANALYSIS

Section	Base Course $E_r$ , psi	Base Course $\nu_r$	Subbase $E_r$ , psi	Subbase $\nu_r$
1	$66350^{.40}$	.38	$16130^{.69}$	.38
2	$23760^{.69}$	.38	$28490^{.56}$	.38
3	$23760^{.69}$	.38	$16130^{.69}$	.38
4	$66350^{.69}$	.38	$28490^{.56}$	.38
5	$25000^{.40}$	.38	$16130^{.69}$	.38
6	$80000^{.40}$	.38	$16130^{.69}$	.38
7	$66350^{.60}$	.38	$16130^{.69}$	.38
8	$66350^{.30}$	.38	$16130^{.69}$	.38
9	$66350^{.40}$	.38	$35000^{.69}$	.38
10	$66350^{.40}$	.38	$70000^{.69}$	.38
11	$66350^{.40}$	.38	$16130^{.45}$	.38
12	$66350^{.40}$	.38	$16130^{.30}$	.38
13	$66350^{.40}$	.45	$16130^{.69}$	.38
14	$66350^{.40}$	.30	$16130^{.69}$	.38
15**	$66350^{.40}$	.38	$E = 150,000 \text{ psi } \nu_r = 0.12$ (stabilized layer)	
16	$25000^{.40}$	.38	$E = 150,000 \text{ psi } \nu_r = 0.12$ (stabilized layer)	
17	$80000^{.40}$	.38	$E = 150,000 \text{ psi } \nu_r = 0.12$ (stabilized layer)	
18	$66350^{.60}$	.38	$E = 150,000 \text{ psi } \nu_r = 0.12$ (stabilized layer)	
19	$66350^{.30}$	.38	$E = 150,000 \text{ psi } \nu_r = 0.12$ (stabilized layer)	
20	$66350^{.40}$	.30	$E = 150,000 \text{ psi } \nu_r = 0.12$ (stabilized layer)	
21	$66350^{.40}$	.45	$E = 150,000 \text{ psi } \nu_r = 0.12$ (stabilized layer)	

\* Reference Section

\*\* Reference Inverted Section

changes in surface deflection and tensile strain in the asphalt are minimal. The changes in subgrade stress and strain appear to be more drastic at first glance. However, viewed in light of the small magnitudes of stress and strain computed, these changes, too, are slight. For example, the maximum compressive strains on the subgrade shown in Table 6.2 are less than one half the limiting strain proposed by Klomp and Dorman (40) for pavements to be subjected to 1,000,000 loads. It should be noted that these limiting strain criteria were developed from the AASHO Road Test data (32) and substantiated by analyses of conventional pavement sections developed from CBR design curves. These analyses yielded maximum subgrade strains of 8 to  $9 \times 10^{-4}$  in/in regardless of soil type (40).

For Sections 3 and 4 the CCP data were substituted for the VCP data for one granular layer at a time. Again, the variations in the pavement response were slight.

### 6.3 K Varied - n Unchanged

For Sections 5 and 6, the value of the coefficient K for the base course was changed to 2500 and 8000 respectively and the subbase modulus was the same as for section one. Note that Section 5, with a decrease in K of over 60 per cent, shows only an 11 per cent increase in surface deflection. For Section 6, the increase in K of about 20 per cent resulted in a decrease in surface deflection of only 0.6 per cent. For each section the changes in the other indicators were similar in magnitude to those in surface deflection. Again, the variations in subgrade stress and strain were numerically greater than the changes in the other indicators.

However, for Sections 16 and 17, the inverted sections for which the K values for the base course underwent identical changes as Sections 5 and 6 the variations in surface deflection and tensile strains in the asphalt were

TABLE 6.2  
EFFECTS OF VARIATIONS IN RESILIENT PARAMETERS ON INDICATORS OF PAVEMENT PERFORMANCE

Section	Surface Deflection $\delta$ , inch	Vertical Stress $\sigma_z$ , psi	Maximum Tensile Strain $\epsilon_t$ in/in	Vertical Strain on Subgrade $\epsilon_z$ in/in
	% Change*	% Change*	% Change*	% Change*
1. Reference Section VCP Parameters For Base and Subbase	.0284	0.0	5.77	0.0
2. CCP Base, CCP Subbase	.0268	-5.6	6.85	+18.5
3. CCP Base, VCP Subbase	.0295	+4.0	6.63	+14.8
4. VCP Base, CCP Subbase	.0256	-9.8	6.06	+5.0
5. $K_{base} = 2500$	.0317	+11.1	6.43	+11.4
6. $K_{base} = 8000$	.0282	-0.6	5.54	-4.0
7. $n_{base} = 0.60$	.0281	-1.0	5.44	-5.6
8. $n_{base} = 0.30$	.0287	+1.0	5.96	+3.4
9. $K_{subbase} = 3500$	.0223	-21.4	6.78	+17.5
10. $K_{subbase} = 7000$	.0198	-30.2	5.93	+2.8
11. $n_{subbase} = 0.45$	.0322	+13.2	5.14	-10.8
			428	0.0
			220	0.0

\* % Change refers to the change in the indicator as compared to the Reference Section

TABLE 6.2 (con't)  
EFFECTS OF VARIATIONS IN RESILIENT PARAMETERS ON INDICATORS OF PAVEMENT PERFORMANCE

Section	Surface Deflection $\delta$ , inch	% Change*	Vertical Stress $\sigma_z$ , psi	% Change*	Maximum Tensile Strain $\epsilon_t$ in/in	% Change*	Vertical Strain on Subgrade $\epsilon_z$ in/in	% Change*
12. $n_{subbase} = 0.30$	.0350	+23.2	4.78	-17.2	488	+14.0	171	-22.2
13. $v_r$ base = 0.45	.0275	-3.0	5.92	+2.5	410	-4.1	242	+10.0
14. $v_r$ base = 0.30	.0298	+5.0	5.27	-8.6	450	+5.0	196	-10.6
15. Reference Section For Inverted Systems	.0143	0.0	5.15	0.0	260	0.0	185	0.0
16. $K_{base} = 2500$	.0204	+42.5	5.12	-0.5	365	+40.5	176	-5.0
17. $K_{base} = 8000$	.0135	-5.6	5.14	0.0	241	-7.2	185	0.0
18. $n_{base} = 0.60$	.0123	-14.0	5.20	+1.0	202	-12.2	188	+1.5
19. $n_{base} = 0.30$	.0154	+7.8	5.10	-1.0	288	+11.0	182	-1.5
20. $v_r$ base = 0.30	.0153	+7.0	5.02	-2.5	268	+3.0	178	-3.8
21. $v_r$ base = 0.45	.0130	-9.0	5.36	+4.0	249	-4.2	195	+5.4

\* % Change refers to the change in the indicator as compared to the Reference Section

much more drastic. Also of interest regarding the inverted sections were the very slight variations in subgrade stress and strain induced by changes in the granular material parameters. This effect must be attributed to the load spreading action of the much stiffer stabilized layer which effectively insulated the subgrade from the rest of the system.

Variations in the value of K for the subbase (Sections 9 and 10) accounted for a wider range of variations in the performance indicators than did the changes in base course parameters (Sections 5 and 6). Most of this variation can be explained by the greater thickness of the subbase and by the fact that the changes in K for the subbase were much greater (+215 per cent for Section 9 and +430 per cent for Section 10.)

#### 6.4 n Varied - K Constant

Changing the value of the exponent n for the base course (Sections 7 and 8) caused very slight variations in the computed indicators. However, for the inverted Sections 18 and 19, the same changes in n of the base course resulted in much larger variation in surface deflections and tensile strains in the asphalt concrete. Again the subgrade stresses and strains were virtually unaffected in the inverted sections.

The variations in n values for the subbase (Sections 11 and 12) resulted in greater changes in the indicators of pavement performance than did the changes in n for the base course for the same reasons stated in connection with the changes in the parameter K.

#### 6.5 Poisson's Ratio Varied

Poisson's ratio,  $\nu_r$ , was varied for the base course in Sections 13 and 14. As shown in Table 6.2, only minimal changes in pavement response resulted.

The changes in response due to variations in the base course  $v_r$  for the inverted Sections 20 and 21 were somewhat greater than those for Sections 13 and 14, but still relatively small as compared to the variations wrought by increasing or decreasing the resilient modulus of the granular layers.

#### 6.6 Interaction of K and n

Examination of Table 6.2 indicates that changes in the coefficient K and exponent n of the granular layers can result in large variations in the computed indicators of pavement response. The greatest variations in response were caused by quite large variations in the parameters and occurred when K and n were both at maxima or both at minima. When varied singly, it appeared that changes in each parameter of the same relative magnitude lead to similar variations in the response indicators. Thus it is difficult to state that one parameter exerts greater influence than the other. When both K and n are varied simultaneously, as is the case when CCP parameters are substituted for VCP parameters (Sections 2, 3, and 4), the computed response indicators undergo little change. This development can only be explained by assuming an interaction of K and n. In Chapter 5 it was stated that for all specimens the regression lines for the VCP and CCP test data were not identical. However, it was pointed out that in no case did both K and n increase or decrease from one test type to another. If one parameter increased, the other decreased; thereby causing the regression curves to intersect or converge. The importance of this observation can be seen from the results of the sensitivity analysis of Sections 2, 3, and 4. The interaction of K and n is such that the effects of an increase in one are largely negated by a decrease in the other and vice-versa.

### 6.7 Significance of Variations in the Resilient Material Parameters

The results of the sensitivity analysis tabulated in Table 6.2 demonstrate the importance of accounting for the stress dependent properties of granular materials. Changes in one parameter K or n without regard to the magnitude of the other parameter can result large variations in the indicators of pavement response, depending upon the magnitude of the changed parameter.

A most significant conclusion to be drawn relates to the interaction of the variables K and n and the manner in which they vary for the two different test types (VCP and CCP) on any one specimen. On the basis of the nature of the variations in K and n, as determined by each type test (Table 5.3) and the effects of the interaction of K and n (Table 6.2), it can be concluded that the predictive equations for the resilient modulus, as determined by the CCP test, are adequate for use in pavement analyses. In other words, Table 6.2 indicates that the stress dependent model for the resilient modulus is of the utmost significance and that the parameters of the model, K and n, developed from either type laboratory test would yield similar analytical results. Because the CCP test can be conducted with standard laboratory triaxial testing equipment and the VCP test requires additional expensive equipment, it appears that the effects of differences in the test results are so slight as to render the more complicated VCP test unnecessary.

Furthermore, because the values of Poisson's ratio computed from CCP test data are unacceptably large and because of the relatively flat slope of the regression line for  $\nu_r$  from the VCP test over the range of  $\sigma_1/\sigma_3$  occurring in granular pavement layers and because pavement response to load is least affected by changes in Poisson's ratio, constant values of  $\nu_r$  in the range of 0.35 to 0.40 can be assigned to the granular layers with only minimal errors resulting.

The results of the sensitivity analysis of the inverted section revealed certain important points. First, as was also mentioned in the stress analysis section in Chapter 3, the use of a stiffer layer underneath the granular base results in drastically reduced surface deflections and tensile strains in the asphalt layer. Furthermore, stresses and strains in the subgrade are less than for conventional sections. Second, the increased stress levels in the overlying granular layers induced by the stabilized layer are such that the stress dependent nature of the granular layer is accentuated. This results in significantly greater variations in surface deflections and tensile strains in the asphalt concrete accompanying changes in the base course parameters K and n than in conventional sections. In addition, the subgrade is effectively insulated from changes in the parameters of the granular layers by the flexural action of the stabilized layer. Finally, it should be noted that the maximum tensile stresses developed in the stabilized layer are quite small ( $\approx 10$  psi) and are only minimally affected by changes in the modulus of the overlying granular material.

In summary, the sensitivity analysis of the data collected during the laboratory investigation phase of this study confirms the applicability of the repeated load triaxial test at constant confining pressures as an effective means of characterizing the resilient response of granular materials. Furthermore, because of the stress dependent nature of the resilient modulus of these materials and the effects on pavement response of variations in the modulus, proper account of the state of stress within granular layers is essential when defining material parameters for pavement structural analysis.

## CHAPTER 7

## SUMMARY AND CONCLUSIONS

### 7.1 Summary

During the course of this study, three materials -- crushed stone, gravel, and a blend of crushed stone and gravel -- were tested in the triaxial apparatus at three levels of density. Two types of repeated-load triaxial tests were carried out on each of the nine specimens: the variable confining pressure test (VCP), in which the chamber pressure was varied simultaneously with the axial stress, and the constant confining pressure test (CCP), in which the chamber pressure was held constant during application of the axial stress. For each test type, predictive equations for the resilient modulus and resilient Poisson's ratio of the specimen were developed through regression analysis of the test data. A highly significant correlation was found to exist between the state of stress in the specimen and the resilient parameters.

A sensitivity analysis was performed utilizing a finite elements computer solution. In this portion of the study a conventional flexible pavement section and an inverted section were analyzed and the effects of changes in the resilient material parameters on four indicators of pavement response were noted.

### 7.2 Conclusions

Conclusions derived from the results of this investigation are as follows:

1. The resilient response of well-graded granular materials, such as those tested in this study, is independent of stress pulse duration. Therefore, any pulse duration in the range of those applied to elements of pavements by wheel loads moving at speeds of about 15 to 70 miles per hour may be used in laboratory investigations.

2. The resilient response of a specimen determined after 25 to 100 stress repetitions is representative of the response after several thousand stress repetitions.

3. One specimen may be used to measure the resilient response over the entire range of stress levels. In addition, the stress sequence tests revealed that these stress levels could be applied to the specimen in any order without incurring testing error.

4. The testing variable most significantly affecting the resilient response of the granular specimens was the applied state of stress. The stress dependent nature of the resilient parameters is typified by the form of the predictive equations for  $E_r$  and  $\nu_r$ :

$$E_r = K\theta^n \quad \text{or} \quad E_r = K' \sigma_3^{n'}$$

and

$$\nu_r = b_0 + b_1 (\sigma_1/\sigma_3) + b_2 (\sigma_1/\sigma_3)^2 + b_3 (\sigma_1/\sigma_3)^3$$

where,  $K$ ,  $n$ ,  $K'$ ,  $n'$ , and the  $b$  coefficients are constants resulting from regression analysis of the test data.

5. The resilient parameters are affected by variations in the dry density of the specimen. Generally, the resilient modulus increases as density increases. Poisson's ratio showed no consistent variation with changes in density. The values of  $\nu_r$  were very similar for all specimens at corresponding values of  $\sigma_1/\sigma_3$  for the VCP test.

6. The effects of material type on the resilient parameters are slight compared with the effects of changes in the state of stress. In general, the crushed stone yielded slightly higher values of  $E_r$  than the gravel. The modulus of the blend material was normally between those of the other materials.

Poisson's ratio varied only minimally from one material to another. The values of  $\nu_r$  calculated for the gravel normally exceeded those for the crushed stone.

7. Indications of anisotropic behavior were observed for both the CCP and VCP tests. Although it was not possible to measure the stiffness in both the lateral and axial directions, it appeared that each specimen was less stiff in the lateral direction.

8. As compared to the VCP test, the CCP test greatly overestimated Poisson's ratio. Most likely, a portion of the large lateral deformations observed were due to nonuniform states of stress and strain within the specimen. However, since the VCP test yielded values of  $\nu_r$  in the range of 0.35 to 0.40 it is felt that conditions of the CCP test are such as to impose greater amounts of volume change on the specimens, as indicated by the computed values of  $\nu_r$  consistently in excess of 0.50.

9. Values of the resilient modulus computed from CCP test data exceeded  $E_r$  computed from the VCP tests for most stress levels. The magnitude of the difference was itself a function of the state of stress and, thus, non-constant. However, on the basis of the observed interaction of the parameters K and n. from the sensitivity analysis and the intersecting nature of the regression lines for  $E_r$  as determined for each type test, it can be concluded that any differences in the predictive equations for  $E_r$  derived from the two test procedures exert only minimal influence on such indicators of pavement response as surface deflection, maximum tensile strain in the asphalt concrete layer, and vertical stress and strain in the subgrade. Therefore the continued use of the CCP triaxial test as a means of characterizing granular materials is justified.

10. Although the CCP test yields unacceptably high values of Poisson's ratio, the use of a constant value of  $\nu_r$  for granular paving materials, in

the range of 0.35 to 0.40, appears to adequately represent this parameter for pavement analysis. This conclusion is formed on the basis of the relatively flat slope of the regression line for  $\nu_r$  over a range of  $\sigma_1/\sigma_3$  from 2 to 7. In addition, the indicators of pavement response are least affected by changes in Poisson's ratio, as shown by the results of the sensitivity analysis.

11. Total plastic axial strains developed in a specimen during the CCP test exceeded those developed during the VCP test by 2 to 56 per cent. Furthermore, the least total plastic axial strains were accumulated by the crushed stone, followed by the blend material and gravel in that order. Also, as the density of each material type increased, plastic axial strains decreased. It appeared that density level and material type effects were more pronounced for plastic response than for resilient response.

12. The sensitivity analysis showed the necessity of accounting for the state of stress in granular layers when computing pavement response to load. The results of the sensitivity analysis also indicate that an investigator can choose reasonable representative values for the resilient granular material parameters for preliminary analysis of a proposed pavement section without the benefit of prior laboratory tests.

13. The merits of the inverted pavement section were also demonstrated by the sensitivity analysis. The use of a stabilized layer below the granular base course results in increased stress levels in the overlying granular layer. Thus the resilient modulus in the granular layer is increased. This in turn leads to such beneficial effects as lower surface deflections, reduced tensile strains in the asphalt, and lower vertical stresses and strains in the subgrade. In addition, the tensile stresses in the stabilized layer of a well designed pavement structure are slight. Furthermore, the heightened stress levels in the granular layer render this material more sensitive to changes in the parameters

K and n; again demonstrating the necessity of proper material characterization. The inverted section represents one technique of exploiting the stress dependent nature of the resilient response of granular materials to the designer's advantage.

### 7.3 Recommended Research

During the course of this study it became apparent that further investigations were necessary in two areas:

1. The anisotropic behavior of granular materials has been noted. Further research is necessary to determine the relative stiffness of compacted granular specimens in the axial and lateral directions as well as the significance of this type behavior for pavement response to load.
2. Further research should be directed towards the prediction of plastic response of granular materials subjected to great numbers of stress repetitions. In addition, methods of reducing the rutting tendencies of granular layers should be investigated. Such methods could take the form of the addition of stabilizing agents to modify the fine materials, altered gradation, or the blending of different material types.

## LIST OF REFERENCES

1. Ahlvin, R. G., "Multiple - Wheel Heavy Gear Load Pavement Tests," Technical Report No. AFWL-TE-70-113, Vol. 1, Air Force Special Weapons Laboratory, Kirtland AFB, New Mexico, 1971 .
2. Ahlvin, R. G., and Ulery, H. H., "Tabulated Values for Determining the Complete Pattern of Stresses, Strains, and Deflections Beneath a Uniform Circular Load on a Homogeneous Half Space," Highway Research Board Bulletin No. 342 (1962), pp. 1-13.
3. Bamert, E., Schnitter, G., and Weber, M., "Triaxial and Seismic Laboratory Tests for Stress-Strain-Time Studies," Proceedings, Sixth International Conference of Soil Mechanics and Foundation Engineering, 1965, Vol. 1, pp. 151-155.
4. Barenberg, E. J., "Mathematical Modeling of Pavement Systems," State of the Art Report, U. S. Army Construction Engineering Research Laboratory, Champaign, Illinois, March, 1970.
5. \_\_\_\_\_, "Behavior and Performance of Aggregate-Soil Systems Under Repeated Loads," Civil Engineering Studies, Highway Engineering Series No. 42, Illinois Cooperative Highway Research Program, Series No. 125, University of Illinois, Urbana, Illinois, August, 1971.
6. \_\_\_\_\_, "A Structural Design Classification of Pavements Based on an Analysis of Pavement Behavior, Material Properties, and Modes of Failure,: Ph.D. Thesis, University of Illinois, 1965.
7. Barkan, D. D., Dynamics of Bases and Foundations, McGraw-Hill, New York, 1962.
8. Barksdale, R. D., "Analysis of Layered Systems," Final Report, Project B-607, National Science Foundation Grant No. GK-1583, Georgia Institute of Technology, Atlanta, 1969.
9. \_\_\_\_\_, "Compressive Stress Pulse Times in Flexible Pavements for Use in Dynamic Testing," Highway Research Record No. 345 (1971), pp. 32-34.
10. \_\_\_\_\_, "Repeated Load Test Evaluation of Base Course Materials," Final Report, Project E20-609, State Highway Department of Georgia, Georgia Institute of Technology, Atlanta, December, 1971.
11. Barksdale, R. D., and Hicks, R. G., "Material Characterization and Layered Theory for Use in Fatigue Analysis," Paper Presented at the Annual Meeting of the Highway Reserch Board, Washington, D. C., January, 1973.
12. Brown, S. F., and Pell, P. S., "A Fundamental Structural Design Procedure for Flexible Pavements," Proceedings, Third International Conference on the Structural Design of Asphalt Pavements, London, September, 1972, pp. 369-381.

13. Burmister, D. M., "The General Theory of Stresses and Displacements in Layered Theory," *Journal of Applied Physics*, Vol. 16, No. 2, 3, and 5, 1945.
14. Burt, M. E., "Progress in Pavement Design," Report LR 508, Transport and Road Research Laboratory, Crowthorne, Berkshire, Great Britain, 1972.
15. Charyulu, M. K., and Sheeler, J. B., "Theoretical Stress Distribution in an Elastic Multi-Layered System," *Highway Research Record No. 228* (1968), pp. 11-17.
16. Compton, J. R., and Strohm, W. E., Jr., "Compaction of Cohesionless Materials," *Miscellaneous Paper S-68-15*, U. S. Army Engineer Waterways Experiment Station, Vicksburg, Mississippi, August, 1968.
17. Deacon, J. A., "Materials Characterization - Experimental Behavior," *Highway Research Board Special Report No. 126* (1971), pp. 150-173.
18. Dehlen, G. L., "The Effect of Non-Linear Material Response on the Behavior of Pavements Subjected to Traffic Loads," Ph.D. Dissertation, University of California, Berkeley, 1969.
19. Dehlen, G. L., and Monismith, C. L., "Effect of Nonlinear Material Response on the Behavior of Pavements Under Traffic," *Highway Research Record No. 310* (1970), pp. 1-16.
20. Dorman, G. M., and Metcalf, C. T., "Design Curves for Flexible Pavements Based on Layered System Theory," *Highway Research Record No. 71* (1965), pp. 69-84.
21. Duncan, J. M., and Chang, C. Y., "Nonlinear Analysis of Stress and Strain in Sails," Proceedings, ASCE, SM-5, 1970, pp. 1629-1654.
22. Duncan, J. M., and Dunlop, P., "The Significance of Cap and Base Restraint," Proceedings, ASCE, SM-1, 1968, pp. 271-290.
23. Duncan, J. M., Monismith, C. L., and Wilson, E. L., "Finite Element Analysis of Pavements," *Highway Research Record No. 228* (1968), pp. 18-33.
24. Dunlap, W. A., "A Report on a Mathematical Model Describing the Deformation Characteristics of Granular Materials," Technical Report No. 1, Study 2-8-62-27, Texas Transportation Institute, Texas A & M University, College Station, 1963.
25. Finn, F. N., Nair, K., and Monismith, C. L., "Applications of Theory in the Design of Asphalt Pavements," Proceedings, Third International Conference on the Structural Design of Asphalt Pavements, London, September, 1972, Vol. 1, pp. 392-409.
26. Finn, W. D. Liam, "Applications of Limit Plasticity in Soil Mechanics," Proceedings, ASCE, SM-5, Part I, 1967, pp. 101-120.
27. Foster, C. R., and Ahlvin, R. G., "Stresses and Deflections Induced by a Uniform Circular Load," Proceedings, Highway Research Board, 1954.

28. Gray, J. E., "Characteristics of Graded Base Course Aggregates Determined by Triaxial Tests," Engineering Bulletin No. 12, National Crushed Stone Association, Washington, D. C., July, 1962.
29. Hardin, B. O., "Constitutive Relations for Airfield Subgrade and Base Course Materials, I. Characterization and Use of Shear Stress-Strain Relations," Technical Report UKY-32-71-CE5, College of Engineering, University of Kentucky, Lexington, 1971.
30. Haynes, J. H., and Yoder, E. J., "Effects of Repeated Loading on Gravel and Crushed Stone Base Course Materials Used in the AASHO Road Test," Highway Research Record No. 39 (1963), pp. 82-97.
31. Hicks, R. G., "Factors Influencing the Resilient Properties of Granular Materials," Ph.D. Dissertation, University of California, Berkeley, 1970.
32. Highway Research Board Special Reports 61A-61G - The AASHO Road Test, 1961.
33. Hoover, J. M. Kumar, S., and Best, T. W., "Degradation Control of Crushed Stone Base Course Mixes During Laboratory Compaction," Highway Research Record No. 301 (1970), pp. 18-27.
34. Huang, Y. H., "Stresses and Displacements in Nonlinear Soil Media," Proceedings, ASCE, SM-1, 1968, pp. 1-19.
35. Huculak, N. A., "Evaluation of Pavements to Determine Maintenance Requirements," Highway Research Record No. 129 (1966), pp. 12-27.
36. Jones, A., "Tables of Stresses in Three-Layer Elastic Systems," Highway Research Board Bulletin No. 342 (1962), pp. 176-214.
37. Kasianchuk, D. A., "Fatigue Considerations in the Design of Asphalt Concrete Pavements," Ph.D. Dissertation, University of California, Berkeley, 1968.
38. Kiewan, R. W., and Glynn, T. E., "Environmental Factors in Analysis of Flexible Pavements," Contract No. DAJA37-70-C-1116, U. S. Army European Research Office, September, 1971.
39. Kirkpatrick, W. M., and Belshaw, D. J., "On the Interpretation of the Triaxial Test," Geotechnique, Vol. 18, No. 3, September, 1968, pp. 336-350.
40. Klomp, A. G. J., and Dormon, G. M., "Stress Distribution and Dynamic Testing in Relation to Road Design," Proceedings, Second Conference of the Australian Road Research Board, Volume II, 1964, pp. 701-728.
41. Ko, H.Y., and Scott, R. F., "A New Soil Testing Apparatus," Geotechnique, Vol. 17, No. 1, March, 1967, pp. 40-57.
42. \_\_\_\_\_, "Deformation of Sand in Hydrostatic Compression," Proceedings, ASCE, SM-3, May, 1967, pp. 137-156.

43. Kondner, R. L. and Zelasko, J. S., "A Hyperbolic Stress-Strain Formula-tion for Sands," Proceedings, Second Pan American Conference of Soil Mechanics and Foundation Engineering, Vol. 1, 1963, pp. 287-324.
44. Kraft, L. M., and Krishnamurthy, N., "Analytical Model for Evaluating Stress-Strain Response of Soils," Journal of Materials, JMLSA, Vol. 6, No. 4, December, 1971, pp. 800-817.
45. Lister, N. W., "Deflection Criteria for Flexible Pavements," TRRL Report LR375, Transport and Road Research Laboratory, Crowthorne, Berkshire, Great Britain, 1972.
46. Love, A. E. H., A Treatise on the Mathematical Theory of Elasticity, Dover Publications, New York, 1944.
47. Makhlof, H. M., and Stewart, J. J., "Factors Influencing the Modulus of Elasticity of Dry Sand," Proceedings, Sixth International Conference of Soil Mechanics and Foundation Engineering, Vol. 1, 1965, pp. 298-302.
48. Mitry, F. G., "Determination of the Modulus of Resilient Deformation of Untreated Base Course Materials," Ph.D. Dissertation, University of California, Berkeley, 1965.
49. Monismith, C. L., Hicks, R. G., and Salam, Y. M., "Basic Properties of Pavement Components," Report No. FHWA-RD-72-19, Federal Highway Administration, 1971.
50. Moore, W. M., Swift, G., and Milberger, L. J., "Deformation Measuring System for Repetitively Loaded, Large Diameter Specimens of Granular Materials," Research Report 99-4, Study 2-8-65-99, Texas Transportation Institute, Texas A & M University, College Station, August, 1969.
51. Moore, W. M., Britton, S. C., and Scrivner, F. H., "A Laboratory Study of the Relation of Stress to Strain for a Crushed Limestone Base Material," Research Report 99-5F, Study 2-8-65-99, Texas Transportation Institute, Texas A & M University, College Station, September 1970.
52. Morgan, J. R., "The Response of Granular Materials to Repeated Loadings," Proceedings, Third Conference of the Australian Road Research Board, Sydney, 1966, pp. 1178-1192.
53. Nair, K., and Chang, C. Y., "Materials Characterization," Final Report, National Cooperative Highway Research Program, Project No. 1-10 and 1-10/1, Highway Research Board, December, 1970.
54. Nair, K., "Solutions and Solutions Techniques for Boundary Value Problems," Highway Research Special Report 126, 1971, pp. 103-113.
55. Nelson, I., and Baron, M. L., "Application of Variable Moduli Models to Soil Behavior," International Journal of Solids and Structures, Vol. 7, 1971, pp. 399-417.

56. Newmark, N. M., "Influence Charts for Computation of Stresses in Elastic Foundations," Bulletin 338, Engineering Experiment Station, University of Illinois, Urbana, 1942.
57. Nichols, F. P., Jr., "Deflections as an Indicator of Pavement Performance," Highway Research Record No. 13 (1963), pp. 46-65.
58. Peattie, K. R., "Stress and Strain Factors for Three-Layer Elastic Systems," Highway Research Bulletin No. 342 (1962), pp. 215-253.
59. Pell, P. S., and Brown, S. F., "The Characteristics of Materials for the Design of Flexible Pavement Structures," Proceedings, Third International Conference on the Structural Design of Asphalt Pavements, Vol. I, 1972, pp. 326-342.
60. Peutz, M. G. F., van Kempen, H. P. M., and Jones, A., "Layered Systems Under Normal Surface Loads," Highway Research Record No. 228 (1968), pp. 34-45.
61. Seed, H. B., Mitry, F. G., Monismith, C. L., and Chan, C. K., "Prediction of Flexible Pavement Deflections from Laboratory Repeated Load Tests," National Cooperative Highway Research Program Report No. 35, 1967.
62. Selig, E. T., and Joyce, R. P., "Planning Soil Dynamics Instrumentation," Instruments and Apparatus for Soil and Rock Mechanics, ASTM Special Technical Publication 392, 1965, pp. 1-19.
63. Schiffman, R. L., "General Analysis of Stresses and Displacements in Layered Elastic Systems," Proceedings, Second International Conference on the Structural Design of Asphalt Pavements, University of Michigan, Ann Arbor, 1962, pp. 365-375.
64. Smith, W. S., and Nair, K., "A Sensitivity Analysis to Determine the Relative Influence of Materials Characterization on a Fatigue Damage Model," Paper Presented at the Annual Meeting of the Highway Research Board, Washington, D. C., January, 1973.
65. Stephenson, R. J., "Report of Triaxial Correlation Tests on Ottawa Sand," U. S. Army Engineer South Atlantic Division Laboratory, Marietta, Georgia, February, 1969.
66. Terazawa, K., "On the Equilibrium of a Semi-Infinite Elastic Solid," Journal, College of Science, Imperial University of Tokyo, 1916.
67. Terzaghi, K., and Peck, R. B., Soil Mechanics in Engineering Practice, John Wiley and Sons, New York, 1967.
68. The Asphalt Institute, "Thickness Design - Full depth Asphalt Pavement Structures for Highways and Streets", Manual MS-1, 1969.
69. Thompson, O. O., "Evaluation of Flexible Pavement Behavior with Emphasis on the Behavior of Granular Layers," Ph.D. Thesis, University of Illinois, Urbana, 1969.

70. Ueshita, K., and Meyerhof, G. G., "Deflection of Multilayer Soil Systems," Proceedings, ASCE, SM-5, 1967, pp. 257-282.
71. Westmann, R. A., "Stress Analysis by Finite Elements," Highway Research Record No. 228 (1968), pp. 46-58.
72. \_\_\_\_\_, "Fundamentals of Material Characterization," Highway Research Board Special Report No. 126, 1971, pp. 91-102.
73. Wilson, E. L., "Structural Analysis of Axially Symmetric Solids," Journal, American Institute of Aeronautics and Astronautics, Vol. 3, No. 12, 1965, pp. 2269-2274.
74. Yang, N. C., Design of Functional Pavements, McGraw, New York, 1972.
75. Yoder, E. J., Principles of Pavement Design, John Wiley and Sons, New York, 1964.
76. Zube, E., and Forsyth, R., "Flexible Pavement Maintenance Requirements as Determined by Deflection Measurement," Highway Research Record No. 129 (1966), pp. 60-75.
77. \_\_\_\_\_, "A Resilience Design Procedure for Flexible Pavements," Highway Research Record No. 189 (1967), pp. 79-104.

## APPENDIX A

## DATA FROM PRIMARY TEST SERIES

The following pages contain the values of applied stresses, resulting strains, and computed resilient moduli and resilient Poisson's ratios from the primary test series. For the VCP results, the axial stress is  $\sigma_1$ . For the CCP results, the axial stress is the repeated deviator stress. The units of stresses and moduli are psi. Strains are in terms of in/in.

TEST SPECIMEN TYPE		AXIAL STRESS	RADIAL STRESS	AXIAL STRAIN	RADIAL STRAIN	RESILIENT MODULUS	POISSONS RATIO
VCP	HD1	7.8	2.0	.000401	.000074	16319.	.33
		11.7	2.0	.000530	.000200	18930.	.42
		15.9	2.0	.000654	.000310	21381.	.48
		10.3	5.0	.000300	.000036	21658.	.34
		14.6	5.0	.000451	.000071	24826.	.34
		21.1	5.0	.000603	.000160	28879.	.37
		34.5	5.0	.000869	.000360	34660.	.44
		44.3	5.0	.001070	.000540	36707.	.50
		23.5	8.0	.000635	.000046	29522.	.30
		39.4	8.0	.001000	.000290	33397.	.37
		55.2	8.0	.001220	.000440	39981.	.40
		21.7	11.0	.000499	.000071	26129.	.39
		42.8	11.0	.001000	.000180	35686.	.32
		64.3	11.0	.001300	.000390	43187.	.37
		24.7	15.0	.000468	.000073	25572.	.42
		45.6	15.0	.001070	.000130	33704.	.32
		59.3	15.0	.001400	.000190	36033.	.29
		73.8	15.0	.001600	.000330	40127.	.32

4

TEST SPECIMEN TYPE	AXIAL STRESS	RADIAL STRESS	AXIAL STRAIN	RADIAL STRAIN	RESILIENT MODULUS	POISSONS RATIO
VCP	MD1					
8.0	2.0	.000476	.000230	12790.	.49	
11.8	2.0	.000740	.000400	13082.	.52	
15.9	2.0	.000845	.000550	15989.	.60	
9.9	5.0	.000378	.000049	15805.	.38	
14.5	5.0	.000612	.000096	18087.	.35	
24.4	5.0	.000920	.000477	20920.	.51	
34.2	5.0	.001148	.000700	24802.	.57	
43.5	5.0	.001268	.000830	29502.	.60	
11.7	8.0	.000301	.000038	15881.	.43	
23.1	8.0	.000720	.000200	23114.	.41	
39.0	8.0	.001148	.000500	27520.	.46	
54.7	8.0	.001384	.000730	33527.	.51	
21.6	11.0	.000540	.000072	24021.	.39	
42.6	11.0	.001050	.000477	30581.	.47	
64.0	11.0	.001280	.000617	41590.	.48	
24.4	15.0	.000422	.000048	28361.	.41	
44.3	15.0	.000980	.000146	34802.	.33	
58.8	15.0	.001148	.000316	41243.	.38	
73.2	15.0	.001283	.000436	47610.	.40	

TEST SPECIMEN TYPE	AXIAL STRESS	RADIAL STRESS	AXIAL STRAIN	RADIAL STRAIN	RESILIENT MODULUS	POISSONS RATIO
VCP	LDI					
12.3	2.0	.000620	.000169	10237.	.37	
16.0	2.0	.000780	.000375	13255.	.48	
9.9	5.0	.000845	.000502	16227.	.56	
14.7	5.0	.000390	.000063	15256.	.39	
24.7	5.0	.000627	.000091	18014.	.34	
34.3	5.0	.001058	.000229	20238.	.32	
44.2	5.0	.001220	.000458	24703.	.42	
12.1	8.0	.001485	.000873	26003.	.56	
23.9	8.0	.000337	.000048	15348.	.43	
39.7	8.0	.000820	.000140	22380.	.35	
55.0	8.0	.001130	.000215	30811.	.31	
21.6	11.0	.001420	.000550	33961.	.42	
43.3	11.0	.000580	.000099	21997.	.40	
64.9	11.0	.001050	.000182	34606.	.32	
43.3	15.0	.001330	.000335	43220.	.34	
57.8	15.0	.000940	.000280	32777.	.41	
71.9	15.0	.001270	.000293	37083.	.36	
		.001490	.000439	40666.	.38	

TEST TYPE	SPECIMEN	AXIAL STRESS	RADIAL STRESS	AXIAL STRAIN	RADIAL STRAIN	RESILIENT MODULUS	POISSONS RATIO
VCP	HD2	9.2	2.0	.000356	.000041	19930.	.28
		11.7	2.0	.000423	.000116	24331.	.35
		15.8	2.0	.000520	.000264	26853.	.46
		14.7	5.0	.000631	.000052	17961.	.34
		24.2	5.0	.000972	.000472	19837.	.49
		34.0	5.0	.001199	.000725	23625.	.57
		43.6	5.0	.001459	.000944	25750.	.60
		23.5	8.0	.000794	.000050	23721.	.29
		39.0	8.0	.001248	.000430	26016.	.41
		54.2	8.0	.001650	.000950	27525.	.55
		20.0	11.0	.000374	.000120	26556.	.46
		41.9	11.0	.000975	.000365	33125.	.44
		63.1	11.0	.001344	.000914	37041.	.61
		23.3	15.0	.000496	.000092	20334.	.44
		42.7	15.0	.000918	.000426	30629.	.49
		56.1	15.0	.001377	.000528	32792.	.45
		70.9	15.0	.001574	.000700	36108.	.47

TEST VCP	SPECIMEN TYPE	AXIAL STRESS	RADIAL STRESS	AXIAL STRAIN	RADIAL STRAIN	REILIENT MODULUS	POISSONS RATIO
MD2	7.7	2.0	•000336	•000114	18073.	•42	
	11.5	2.0	•000487	•000161	20357.	•39	
	15.1	2.0	•000604	•000240	22082.	•43	
	9.7	5.0	•000268	•000074	19949.	•44	
	14.3	5.0	•000536	•000137	19291.	•40	
	23.7	5.0	•000906	•000294	21785.	•40	
	33.1	5.0	•001208	•000553	23500.	•47	
	42.8	5.0	•001527	•001008	24000.	•61	
	12.0	8.0	•000227	•000074	19470.	•47	
	22.7	8.0	•000738	•000248	21395.	•43	
	38.0	8.0	•001174	•000347	27184.	•38	
	53.4	8.0	•001577	•000597	29637.	•42	
	21.1	11.0	•000520	•000075	23778.	•40	
	41.6	11.0	•001275	•000422	25490.	•41	
	62.4	11.0	•001644	•000503	32943.	•38	
	23.6	15.0	•000369	•000173	23775.	•49	
	42.7	15.0	•001040	•000399	27958.	•45	
	57.1	15.0	•001376	•000429	32702.	•40	
	71.1	15.0	•001611	•000527	36693.	•40	

TEST TYPE	SPECIMEN	AXIAL STRESS	RADIAL STRESS	AXIAL STRAIN	RADIAL STRAIN	RESILIENT MODULUS	POISSONS RATIO
VCP	LD2	8.0	2.0	.000661	.000119	10081.	.32
		11.2	2.0	.000780	.000225	12490.	.36
		15.0	2.0	.000949	.000405	13860.	.45
		9.6	5.0	.000626	.000059	9267.	.38
		14.3	5.0	.000864	.000121	12674.	.34
		24.5	5.0	.001169	.000303	17897.	.35
		33.3	5.0	.001356	.000630	21013.	.48
		42.9	5.0	.001644	.000993	22739.	.55
		11.8	8.0	.000254	.000065	17585.	.46
		22.8	8.0	.000720	.000194	22759.	.40
		38.4	8.0	.001356	.000291	23892.	.37
		53.2	8.0	.001593	.000753	28573.	.48
		20.8	11.0	.000492	.000135	22531.	.44
		42.0	11.0	.001153	.000221	30074.	.33
		63.1	11.0	.001559	.000369	35860.	.33
		23.4	15.0	.000492	.000099	20422.	.44
		42.2	15.0	.001085	.000208	28752.	.37
		56.1	15.0	.001322	.000246	34867.	.33
		69.8	15.0	.001559	.000309	38658.	.32

4

TEST SPECIMEN TYPE	Axial Stress	Radial Stress	Axial Strain	Radial Strain	Resilient Modulus	Poissons Ratio
VCP	HD3	8.1	2.0	.000334	.000072	20096.
	11.8	2.0	.000435	.000119	23946.	.35
	15.6	2.0	.000510	.000167	27561.	.38
	10.3	5.0	.000201	.000060	29327.	.44
	14.7	5.0	.000368	.000145	27652.	.46
	24.3	5.0	.000652	.000180	31606.	.37
	33.8	5.0	.000786	.000324	37339.	.44
	44.4	5.0	.000987	.000523	39660.	.52
	12.2	8.0	.000134	.000047	34243.	.48
	23.1	8.0	.000418	.000167	37624.	.46
	39.8	8.0	.000769	.000229	43871.	.38
	54.2	8.0	.000987	.000373	48128.	.42
	21.6	11.0	.000334	.000096	35485.	.44
	42.0	11.0	.000786	.000252	42032.	.41
	62.5	11.0	.001037	.000314	52301.	.37
	23.5	15.0	.000201	.000096	42575.	.50
	42.8	15.0	.000601	.000310	46023.	.51
	57.4	15.0	.000886	.000343	49784.	.44
	71.1	15.0	.001003	.000376	58089.	.43

TEST SPECIMEN TYPE	AXIAL STRESS	RADIAL STRESS	AXIAL STRAIN	RADIAL STRAIN	RESILIENT MODULUS	POISSONS RATIO
VCP MD3	7.6	2.0	.000385	.000107	15752.	.38
	11.9	2.0	.000544	.000118	19594.	.31
	15.3	2.0	.000653	.000166	21476.	.32
	9.3	5.0	.000218	.000091	20464.	.48
	14.4	5.0	.000436	.000141	23146.	.43
	23.5	5.0	.000812	.000245	24229.	.38
	33.3	5.0	.001106	.000462	26120.	.45
	42.8	5.0	.001407	.000718	26813.	.51
	11.5	8.0	.000167	.000046	24108.	.47
	22.6	8.0	.000616	.000179	26040.	.41
	38.5	8.0	.001105	.000278	29801.	.35
	54.1	8.0	.001575	.000570	30242.	.41
	21.8	11.0	.000436	.000146	27011.	.46
	42.2	11.0	.001122	.000325	29968.	.39
	63.3	11.0	.001608	.000732	32874.	.47
	23.8	15.0	.000410	.000065	26511.	.43
	42.1	15.0	.000955	.000248	31552.	.40
	57.6	15.0	.001306	.000430	34645.	.41
	71.0	15.0	.001608	.000584	36301.	.42

TEST TYPE	SPECIMEN	AXIAL STRESS	RADIAL STRESS	AXIAL STRAIN	RADIAL STRAIN	RESILIENT MODULUS	POISSONS RATIO
VCP	LD3	8.1	2.0	.000438	.000094	15473.	.34
		11.7	2.0	.000572	.000153	18008.	.35
		15.3	2.0	.000675	.000235	20419.	.39
		9.7	5.0	.000350	.000049	16299.	.40
		14.5	5.0	.000623	.000131	17208.	.37
		24.4	5.0	.000926	.000200	22813.	.33
		33.6	5.0	.001077	.000475	25393.	.44
		42.8	5.0	.001549	.000731	24540.	.48
		11.2	8.0	.000303	.000049	13185.	.45
		23.5	8.0	.000825	.000196	20997.	.38
		39.2	8.0	.001212	.000250	28121.	.32
		54.2	8.0	.001785	.000556	27061.	.37
		21.5	11.0	.000724	.000075	16107.	.38
		42.7	11.0	.001246	.000273	28128.	.35
		64.0	11.0	.001818	.000423	31265.	.32
		24.7	15.0	.000695	.000123	16869.	.43
		43.4	15.0	.001145	.000247	28111.	.38
		56.9	15.0	.001380	.000396	32735.	.39
		71.7	15.0	.001684	.000471	36010.	.37

TEST TYPE	SPECIMEN	AXIAL STRESS	RADIAL STRESS	AXIAL STRAIN	RADIAL STRAIN	RESILIENT MODULUS	POISSONS RATIO
CCP	HD1	7.7	2.0	.000569	.000238	13497.	.42
		11.5	2.0	.000670	.000381	17200.	.57
		15.7	2.0	.000803	.000463	19600.	.58
		10.0	5.0	.000467	.000190	21200.	.41
		14.7	5.0	.000586	.000321	25000.	.55
		24.6	5.0	.000869	.000488	28300.	.56
		34.2	5.0	.000941	.000608	36400.	.64
		44.7	5.0	.001060	.000737	42000.	.68
		12.2	8.0	.000435	.000143	28092.	.33
		23.9	8.0	.000735	.000394	32500.	.53
		39.6	8.0	.000920	.000596	43100.	.64
		55.0	8.0	.001110	.000669	49000.	.60
		22.0	11.0	.000601	.000280	36600.	.46
		43.3	11.0	.000920	.000536	47000.	.58
		65.4	11.0	.001150	.000738	56000.	.64
		25.6	15.0	.000602	.000238	42650.	.39
		44.7	15.0	.000853	.000477	52000.	.55
		58.6	15.0	.001000	.000583	57000.	.58
		69.8	15.0	.001135	.000669	61400.	.59

TEST TYPE	SPECIMEN	AXIAL STRESS	RADIAL STRESS	AXIAL STRAIN	RADIAL STRAIN	RESILIENT MODULUS	POISSONS RATIO
CCP	MD1	7.9	2.0	.000474	.000280	16582.	.60
		11.9	2.0	.000609	.000375	19507.	.65
		15.6	2.0	.000677	.000480	22969.	.71
		10.0	5.0	.000406	.000245	24532.	.60
		14.7	5.0	.000609	.000426	24105.	.70
		24.5	5.0	.000880	.000620	27795.	.72
		34.2	5.0	.001218	.000970	28112.	.80
		44.7	5.0	.001591	.001150	28108.	.72
		11.9	8.0	.000440	.000210	27068.	.47
		23.8	8.0	.000897	.000455	26555.	.56
		38.7	8.0	.001218	.000660	31740.	.58
		55.2	8.0	.001489	.000860	37092.	.60
		21.2	11.0	.000745	.000450	28497.	.60
		42.8	11.0	.001184	.000700	36149.	.64
		64.0	11.0	.001557	.001090	41124.	.73
		24.2	15.0	.000677	.000330	35687.	.49
		43.7	15.0	.001083	.000600	40323.	.58
		58.2	15.0	.001354	.000810	42954.	.60
		69.0	15.0	.001489	.000939	46367.	.63

TEST SPECIMEN TYPE	AXIAL STRESS	RADIAL STRESS	AXIAL STRAIN	RADIAL STRAIN	RESILIENT MODULUS	POISSONS RATIO
CCP	LD1	7.6	2.0	.000753	.000339	.45
11.5	2.0		.000959	.000485	11981.	.51
15.2	2.0		.001096	.000651	13878.	.59
9.8	5.0		.000479	.000192	20459.	.40
14.4	5.0		.000651	.000326	22058.	.50
23.7	5.0		.000959	.000518	24672.	.54
33.8	5.0		.001027	.000741	32911.	.72
43.3	5.0		.001233	.001059	35085.	.86
11.5	8.0		.000377	.000158	30477.	.42
23.0	8.0		.000685	.000497	33547.	.73
38.9	8.0		.001164	.000775	33385.	.67
53.4	8.0		.001370	.001091	38978.	.80
21.0	11.0		.000582	.000327	35997.	.56
41.9	11.0		.001027	.000702	40808.	.68
62.9	11.0		.001370	.000969	45883.	.71
24.7	15.0		.000599	.000279	41185.	.47
42.7	15.0		.001062	.000606	40254.	.57
56.8	15.0		.001267	.000752	44815.	.59
67.6	15.0		.001438	.000847	47003.	.59

TEST TYPE	SPECIMEN	AXIAL STRESS	RADIAL STRESS	AXIAL STRAIN	RADIAL STRAIN	RESILIENT MODULUS	POISSONS RATIO
CCP	HD2	7.9	2.0	.000347	.000280	22767.	.80
		11.8	2.0	.000454	.000404	26000.	.89
		15.6	2.0	.000583	.000539	26800.	.92
		9.9	5.0	.000374	.000245	26500.	.65
		14.5	5.0	.000567	.000381	25573.	.67
		24.2	5.0	.000859	.000717	28172.	.83
		33.9	5.0	.001150	.001150	29500.	1.00
		44.5	5.0	.001620	.001620	27500.	1.00
		11.5	8.0	.000519	.000364	22200.	.70
		23.1	8.0	.001053	.000995	21937.	.94
		38.6	8.0	.001491	.001387	25889.	.93
		54.3	8.0	.001945	.002284	27918.	1.17
		20.1	11.0	.000525	.000389	38286.	.74
		42.0	11.0	.001082	.000908	38817.	.84
		60.4	11.0	.001574	.001507	38374.	.95
		22.8	15.0	.000454	.000389	50000.	.86
		42.9	15.0	.000780	.000648	55000.	.83
		56.4	15.0	.001040	.000972	54500.	.93
		67.0	15.0	.001115	.001183	60000.	1.06

TEST TYPE	SPECIMEN	AXIAL STRESS	RADIAL STRESS	AXIAL STRAIN	RADIAL STRAIN	RESILIENT MODULUS	POISSONS RATIO
CCP	MD2	7.3	2.0	.000403	.000191	18189.	.47
		10.6	2.0	.000520	.000425	20288.	.82
		15.0	2.0	.000671	.000588	22280.	.88
		9.5	5.0	.000386	.000212	24715.	.55
		14.0	5.0	.000570	.000359	24474.	.63
		23.8	5.0	.000889	.000720	26772.	.81
		33.0	5.0	.001477	.001373	22343.	.93
		42.8	5.0	.001779	.001789	24058.	1.01
		11.2	8.0	.000461	.000248	24403.	.92
		22.5	8.0	.000923	.000584	24377.	.96
		37.8	8.0	.001443	.001136	26195.	.79
		53.0	8.0	.001980	.001721	26768.	.87
		20.5	11.0	.000872	.000471	23509.	.54
		42.1	11.0	.001510	.001039	27881.	.69
		61.5	11.0	.002148	.001542	28608.	.72
		23.1	15.0	.000671	.000279	34426.	.42
		41.6	15.0	.001107	.000619	37624.	.56
		56.4	15.0	.001477	.000961	38186.	.65
		66.9	15.0	.001745	.001216	38338.	.70

TEST TYPE	SPECIMEN	AXIAL STRESS	RADIAL STRESS	AXIAL STRAIN	RADIAL STRAIN	RESILIENT MODULUS	POISSONS RATIO
CCP	LD2	7.9	2.0	.000576	.000377	13715.	.65
		11.0	2.0	.000729	.000618	15021.	.85
		15.4	2.0	.000949	.000950	16228.	1.00
		9.9	5.0	.000492	.000295	20203.	.60
		14.1	5.0	.000661	.000475	21331.	.72
		24.3	5.0	.001119	.000951	21716.	.85
		33.6	5.0	.001627	.001426	20652.	.88
		41.8	5.0	.001763	.001967	23710.	1.12
		10.8	8.0	.000475	.000246	22695.	.52
		22.9	8.0	.000949	.000683	24131.	.72
		37.9	8.0	.001441	.001220	26329.	.85
		52.6	8.0	.001932	.001837	27226.	.95
		21.0	11.0	.000898	.000515	23385.	.57
		41.9	11.0	.001559	.001156	26876.	.75
		61.5	11.0	.002034	.001626	30236.	.80
		23.6	15.0	.000610	.000270	38689.	.44
		41.7	15.0	.001017	.000615	41052.	.0
		56.6	15.0	.001288	.000878	43944.	.69
		67.4	15.0	.001593	.001106	42310.	.69

TEST TYPE	SPECIMEN	AXIAL STRESS	RADIAL STRESS	AXIAL STRAIN	RADIAL STRAIN	RESILIENT MODULUS	POISSONS RATIO
CCP	HD3	7.6	2.0	.000334	.000229	22904.	.69
		11.6	2.0	.000480	.000311	24104.	.65
		15.3	2.0	.000569	.000393	26889.	.69
		9.5	5.0	.000326	.000167	29233.	.51
		14.3	5.0	.000443	.000262	32280.	.59
		23.8	5.0	.000645	.000442	36899.	.69
		34.7	5.0	.000936	.000736	37073.	.79
		43.5	5.0	.001204	.001129	36171.	.94
		11.6	8.0	.000318	.000155	36352.	.49
		23.1	8.0	.000619	.000425	37383.	.69
		38.8	8.0	.000953	.000784	40714.	.82
		54.5	8.0	.001237	.001127	44018.	.93
		21.3	11.0	.000569	.000327	37346.	.57
		42.9	11.0	.000987	.000768	43465.	.78
		62.6	11.0	.001288	.001070	48602.	.83
		23.1	15.0	.000435	.000204	53103.	.47
		42.8	15.0	.000736	.000466	58220.	.63
		55.8	15.0	.000920	.000601	60652.	.65
		67.4	15.0	.001087	.000768	62000.	.71

TEST SPECIMEN TYPE	AXIAL STRESS	RADIAL STRESS	AXIAL STRAIN	RADIAL STRAIN	RESILIENT MODULUS	POISSONS RATIO
CCP MD3	7.2	2.0	.000419	.000246	17184.	.59
	11.3	2.0	.000586	.000361	19283.	.62
	15.6	2.0	.000704	.000530	22131.	.75
	9.6	5.0	.000385	.000197	24909.	.51
14.4	5.0	.000586	.000328	.24539.	.56	
23.5	5.0	.000854	.000620	27471.	.73	
35.3	5.0	.001374	.001197	25691.	.87	
43.8	5.0	.001910	.001721	22946.	.90	
11.2	8.0	.000452	.000220	24668.	.49	
22.5	8.0	.000938	.000684	23955.	.73	
37.8	8.0	.001441	.001221	26266.	.85	
53.3	8.0	.001910	.001792	27906.	.94	
21.6	11.0	.000812	.000489	26638.	.60	
41.9	11.0	.001441	.001221	29077.	.85	
61.7	11.0	.002010	.001792	30697.	.89	
23.2	15.0	.000620	.000292	37339.	.47	
43.0	15.0	.001089	.000682	39486.	.63	
56.7	15.0	.001340	.000990	42313.	.74	
67.1	15.0	.001642	.001218	40865.	.74	

TEST TYPE	SPECIMEN	AXIAL STRESS	RADIAL STRESS	AXIAL STRAIN	RADIAL STRAIN	RESILIENT MODULUS	POISSONS RATIO
CCP	LD3	7.9	2.0	.000505	.000263	15683.	.52
		11.7	2.0	.000623	.000394	18764.	.63
		14.5	2.0	.000758	.000624	19103.	.82
		9.6	5.0	.000488	.000235	19754.	.48
		14.4	5.0	.000657	.000378	21963.	.58
		24.1	5.0	.001027	.000698	23447.	.68
		33.7	5.0	.001448	.001281	23273.	.88
		43.0	5.0	.001515	.001461	28383.	.96
		11.2	8.0	.000438	.000229	25639.	.52
		23.1	8.0	.000875	.000654	26423.	.75
		39.6	8.0	.001347	.001225	28656.	.91
		53.7	8.0	.002020	.001961	26609.	.97
		21.0	11.0	.000707	.000489	29632.	.69
		42.6	11.0	.001306	.001107	32619.	.85
		63.0	11.0	.001818	.001629	34653.	.90
		24.2	15.0	.000572	.000308	42238.	.54
		42.3	15.0	.000909	.000731	46590.	.80
		57.1	15.0	.001145	.000925	49869.	.81
		67.2	15.0	.001347	.001218	49852.	.90

## APPENDIX B

## NOMENCLATURE

- $\epsilon_l$  = lateral strain, in/in  
 $\epsilon_a$  = axial strain, in/in  
 $t$  = time  
 $T$  = temperature  
 $\tau$  = shear stress, psi  
 $\sigma_a$  = axial stress, psi  
 $\sigma_r$  = radial stress, psi  
 $\theta$  = first invariant of the stress tensor; numerically equal to the sum of the principal stresses. For a triaxial test specimen,  $\theta = \sigma_1 + 2\sigma_3$ .  
 $\beta$  = soil constant, proposed by Barkan (7), relating the elastic modulus to the stress invariant,  $\text{psi}^{-1}$   
 $M_z$  = soil modulus of deformation proposed by Dunlap (24), psi  
 $M_r$  = resilient modulus, psi  
 $K_1, K_2, K_1', K_2'$  = constants in the equations for  $M_r$   
 $\nu_r$  = resilient Poisson's ratio  
 $\gamma_d$  = dry density,  $\text{lb}/\text{ft}^3$   
 $p$  = distributed surface pressure, psi  
 $w_z$  = vertical displacement at depth  $z$  within a pavement structure, inches  
 $a$  = radius of surface load, inches  
 $\nabla^2$  = LaPlace Operator,  $\frac{\partial^2}{\partial r^2} + \frac{1}{r} \frac{\partial}{\partial r} + \frac{\partial^2}{\partial z^2}$   
 $\phi, \psi$  = stress functions  
 $J_0$  = Bessel function of first kind and zero order  
 $[Q]$  = matrix of concentrated node point loads  
 $[K]$  = stiffness matrix  
 $[U]$  = matrix of node point displacements in the  $r-z$  plane

[B] = elasticity matrix

C,  $\phi$  = Coulomb shear strength parameters

$R_f$  = constant relating compressive strength to asymptotic stress different in the hyperbolic stress-strain law

$E_r$  = resilient modulus, psi

K, n, K', n' = constants in the predictive equations for  $E_r$

VCP = variable confining pressure repeated-load triaxial test

CCP = constant confining pressure repeated-load triaxial test

$\varepsilon_p$  = plastic axial strain, in/in

$\frac{\Delta V}{V}$  = volumetric strain

**VITA**

John J. Allen was born in Corsicana, Texas on January 30, 1943. He graduated from Corsicana High School in 1961. He attended Texas A. & M. University for one year and graduated from the United States Air Force Academy in 1966, winning the Theodore R. Loeschner, Jr. Award as the outstanding civil engineering graduate.

After completion of navigator training, he flew as an instructor navigator in C-130A aircraft in Southeast Asia until May, 1970. His decorations include the Distinguished Flying Cross with oak leaf cluster and the Air Medal with eight oak leaf clusters. Upon completion of this study he will join the faculty of the Department of Civil Engineering at the U.S. Air Force Academy.

In 1972 he received his Master's Degree from the University of Illinois at Urbana-Champaign. He is a member of Chi Gamma Iota, Phi Kappa Phi, and Sigma Xi. He also holds membership in the Society of American Military Engineers.